UNIVERSIDAD DE CÓRDOBA

TESIS DOCTORAL

POR COMPENDIO DE PUBLICACIONES

PROGRAMA DE DOCTORADO EN INGENIERÍA AGRARIA, ALIMENTARIA, FORESTAL Y DEL DESARROLLO RURAL SOSTENIBLE

NUEVOS DESARROLLOS TEÓRICOS EN LA CAPTACIÓN SOLAR EN ESTRUCTURAS FIJAS Y MÓVILES.

NEW THEORETICAL DEVELOPMENTS IN SOLAR CAPTURE FOR STATIC AND MOBILE STRUCTURES

Autor: Luis Manuel Fernández de Ahumada

Directores: ***Dr. D. Rafael López Luque.***

Dr. D. José Cristóbal Ramírez Faz.

Córdoba, noviembre 2019

TITULO: *New theoretical developments in solar capture for static and mobile structures*

AUTOR: *Luis Manuel Fernández de Ahumada*

Campus de Rabanales
Ctra. Nacional IV, Km. 396 A
14071 Córdoba

https://www.uco.es/ucopress/index.php/es/
ucopress@uco.es

Lista de publicaciones originales

Esta tesis se presenta en forma de compendio de publicaciones, de acuerdo con el artículo 24 de la normativa reguladora de los estudios de Doctorado de la Universidad de Córdoba (Aprobado en el consejo de gobierno de 21 de diciembre de 2011 y modificada por el mismo órgano el 29 de mayo de 2013 y el 23 de julio de 2013) que desarrolla el RD 1393/2007 y el RD 99/2011 por el que se regulan las enseñanzas de doctorado. Dichas publicaciones recogen los resultados que han sido obtenidos en los diferentes trabajos de investigación desarrollados con el fin de alcanzar el objetivo fijado para la realización de la tesis. A continuación, se listan las referidas publicaciones (3) que constituyen los anexos de la presente memoria de tesis.

Artículo 1 (se puede consultar en el Anexo I de este documento)

Fernández-Ahumada, L.M.; Casares, F.J.; Ramírez-Faz, J.; López-Luque, R. Mathematical study of the movement of solar tracking systems based on rational models. *Sol. Energy* **2017**, *150*, 20–29. ISSN 0038-092X. https://doi.org/10.1016/j.solener.2017.04.006

Solar Energy**.** Factor de impacto (2017): 4,374

Q1 en el área de ENERGY&FUELS (JCR), posición: 23/97

Artículo 2 (se puede consultar en el Anexo II de este documento)

Fernández-Ahumada, L.M.; Ramírez-Faz, J.; López-Luque, R.; Varo-Martínez, M.; Moreno-García, I.M.; Casares de la Torre, F. A novel backtracking approach for two-axis solar PV tracking plants. *Renew. Energy* **2020**, *145*, 1214–1221. ISSN 0960-1481, https://doi.org/10.1016/j.renene.2019.06.062.

Renewable Energy**.** Factor de impacto (2018): 5,439

Q1 en el área de ENERGY&FUELS (JCR), posición: 17/103

Artículo 3 (se puede consultar en el Anexo III de este documento)

Fernández-Ahumada, L.M.; Ramírez-Faz, J.; López-Luque, R.; Márquez-García, A.; Varo-Martínez, M. A Methodology for Buildings Access to Solar Radiation in Sustainable Cities. *Sustainability* **2019**, *11.* ISSN: 2071-1050. https://doi.org/10.3390/su11236596

Sustainability**.** Factor de impacto (2018): 2,592

Q2 en el área de ENVIRONMENTAL SCIENCES (JCR), posición: 105/251

Otras publicaciones

Ponencia presentada en Congreso internacional

Fernández-Ahumada, L.M.; Ramírez-Faz, J.; López-Luque, R.; Varo-Martínez, M.; Moreno-Garca, I.M.; Casares de la Torre, F. A new methodology to prevent shadows in two-axis solar tracking plants. *In Proceedings of the 2019 IEEE International Conference on Environment and Electrical Engineering and 2019 IEEE Industrial and Commercial Power Systems Europe* (EEEIC / I&CPS Europe); IEEE, **2019**; pp. 1–4, ISBN: 978-1-7281-0653-3, doi: 10.1109/EEEIC.2019.8783819**.**

TÍTULO DE LA TESIS: NUEVOS DESARROLLOS TEÓRICOS EN LA CAPTACIÓN SOLAR EN ESTRUCTURAS FIJAS Y MÓVILES

DOCTORANDO/A: Luis Manuel Fernández de Ahumada

INFORME RAZONADO DEL/DE LOS DIRECTOR/ES DE LA TESIS

La presente tesis desarrolla herramientas que permiten modelizar la radiación solar en tres ámbitos, a saber: instalaciones fotovoltaicas sin sombreo, instalaciones fotovoltaicas con sombreo y edificios en ámbitos urbanos de construcción compleja. Concretamente, el doctorando ha definido ecuaciones matemáticas que optimizan el seguimiento fotovoltaico primando la obtención de mejoras en la generación energética, ha planteado un novedoso enfoque (retroseguimiento) para evitar sombreos en instalaciones fotovoltaicas bajo la premisa antes señalada de la optimización en la generación energética y, por último, ha caracterizado de manera precisa la irradiancia recibida en edificios teniendo en cuenta el efecto que sobre ella tienen la geometría propia del edificio, así como el entorno arquitectónico.

A lo largo del proceso de elaboración de la tesis, el doctorando ha demostrado una elevada capacidad autónoma de adaptación a las diferentes dificultades que se han ido planteando. Ha quedado patente la adquisición de competencias específicas para el desempeño de una futura carrera en el ámbito científico.

Por todo esto, consideramos que se trata de una Tesis de gran calidad, que aborda un problema real, de gran actualidad y con gran aplicabilidad a los sectores fotovoltaico y de la construcción.

La Tesis se presenta como un compendio de tres publicaciones en algunas de las revistas más prestigiosas en el área de investigación, 2 en el primer cuartil y 1 en el segundo cuartil (JCR).

- SOLAR ENERGY (2017, Vol. 150, págs. 20-29), Factor de impacto: 4,374.
- RENEWABLE ENERGY (2020, Vol. 145, págs. 1214-1221), Factor de impacto (2018): 5,439.
- SUSTAINABILITY (2019, Vol. 11, issue 23), Factor de impacto (2018): 2,592

Por todo ello, se autoriza la presentación de la tesis doctoral.

Córdoba, 22 de noviembre de 2019

Firma de los directores

Fdo.: RAFAEL LÓPEZ LUQUE Fdo.: JOSÉ CRISTÓBAL RAMÍREZ FAZ

A Rocío y Julieta que aparecieron para no irse;

a mis padres que siempre creyeron.

Agradecimientos

Cuando algo importante se lleva a cabo, se da uno cuenta de lo difícil que es hacer las cosas solo. Jugador de banquillo, tardé en darme cuenta de que, en el mundo científico, al igual que en el baloncesto, no se llega muy lejos solo con las herramientas que uno trae de casa. En lo que de bueno tenga esta tesis han participado muchas personas que espero no olvidar. Mis directores de tesis, Rafa y Pepe, me han enseñado no solo lo que en este documento puede verse sino a trabajar de una manera constante y a no decaer aun cuando las circunstancias no fueran las más apropiadas. Gracias por confiar, por dejar hacer y por hacerme mejorar. Quiero expresar mi gratitud al resto de miembros del grupo de investigación “Física para las Energías Renovables” y en especial a Marta Varo que se ha desvivido para que esta tesis saliera a flote.

Mis compañeros de área de conocimiento siempre han sido un apoyo y tenían casi tantas ganas como yo de que esto fuera para arriba. De igual modo, quiero agradecer al equipo de dirección de la EPSC su apoyo constante cuando he necesitado el tiempo que no tenemos.

Por último , me gustaría agradecer a mi compañera de travesía en la vida, Rocío, haber podido dedicarme estos últimos meses a esta tesis y tirar del carro. Espero poder explicar a Julieta en qué consistieron estos años. El tiempo no se devuelve, pero lo que viene a continuación no nos lo quitará nadie.

Mis padres siempre confiaron en que lo que se había regado durante tanto tiempo diera sus frutos. Gracias por creer en mí.

No me olvido de mi hermana Elvira, mi compañera de juegos de pequeños y de mayor mi gurú de ciencia. Mi hermano Manolo me hace ser un poco más grande y siempre tiene una palabra que me hace reflexionar. Gracias a los dos.

Resumen

La irradiancia solar es una variable fundamental para la caracterización del recurso solar como fuente de energía. La escasez de datos de esta variable ha provocado que se hayan desarrollado modelos explicativos de la misma (modelos isotrópicos, anisotrópicos, etc.). Sin embargo, los modelos de irradiancia solar han sido hasta la fecha poco explotados en la generación de conocimiento de pautas relativas a una captación óptima. De manera particular, esta falta de desarrollo se manifiesta en el estudio de seguidores solares de instalaciones fotovoltaicas y en la radiación incidente sobre edificios de núcleos urbanos. Matemáticamente, las ecuaciones que rigen los modelos de irradiancia pueden ser derivadas respecto de las variables de posición y, de esta manera, generar resultados de movimiento que optimizan la captación y, por tanto, la producción energética. Asimismo, la explotación de estos modelos permite explicar resultados conocidos en el ámbito energético sostenible. Valga como ejemplo el caso de los seguidores solares basados en la maximización de la captación solar que presentan mejores tasas de generación energética que los basados en seguimiento astronómico.

Esta tesis presenta la deducción analítica de las ecuaciones genéricas y unificadas de movimiento de seguidores solares. Muestran como novedad ser más genéricas, permitiendo la optimización del posicionamiento en instalaciones fotovoltaicas aprovechando las componentes difusa y reflejada de la irradiancia frente a las habitualmente publicadas que solo tienen en cuenta la posición del sol (ecuaciones de movimiento astronómico). El análisis de los resultados obtenidos refuta la idea axiomática, ampliamente difundida por numerosos autores, que establece como seguidor ideal en instalaciones fotovoltaicas aquel que procura el mejor alineamiento posible con los rayos solares directos.

Además, en las instalaciones fotovoltaicas con seguidores solares aparecen durante las horas de altura solar baja, sombreos entre colectores que provocan una drástica caída de producción. Esta tesis presenta una nueva estrategia óptima de seguimiento que evita la creación de estas sombras. El método propuesto determina si hay o no sombra entre los colectores de una instalación. Por lo tanto, cuando los colectores no están

sombreados, se propone una trayectoria de seguimiento para obtener la máxima irradiancia en los colectores. Cuando los colectores estuviesen sombreados se propone el retroseguimiento. La producción energética en las plantas con este novedoso método de seguimiento puede ser un 1,31% superior a la de instalaciones fotovoltaicas con seguimiento astronómico y sin intersombreo. Además, este método permite estudiar instalaciones para las que actualmente no existen enfoques publicados, como instalaciones con colectores no rectangulares o aquellas situadas en terrenos con topografía no plana.

Por otro lado, la creciente necesidad de mejorar la sostenibilidad ambiental y energética de los edificios implica el aprovechamiento de la radiación solar incidente en sus superficies. Sin embargo, en las ciudades esta tarea se complica debido a la geometría constructiva que provoca el sombreo entre los edificios. En este contexto, esta tesis presenta un estudio del acceso solar a las fachadas de los edificios de las ciudades. La metodología se basa en la determinación de la radiación solar anual incidente en 121 puntos significativos de cada fachada considerando los doce días más representativos del año. Para caracterizar la influencia de las diferentes tipologías de edificaciones respecto al acceso solar, se propone el Coeficiente Solar Urbano (relación entre la irradiancia recibida en un punto de un edifico y la total recibida en el barrio en que se encuentra dicho edificio). Se ha analizado un estudio en dos barrios de Córdoba (España) con diferentes entornos urbanos. En concreto, se han comparado dos tipologías de barrios: uno con "bloques en forma de L" y "bloques en forma de U" y otro con "bloques agrupados". Para ambos se ha calculado el Coeficiente Solar Urbano, obteniendo un valor medio superior para el barrio con "bloques en forma de L" y "bloques en forma de U" (0,317) que para el barrio con "bloques agrupados" (0,260). En consecuencia, los resultados muestran que la morfología urbana puede influir en el Coeficiente Solar Urbano y el acceso solar. Finalmente, se ha obtenido un modelo de regresión para cada barrio con el fin de determinar la dependencia del Coeficiente Solar Urbano respecto a los factores geométricos del barrio.

Con esta tesis se ha abordado una caracterización de la irradiancia en aplicaciones móviles y fijas, planteando problemas reales cuyas soluciones son de una aplicabilidad plena en los ámbitos del urbanismo y la energía fotovoltaica.

Palabras clave: Plantas solares FV, seguimiento Solar, pérdidas por sombreo, retroseguimiento, ciudades sostenibles; acceso solar; radiación solar en edificios.

Abstract

Solar irradiance is a fundamental variable for the characterization of the solar resource as an energy source. The scarcity of data on this variable has encouraged the development of explanatory models (isotropic models, anisotropic models, etc.). However, the models of solar irradiance have not been exploited so far in the generation of knowledge of patterns relating to optimal capture. In particular, this lack of development is evident in the study of solar trackers of photovoltaic facilities and in the radiation incident on buildings in cities. Mathematically, equations governing irradiance models can be derived with respect to position variables and, in this way, generate movement results that optimise capture and, therefore, energy production. Likewise, the exploitation of these models enables to explain known results in the sustainable energy field. A good example is the case of solar trackers based on the maximization of solar capture which have greater energy generation rates than those based on astronomical tracking.

This thesis presents the analytical deduction of generic and unified equations of the movement of solar tracking systems. As a novelty, these equations are more generic, thus allowing the optimization of the positioning of photovoltaic (PV) facilities where diffuse and reflected irradiance are usable as opposed to those usually published that just consider the position of the sun (astronomical motion equations). The analysis of the results obtained criticizes the axiomatic idea – widely considered by numerous authors – establishing that the ideal tracking system in PV facilities is that tracker providing the best possible alignment with direct sunbeams.

In PV plants based on solar tracking, during low-elevation solar angle hours, shadows appear between the collectors causing a dramatic decrease in production. This thesis presents a novel optimal tracking strategy to prevent the creation of these shadows. The presented method determines whether or not there is shading between collectors. Thus, when the collectors are not shaded, a tracking trajectory for maximum irradiance on the collectors is suggested. When the collectors are shaded, backtracking is proposed. Therefore, energy production in plants with this novel tracking method can be 1.31 % higher than that in PV plants with astronomical tracking. Moreover, this

method allows the study of PV facilities for which there have been no published approaches, such as plants with non-rectangular collectors or those located on topographically heterogeneous surfaces.

The growing need to improve the environmental and energy sustainability of buildings involves the use of solar radiation incident on their surfaces. However, in cities this task is complicated due to the constructive geometry that leads to shading between buildings. In this context, this work presents a study of solar access to the façades of buildings in cities. The methodology is based on the determination of the incident annual solar radiation in 121 significant points of each façade considering the twelve representative days of the year. To characterize the influence of the different city typologies on solar access, the Urban Solar Coefficient (the ratio of the irradiance received at one point in a building to the total irradiance received in the neighbourhood in which the building is located) is proposed. A study in two neighborhoods in Cordoba (Spain) with different urban settings have been analyzed. Specifically, two typologies of neighborhoods have been compared: one with ”L-shaped” and “U-shaped blocks” and another with “Grouped blocks”. For both of them, the Urban Solar Coefficient has been calculated, obtaining a higher mean value for the neighborhood with ”L-shaped” and “U-shaped blocks” (0.317) than for the one with “Grouped blocks” (0.260). Accordingly, the results show that urban morphology can influence the Urban Solar Coefficient and solar access. Finally, a regression model for each neighborhood has been obtained in order to determine the dependence of the Urban Solar Coefficient on neighborhood geometry factors.

This thesis has addressed a characterization of irradiance in mobile and fixed structures, proposing real problems whose solutions are fully usable in the domains of urbanism and photovoltaic energy.

Keywords: PV solar plants, solar tracker, lower losses by shading, backtracking, sustainable cities, solar access; solar radiation on buildings

Índice de Contenidos

Índice de figuras

Índice de tablas

Lista de símbolos

a_P, b_P, F_1, F_2 = parámetros del modelo de Pérez

b_M = parámetros del modelo de Muneer

$\vec{e}$ = vector unitario del eje de rotación

F = parámetros del modelo de Klucher

H = radiación diaria global

$\vec{\imath}, \vec{\jmath}, \vec{k}$ = vectores unitarios asociados a un sistema cartesiano

I = irradiancia solar global sobre un colector inclinado

I_B = irradiancia solar directa sobre plano horizontal

I_D= irradiancia solar difusa

I_{DN}= irradiancia directa normal

$I_{D\beta}$= irradiancia solar difusa sobre plano horizontal

I_G= irradiancia solar global ($I_B + I_D$)

I_{OH} = irradiancia extraterrestre

$\vec{n}$ = vector normal a la superficie

$\vec{p}$ = vector unitario, coplanar con $\vec{u}$ y $\vec{e}$ y perpendicular a $\vec{e}$

$\vec{u}$ = gradiente de irradiancia

$\vec{s}$ = vector solar

s_x , s_y , s_z = componentes del vector solar

$\vec{u}_f, \vec{v}_f$ = vectores unitarios del sistema de referencia del plano contenido en el colector

P_o = origen del colector de referencia

P_i = origen del colector genérico que puede sombrear

A_0 = punto equivalente a P_o en la superficie del colector

A_i = punto equivalente a P_i en la superficie del colector

$\vec{d}_i$ = vector de traslación del colector Π_0 hacia la proyección Π'_i

d_x , d_y = componentes del vector $\vec{d}_i$

$\overline{H_{g,a}}$ = radiación solar horizontal media anual en el emplazamiento elegido

$\overline{H_{g,a,p}}$ = radiación solar media anual en un punto concreto de un edificio del emplazamiento

H = altura del punto estudiado

D = distancia entre la fachada estudiada y la más cercana

c_1, c_2, c_3, c_4, c_5 = coeficientes de correlación para las topologías de edificación

k_1, k_2, k_3, k_4 = constantes de la regresión lineal entre USC y H, D_s, y ϑ_{ff}

D_s = ancho de la calle

Símbolos griegos

β = ángulo de inclinación del colector

δ = declinación solar

θ = ángulo de incidencia de los rayos de sol sobre un plano inclinado

θ_z = ángulo solar cenital

λ, μ, ν= multiplicadores de Lagrange

τ = ángulo genérico formado por el plano horizontal y el eje de rotación en un seguidor de un solo eje

Φ = función de Lagrange

φ = latitud

ρ = albedo

γ = ángulo azimut del colector

α = ángulo de elevación del colector

θ_1, θ_2 = ángulos de rotación de los ejes primario y secundario respectivamente de un seguidor

τ_{ap} = escalar que multiplica al vector solar para cumplir la regla del paralelogramo

Π_0= colector de referencia

ψ= plano que contiene el seguidor de referencia

Π_i = colector cualquier colector del campo fotovoltaico

Π'_i = proyección de Π_i sobre el plano ψ

Σ = envolvente de los polígonos resultante de las proyecciones de los colectores Π_i en ψ

ϑ_{ff} = orientación de la fachada

Acrónimos

GCR = Ground Cover Ratio

ATNS = Astronomical Tracking with No Shading

MITNS = Maximum Irradiance Tracking with No Shading

MIBT =Maximum Irradiance BackTracking

USC = Urban Solar Coefficient

SVF = Sky View Factor

Capítulo 1 .
Introducción

El progreso de las sociedades está ligado de manera directa con el consumo energético. La dependencia energética de fuentes fósiles se ha convertido en un problema de grandes dimensiones. La Humanidad se enfrenta a una necesidad cada vez mayor de utilización de fuentes renovables de energía, sirva como ejemplo el aumento de la demanda mundial de energía primaria en 2018 hasta las 14.301 Mtep (un 2,3% más que el año anterior y un 30% mayor que el de hace 7 años) de las que solo el 15% son de origen renovable [1]. El incremento de las necesidades energéticas no es un hecho aislado. El crecimiento de la población mundial desde los actuales 7.700 millones de personas a los 8.500 millones en 2030 o 9.700 millones en 2050 [2] es un reto de gigantescas dimensiones para nuestra sociedad. Las continuas migraciones, desde el medio rural al urbano y desde los países empobrecidos a aquellos con economías más avanzadas, ligadas al cambio climático representan otro significativo desafío para nuestra generación [3]. Las consecuencias de estos fenómenos son diversas y van desde problemas asociados al impacto cada vez mayor que el uso de combustibles fósiles tiene en el transporte de personas y mercancías [4], hasta el empeoramiento de la calidad del aire respirado relacionado con las emisiones producidas por combustibles fósiles [5]. Los fenómenos descritos están a su vez muy interrelacionados, lo que sugiere que el enfoque de actuación deba ser transversal y global. Se pueden destacar como iniciativas internacionales el acuerdo del Clima de París (con medidas de obligado cumplimiento para los países firmantes) [6] o los Objetivos de Desarrollo Sostenible promovidos por Naciones Unidas y que, de manera explícita, abordan en sus puntos séptimo (Energía asequible y no contaminante) y décimo tercero (Acción por el Clima) temáticas relacionadas directamente con la sostenibilidad y los problemas ambientales [7].

Estas circunstancias han fomentado la investigación y el desarrollo de energías renovables para mejorar la eficiencia energética y la sostenibilidad global [8]. Entre estas fuentes de energía renovable, la energía solar destaca como una fuente de energía limpia, abundante y disponible, en mayor o menor medida, en toda la Tierra [9]. Esta situación junto con el vertiginoso abaratamiento de costes durante los últimos quince años en los materiales utilizados en el sector solar (principalmente en fotovoltaica) explican que las diferentes tecnologías asociadas al uso de la energía solar hayan experimentado un aumento espectacular [1].

En este contexto, esta tesis doctoral pretende, teniendo como hilo conductor la captación solar, caracterizar diferentes metodologías que optimicen dicha captación en el ámbito de instalaciones fotovoltaicas y de edificios urbanos. Los tres trabajos presentados abordan por un lado dos enfoques completamente novedosos de mejora en el seguimiento solar fotovoltaico y

por otro, la definición de la influencia de la tipología constructiva en los edificios respecto al acceso solar.

1.1. Optimización del seguimiento en instalaciones fotovoltaicas

El sector fotovoltaico, gracias a significativas mejoras tecnológicas y de competitividad, se convierte en una prometedora fuente básica de generación eléctrica. En esta tecnología aún existe margen posible para una optimización en la eficiencia de la gestión de las instalaciones basadas en ella, así como en la configuración de su diseño, lo que nos llevaría a un potencial incremento del desarrollo de dicha fuente [10,11]. Estas mejoras, sin embargo, no siempre llevan aparejadas prácticas idóneas de diseño y manejo de instalaciones. En consecuencia, pueden obstaculizar el progreso de la tecnología fotovoltaica, impidiendo un uso óptimo de instalaciones.

En el primer trabajo académico de esta tesis se muestra cómo las ecuaciones para el seguimiento astronómico, generalmente recomendadas, pueden ser inadecuadas ya que limitan la producción en porcentajes incluso por encima del 10%. Esta crítica surge del análisis de las ecuaciones también presentadas en este trabajo, deducidas para realizar un seguimiento solar óptimo.

Los sistemas de seguimiento solar, en general, se clasifican en dos categorías: i) sistemas de seguimiento de un solo eje, en los que un elemento móvil adapta su posición girando alrededor de un eje fijo, y ii) sistemas de seguimiento de dos ejes, en los que el plano colector gira en torno a dos ejes fijos, lo que permite la orientación hacia cualquier dirección de la esfera celeste [12]. En ambos casos, el movimiento en azimut y elevación de la superficie captadora puede estar predeterminado por un conjunto de ecuaciones (control en bucle abierto) o recalculado permanentemente a partir de las lecturas de sensores de radiación (control en bucle cerrado). Los incrementos productivos según los tipos de sistemas de seguimiento para diferentes latitudes y tecnologías han sido ampliamente estudiados, mostrando que el proceso de seguimiento es más efectivo a medida que la latitud es mayor [13–16]. Los mayores incrementos son del orden del 57% [11,17]. El seguimiento es obligatorio en aquellas aplicaciones en las que se concentra la radiación solar [18].

Las ecuaciones presentadas en la bibliografía para determinar la orientación de los sistemas de seguimiento se basan exclusivamente en el movimiento astronómico del sol. El desarrollo de ecuaciones astronómicas permite predecir la posición solar en la esfera celeste con una precisión del orden de los milirradianes [19–21]. De esta manera, Duffie y Beckman [22], Braun

y Mitchell [23], Meinel y Meinel [24], Neville [25], Narvarte y Lorenzo [26] y Riley y Hansen [27] presentan las ecuaciones para seguidores de un eje y dos ejes obtenidas mediante la aplicación de la trigonometría esférica al movimiento solar. Más recientemente, se ha abierto una nueva línea que describe el movimiento del sol y de los seguidores solares mediante la aplicación del álgebra vectorial [28–32]. El vector solar $\vec{s}$ se define pues como el vector unitario dirigido al centro del disco solar. Todas las relaciones astronómicas se deducen cuando se hacen cambios de sistemas coordinados usando álgebra matricial o aplicando las definiciones del producto vectorial y escalar.

1.1.1. Estudio matemático para el seguimiento

La aplicación del modelo astronómico al seguimiento solar se materializa mediante la condición de minimización del ángulo de incidencia θ que los rayos solares directos forman con la normal de la superficie del colector. En términos de irradiancia solar, es un sistema de seguimiento que solo considera la maximización de la componente directa de la irradiancia [16]. Por consiguiente, es apropiado para aplicaciones que solo pueden utilizar esta componente (normalmente aplicaciones con concentración). Este movimiento de los planos del seguidor no es el más adecuado para la energía fotovoltaica, donde todas las componentes de la radiación son aprovechables. Este efecto es especialmente evidente en aquellos días en los que la radiación directa no llega a los colectores y el disco solar no es visible. Un seguimiento astronómico del sol implica una menor captación de energía en todos los momentos del día en comparación con la energía obtenida en un plano horizontal fijo. Duffie y Beckman [22] y Mousazadeh et al. [11] muestran este efecto en días con una baja incidencia de radiación directa. La literatura, sin embargo, no incluye trabajos orientados al desarrollo de ecuaciones de seguimiento solar para esos días.

De esta forma, es necesario el estudio del efecto de las componentes difusa y reflejada sobre el seguimiento solar para obtener las ecuaciones que impliquen captación radiativa máxima.

1.1.2. Sombreo y retroseguimiento

Adicionalmente, uno de los aspectos de gran importancia a tener en cuenta en las instalaciones con seguimiento solar astronómico es el sombreo entre módulos, que principalmente ocurre en las primeras y últimas horas del día y que da lugar a pérdidas productivas, así como a la aparición de puntos calientes en los módulos [17].

En la bibliografía, son multitud los estudios académicos que, teniendo en cuenta la influencia del sombreo, han tratado de caracterizar y optimizar el diseño de plantas seguidoras. Díaz-

Dorado et al. [33,34] han desarrollado un modelo que considera la disposición de las células dentro de los módulos fotovoltaicos, así como la posición exacta de cada módulo dentro de la superficie seguidora, de modo que los efectos del sombreo se determinan para todas las células del seguidor. En su trabajo, los sombreos son caracterizados considerando una estrategia de seguimiento convencional que procura la perpendicularidad de los rayos solares directos con la superficie colectora [33,34].

Para estimar las pérdidas de potencia causadas por el sombreado, Martínez-Moreno et al. [35] han propuesto un modelo predictivo que no requiere de ninguna información específica sobre las conexiones entre las células y los módulos. Este modelo ha sido validado por diferentes autores [36,37] quienes han desarrollado modelos más extensos basados en el modelo de Martínez-Moreno para determinar la productividad de las plantas fotovoltaicas. Asimismo, Perpiñan [38] ha desarrollado un método de estimación y optimización del coste energético basado en los parámetros de diseño de la planta, concretamente en la relación de cobertura del suelo (Ground Cover Ratio o GCR, que es la relación entre la superficie de los módulos fotovoltaicos y el terreno ocupado por la planta fotovoltaica). Para ello, el método utiliza la hipótesis de Gordon y Wenger [39] al determinar las pérdidas de energía debidas al sombreado, que las considera proporcionales al porcentaje de área sombreada. Narvarte y Lorenzo [26] estudiaron la productividad de una planta fotovoltaica considerando diferentes tipos de seguimiento solar y tres hipótesis simplificadas para estimar las pérdidas por sombreado.

Con esta idea de minimizar los efectos del sombreado, Panico et al. [40] propusieron el retroseguimiento (*backtracking)*. Esta técnica consiste en desviar la dirección de los seguidores de la dirección solar para evitar el sombreado entre los colectores cuando sea necesario. Diferentes autores [17,40,41] han demostrado las ventajas del retroseguimiento, destacando:

A. Ventajas de aprovechamiento del terreno: Al evitar los efectos del sombreado, se pueden reducir las distancias entre los seguidores, consiguiendo un GCR mayor.

B. Ventajas operativas: El trabajo realizado por Lorenzo y Narvarte [17] indica que, en todos los casos, el balance energético es más favorable en las plantas con retroseguimiento que en las que permiten el sombreado entre colectores.

C. Ventajas de diseño: La ausencia de sombras y, por lo tanto, de puntos calientes, implica menores costes de mantenimiento.

Por lo tanto, la fiabilidad de las plantas con retroseguimiento es mayor que la de las plantas que permiten el sombreado [17,41].

Para determinar la orientación de los colectores durante el retroseguimiento, se han propuesto diferentes métodos basados en la determinación geométrica de las sombras entre polígonos [13,17,42]. Sin embargo, estos métodos a menudo se limitan a situaciones geométricas simplistas como:

i. Colectores exclusivamente rectangulares.

ii. Mallas geométricas regulares en las que sólo se considera el sombreamiento entre colectores contiguos

iii. Superficies topográficas planas y horizontales.

iv. Movimiento alrededor de los ejes azimutal y de elevación. Otras posibilidades que implican diferentes opciones de giros de la superficie colectora no son consideradas (Equatorial, Elevation-Rolling, Rolling-Elevation).

Teniendo en cuenta las limitaciones anteriores, se plantea un método de retroseguimiento más simple y genérico para evitar sombras y optimizar la captación de energía solar.

1.2. Radiación en el ámbito urbano

El aprovechamiento de la energía solar en las ciudades se ha convertido en una obligación en las nuevas viviendas para hacerlas más sostenibles. Sin embargo, los niveles de radiación solar no suelen tenerse en cuenta a la hora de tomar decisiones sobre la planificación urbana. De hecho, para desarrollar medidas de eficiencia energética en edificios nuevos es necesario conocer los niveles de radiación solar que llega a cada una de las partes del edificio y que podrían utilizarse para instalar paneles fotovoltaicos o colectores térmicos [43,44]. Además, esta información sobre la radiación solar también puede utilizarse para la estimación de la iluminación natural de sus ventanas y, en consecuencia, para garantizar los derechos solares [45], especialmente en ciudades con baja incidencia solar (presencia de rascacielos, orografía, zonas con elevada latitud, etc.). La luz natural también influye positivamente en la salud y el comportamiento humano de los residentes [46,47] y contribuye a mejorar el clima interior, aumentar el confort térmico y, en consecuencia, reducir la demanda energética de una vivienda [47–52]. Por todas estas razones, es necesario un conocimiento profundo del nivel de radiación solar disponible en las fachadas de los edificios de las ciudades [53].

Además, un conocimiento completo de la radiación solar en fachadas de ciudades con geometría edificatoria compleja permite desarrollar nuevos diseños de edificios solares pasivos [54]. De esta forma, se facilita la elección de los materiales ideales para las ventanas (como polímeros transparentes o translúcidos, protecciones solares o acristalamientos con alta selectividad térmica entre otros) y su disposición en cada caso [55]. Estas técnicas resultan especialmente interesantes en zonas donde las cargas de calefacción de los edificios representan una parte importante de la demanda energética. Así, las herramientas de simulación de rendimiento de edificios (Building Performance Simulation o BPS) comparan diferentes alternativas de diseño relacionadas con la eficiencia y el consumo de energía en los edificios, proporcionando información útil y rápida a los técnicos [56]. Debido a la importancia del nivel de radiación solar en fachadas y cubiertas [57,58], los profesionales del ámbito de la arquitectura deberían tenerlo en cuenta en las fases iniciales de sus proyectos. En esta línea de trabajo, Tang Minfang [59] estudió el efecto del ángulo azimut y la altura de las fachadas principales de un edificio sobre la radiación solar disponible y Salazar Trujillo [60] describió la influencia de la radiación solar sobre las temperaturas en el interior de las habitaciones para mejorar la eficiencia energética.

Sin embargo, este análisis puede resultar complejo en las ciudades [51] debido a las diversas interacciones existentes, incluyendo aquellas con edificios colindantes o con arboleda cercana [61] y el hecho de que cada barrio debe ser estudiado independientemente [62].

Las técnicas basadas en Sistemas de Información Geográfica (SIG) permiten representar ciudades complejas y pueden utilizarse para la estimación de los paramentos más apropiados de un edificio, para la instalación de paneles fotovoltaicos [63] o para identificar las zonas de óptimo potencial de energía solar [64]. Además, utilizando estas técnicas, los resultados pueden ser escalables y automatizados [65]. Un buen ejemplo de una metodología basada en SIG es la Planificación de Energía Solar (SEP) desarrollada por Gadsden et al. [66], que no sólo predice la energía consumida por las viviendas, sino también el ahorro de energía que se puede lograr cuando se utilizan sistemas fotovoltaicos, agua caliente sanitaria solar o diseño solar pasivo.

Se han desarrollado varias aplicaciones informáticas para estudiar la distribución de la radiación solar en ambientes urbanos complejos. Destaca la herramienta *Heliodon*, diseñada por Benoit Beckers y Luc Masset, que representa gráficamente la irradiancia solar que llega a las fachadas de los edificios. Sin embargo, para minimizar el tiempo de cálculo, sólo considera la componente directa de la radiación solar [67]. Destaca también el software *Solene*, diseñado por el Centre de Recherche Méthodologique d'Architecture (CERMA), que analiza la luz solar en las ciudades [68]. Permite determinar las sombras entre edificios, así como la luz natural tanto dentro como fuera

de un edificio. Por lo tanto, es una herramienta muy útil para los profesionales del mundo de la arquitectura que pueden simular fácilmente la luz natural a la hora de decidir la distribución de las ventanas en fachadas y tejados.

Se hace patente que la caracterización de la radiación solar que llega a los edificios es un importante hito en la planificación de los desarrollos urbanos.

Tras la definición de la problemática planteada a lo largo de este primer capítulo introductorio, se ha demostrado la necesidad de abordar los retos científicos presentados a partir de las hipótesis y objetivos que se detallan en el segundo capítulo de este documento. Los capítulos tercero, cuarto y quinto sustentan el aporte científico de la tesis mediante los tres artículos publicados en las revistas referenciadas en el *Listado de publicaciones*. El sexto capítulo está dedicado a las conclusiones de cada uno de los artículos. Se añaden posteriormente, la bibliografía global de la tesis y tres anexos correspondientes a los artículos tal y como se han publicado en las respectivas revistas.

Capítulo 2 . Hipótesis y objetivos

2.1. Hipótesis

2.2. Objetivos

2.1. Hipótesis.

- **Hipótesis global (artículos 1, 2 y 3)**.

Los modelos de estimación de irradiancia solar habitualmente se aplican a planos inclinados e instalaciones estáticas. Esta estrategia ignora la capacidad de generar conocimiento en seguimiento y captación en ambientes complejos. Los mismos modelos rigen para trayectorias de seguimiento bajo tres prismas: i) sin intersombreo, ii) con intersombreo y iii) en geometrías complejas.

- **Hipótesis A (artículos 1 y 2)**

Todos los modelos de irradiancia estudiados son funciones matemáticas derivables mediante cálculo simbólico y cuya optimización se basa en la diferenciación respecto al vector unitario, con la posibilidad de aplicar el método analítico de Lagrange.

- **Hipótesis B (artículos 1 y 2)**

La geometría de las expresiones vectoriales puede realizarse mediante la combinación de los productos escalares de tres vectores (solar $\vec{s}$, normal $\vec{n}$, unitario cenital $\vec{k}$; $\vec{s} \cdot \vec{n}$, $\vec{k} \cdot \vec{n}$, $\vec{s} \cdot \vec{k}$).

- **Hipótesis C (artículo 2)**

Los seguidores solares raramente están aislados y se encuentran agrupados en instalaciones fotovoltaicas donde es probable el sombreo entre ellos.

- **Hipótesis D (artículo 2)**

Los seguidores solares se mueven de manera que los planos captadores son paralelos entre sí.

- **Hipótesis E (artículo 2)**

La condición de sombreo entre colectores se deriva de la aplicación de un test basado en álgebra de Minkowski [69–71]*, que se determina si se cumple que:*

i) el colector que puede dar sombra es visible desde el colector de referencia

ii) el sol no irradia sobre la parte trasera de los colectores

iii) es de día.

- **Hipótesis F (artículo 3)**

El factor adimensional Coeficiente Solar Urbano (Urban Solar Coefficient o USC), definido como la relación existente entre la radiación solar media anual que alcanza un punto concreto de la fachada tipo de las edificaciones en un barrio y la radiación horizontal solar media anual de dicho barrio, es un indicador adecuado para el cálculo del acceso solar.

- **Hipótesis G (artículo 3)**

Existe una adecuada caracterización de la componente difusa de la irradiancia en función del factor Sky View Factor o SVF, definido como la fracción eficaz de cielo visible desde un punto en un ambiente obstruido.

2.2. Objetivos.

- **Objetivo A (artículos 1 y 2)**

Generar conocimiento a partir de las ecuaciones de modelización de la irradiancia para la obtención de trayectorias óptimas de seguimiento en instalaciones fotovoltaicas de uno y dos ejes sin considerar el intersombreo.

- **Objetivo B (artículo 2)**

Generar conocimiento a partir de las ecuaciones de modelización de la irradiancia para la obtención de trayectorias óptimas de seguimiento en instalaciones fotovoltaicas de uno y dos ejes considerando el intersombreo.

- **Objetivo C (artículo 3)**

Generar conocimiento a partir de las ecuaciones de modelización de la irradiancia para caracterizar la radiación solar que alcanza las fachadas de edificios urbanos de diferentes tipologías.

- **Objetivo D (artículo 2)**

Obtener un método de retroseguimiento para seguidores solares que pueda ser aplicado en superficies colectoras no rectangulares.

- **Objetivo E (artículo 2)**

Obtener un método de retroseguimiento para seguidores solares en instalaciones donde los colectores no están necesariamente situados en los nodos regulares de una red.

- **Objetivo F (artículo 2)**

Obtener un método de retroseguimiento para seguidores solares en superficies topográficas reales, no solo sobre superficies planas u horizontales.

- **Objetivo G (artículo 2)**

Obtener un enfoque de retroseguimiento para seguidores solares que considere la irradiancia global sobre los colectores en lugar de limitarse a la componente directa y que permita determinar y comparar los efectos de los diferentes modos de seguimiento

- **Objetivo H (artículo 3)**

Determinar la influencia de la morfología de los edificios en el acceso solar de los mismos.

- **Objetivo I (artículo 3)**

Determinar la correlación en la estimación de la radiación solar entre las fachadas de los edificios respecto a variables auxiliares (azimut, ancho de calle, altura, etc.)

Capítulo 3 .

Mathematical study of the movement of solar tracking systems based on rational models

MATHEMATICAL STUDY OF THE MOVEMENT OF SOLAR TRACKING SYSTEMS BASED ON RATIONAL MODELS

Solar Energy, Volume 150, 1 July 2017, Pages 20-29

L.M. Fernández-Ahumada[a], F.J. Casares[b], J. Ramírez-Faz[b]*, R. López-Luque[b]

[a] Computing and Numeric Analysis. University of Córdoba. Campus de Rabanales, 14071 Córdoba, Spain.

[b] Electrical Engineering. University of Córdoba. Campus de Rabanales, 14071 Córdoba, Spain.

[c] Applied Physics. University of Córdoba. Campus de Rabanales, 14071 Córdoba, Spain.

*Corresponding Author: Phone: + 34957218474 Fax: + 34957218474 e-mail address: jramirez@uco.es

ABSTRACT

This paper presents the analytical deduction of generic and unified equations of the movement of solar tracking systems. These equations reproduce published equations, which only consider the sun position, or the equations of the astronomical movement. As a novelty, these equations are more generic, thus allowing the optimization of the positioning of PV installations where diffuse and reflected irradiance are usable. The analysis of the results obtained criticizes the axiomatic idea – widely considered by numerous authors – establishing that the ideal tracking system in PV installations is that tracker providing the best possible alignment with direct sunbeams.

KEYWORDS:

Solar tracking, Photovoltaic, Equations.

3.1. Introduction.

The use of renewable energy sources is one of the main problems of humanity in the short term. This situation entails that different technologies associated to the use of solar energy are experiencing a dramatic increase. This is the case of the photovoltaic sector, where scientific and industrial progress are creating a sustainable energy alternative [10,11]. These improvements, however, do not always have adequate design practices and proper installation management. As a consequence, they may hinder the progress of PV technology not allowing the optimal use of the installation. This paper presents that equations for astronomical tracking, generally recommended, may be unsuitable since they limit production in percentages even over 10%. This criticism arises from the analysis of the equations also included in this paper and is deducted to perform an optimal solar tracking.

Solar tracking systems, in general, are classified into two categories: (i) single-axis tracking systems, where a mobile element adopts its position by rotating about a fixed axis; and (ii) two-axis tracking systems, where the collector plane rotates about two fixed axes, allowing the orientation towards any direction of the celestial sphere [12]. In cases, the movement in azimuth and the elevation of the collector surface could be predetermined by a set of equations (open-loop control) or permanently recalculated from the reading of the radiation sensors (closed-loop control). Lorenzo et al., Perpiñan et al., Huld et al. and Huld et al. [13–16] present the productive increases according to the types of tracking systems for different latitudes and technologies, showing that the tracking process is more effective as the latitude is higher. The biggest increases are of the order of 57% [11]. Tracking is compulsory in those applications where solar radiation is concentrated [18].

The equations included in the references to determine the orientation of the tracking systems are exclusively based on the astronomical movement of the sun. The development of astronomical equations enables the prediction of the solar position on the celestial sphere with a precision of the order of miliradians [19–21]. According to this, Duffie and Beckman, Braun and Mitchell, Meinel and Meinel, Neville, Narvarte and Lorenzo and Riley and Hansen [22–25,27,72] present the equations for both single-axis and two-axis trackers obtained by the application of the spherical trigonometry to the solar movement. More recently, papers including Jolly, Sproul, Parkin, Chong and Wong, Rapp-Arrarás and Domingo-Santos [28–32] have opened a new line to describe the solar movement, as well as solar tracking systems, thanks to the application of vectorial algebra. The solar vector $\vec{s}$ thus is defined as the unit vector directed to the center of the solar disc. All the astronomical relations are deducted when changes of coordinated systems are made by using matricial algebra, or by applying the definitions of the dot and cross product.

The application of the astronomical model to the solar tracking is materialized thanks to the condition of minimizing the incidence angle θ that sunbeams create with the normal of the collector surface. In

terms of solar irradiance, it is a tracking system that only considers the maximization of the direct component [16]. Consequently, it is appropriate for applications that can only use this component (usually applications with concentration). This movement of tracker planes is not the most adequate for PV, where all the radiation components are usable. This effect is especially evident on those days when direct radiation does not reach the collectors and the solar disc is not visible. An astronomical tracking of the sun involves a lower energy collection at all moments of the day compared to the energy obtained in a fixed horizontal plane. Duffie and Beckman and Mousazadeh et al. [11,22]show this effect on days with a low incidence of direct radiation. Literature, however, does not include papers oriented towards the development of solar tracking equations for those days. This way, there is a need to study the effect of the diffuse and reflected components on the solar tracking in order to obtain the equations for the maximum radiation collection.

The characterization of solar radiation on tilted collector planes has been studied by numerous authors, who have proposed several semi-empirical approaches [73–80]. Klucher, Loutzenhiser et al. and Yoon et al.[75,81,82] compare the irradiance models with a series of measures recorded in different localities for the most explanatory irradiance model. Yadav and Chandel Ahmad and Tiwari, Tsalides and Thanailakis, Evseev and Kudish, Khorasanizadeh et al. Stanciu and Stanciu and Bakirci [83–89] have used these models to determine the optimal inclination of collectors in different localities. These authors consider that the optimal inclination allows to collect the maximum radiation, ignoring other factors like collector temperature, dust or Fresnel reflection losses. In this light, Baltas et al. and Martin and Ruiz [90,91] propose models to consider these effects on static collectors. These losses should be insignificant for collectors on solar trackers as they are only significant for high incidence values [90,91]. The absence of papers about the problem to obtain the optimal position of tracking collectors from the irradiance models has also been observed when analyzing the studies by authors like Drago, Cruz-Peragón et al., Chang, Huang and Sun, Li et al. and Chang [92–97] Focusing on the purpose of knowing the maximum energy available for PV installations, they integrate the incident modelled irradiance on collectors with astronomical movement. Nevertheless, they ignore the fact that all irradiance models implicitly entail the optimal position where the tracker should be located.

This paper presents a rational model to study the movement equations of solar tracking systems using vectorial algebra and differential calculus. It is aimed that this model is unified, valid for all types of solar tracking systems, including all the rational equations currently described in the literature. It is also aimed that this model includes explicitly actually usable irradiance models. The proposed methods are based on the mathematical maximization of the usable irradiance on the collector plane.

3.2. Proposal of the model.

3.2.1. Astronomical bases of solar tracking.

This paper departs from the description of the solar vector $\vec{s}$ in a local system of axes, following the represented in Figure 3.1.

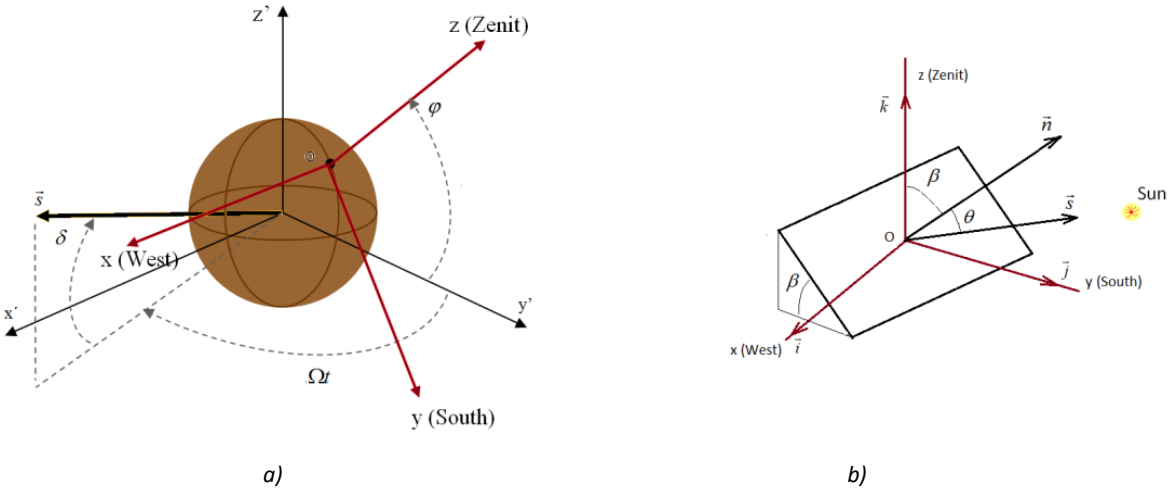

a) *b)*

Figure 3.1. Earth reference system.

Figure 3.1 (a) shows the solar vector on an equatorial reference system with the origin in the center of the Earth, the $Ox´y´$ plane coinciding with the equator plane. Therefore, the $Oz´$ axis is parallel to the Earth's rotational axis, and the $Oz\acute{y}´$ plane coincides with the plane of the local meridian [50]. In this coordinate system the hour angle, given by the product of the rotation speed $\Omega = 2\pi/24\, rad/h)$ by the time elapsed after the solar midday, and declination δ can be represented as the angle φ. Figure 3.1 shows the terrestrial reference system, where the following axes are used: Ox: direction to the West; Oy: direction to the South; and Oz: zenithal direction; in which $\vec{\imath}, \vec{\jmath}, \vec{k}$ are the respective unit vectors. The solar vector, thus, is given by Eq. (3.1) as shown in Ramírez-Faz and López-Luque [98].

$$\vec{s} = s_x\,\vec{\imath} + s_y\,\vec{\jmath} + s_z\,\vec{k} = sin\Omega t\, cos\,\delta\,\vec{\imath} + (cos\,\Omega t\, cos\,\delta\, sin\,\varphi - sin\,\delta\, cos\,\varphi)\vec{\jmath} + \\ +(cos\,\Omega t\, cos\,\delta\, cos\,\varphi + sin\,\delta\, sin\,\varphi)\vec{k} \tag{3.1}$$

Figure 3.1 (b) also represents the unit vector $\vec{n}$, orthogonal to the collector plane and representative of the spatial position of the collector. The angle between vector $\vec{n}$ and vector $\vec{s}$ is θ, while the angle between $\vec{n}$ and $\vec{k}$ is β

3.2.2. Models to calculate usable irradiance.

In general, the direct, diffuse and reflected components can be distinguished in the solar irradiance incidental on a plane. Direct irradiance is closely related to Sun-Earth geometry, as the electromagnetic rays of this component come directly from the positional direction of the Sun Studies of direct shadowing are actually geometric studies based on the astronomical movement, which enable the characterization of the effect of obstructions on the collector plane. The diffuse component is formed by all rays incoming from all directions of celestial vault, except the Earth-Sun direction. The atmospheric scattering and the reflection of the solar radiation entail greater difficulties for its characterization. Models normally consider diffuse irradiance as climatic variable obtained from measurements of multiple years [22].

As several empirical models are available to describe the diffuse irradiance, it is necessary to select the most adequate for each location. Calibration of parameters and statistical comparison between models are the main steps to choose the most adequate model [80].

We present below six models of proven validity. The first can be applied regardless of climate, as long as direct irradiance is usable. If it is an application that uses all the components, a model (like one of the five suggested here) should be validated.

The models proposed in this paper are:

a. Direct irradiance model. Eq. (3.2) describes the irradiance to be considered on the collector plane in all cases where only direct irradiance is usable. This is the case of solar concentration.

$$I = \frac{cos\,\theta}{cos\,\theta_z}\, I_B \tag{3.2}$$

b. Isotropic sky model. Described by Duffie and Beckman and Liu and Jordan [22,73], this model assumes that diffuse radiation is isotropically distributed in the sky dome. This model establishes Eq. (3.3).

$$I = \frac{cos\,\theta}{cos\,\theta_z}\, I_B + \frac{1+cos\,\beta}{2}\, I_D + \rho\frac{1-cos\,\beta}{2}\,(I_B + I_D) \tag{3.3}$$

c. Hay-Davies model [74]. This model establishes that a determined fraction I_B/I_{OH} of the diffuse irradiance is directed from the direction of the solar disc.

$$I = \frac{cos\,\theta}{cos\,\theta_z}\, I_B + \left[\left(\frac{cos\,\theta}{cos\,\theta_z}\right)\frac{I_B}{I_{OH}} + \left(1-\frac{I_B}{I_{OH}}\right)\frac{1+cos\,\beta}{2}\right] I_D + \rho\frac{1-cos\,\beta}{2}\,(I_B + I_D) \tag{3.4}$$

d. Klucher model [75]. It is known that the isotropic model (Eq. (3.3)) underestimates irradiance on tilted planes during clear days. The Klucher model aims to correct this effect.

$$I = \frac{cos\,\theta}{cos\,\theta_z}\,I_B + \frac{1+cos\,\beta}{2}\left(1 + Fsin^3\frac{\beta}{2}\right)(1 + Fcos^2\theta sin^3\theta_z)\,I_D + \rho\frac{1-cos\,\beta}{2}\;\;(I_B + I_D) \tag{3.5}$$

where

$$F = 1 - \left(\frac{I_B}{I_B + I_D}\right)^2 \tag{3.6}$$

e. Reindl model [76]. It is a non-isotropic model that establishes Eq. (3.7).

$$I = \frac{cos\,\theta}{cos\,\theta_z}\,I_B + \left[\left(\frac{cos\,\theta}{cos\,\theta_z}\right)\frac{I_B}{I_{OH}} + \left(1 - \frac{I_B}{I_{OH}}\right)\frac{1+cos\,\beta}{2}\left(1 + \sqrt{\frac{I_B}{I_B + I_D}}sin^3\frac{\beta}{2}\right)\right] I_D + \rho\frac{1-cos\,\beta}{2}\,(I_B + I_D) \tag{3.7}$$

f. Muneer model [77]. This model considers that non-isotropy of diffuse irradiance is modulated by factor b_M thanks to Eqs. (3.8) and (3.9). In fact, Eq. (3.8) coincides with Eq. (3.3) when b_M=0.

$$I = \frac{\cos\theta}{\cos\theta_z}\,I_B + \left[\left(\frac{\cos\theta}{\cos\theta_z}\right)\frac{I_B}{I_{OH}} + \left(1 - \frac{I_B}{I_{OH}}\right)\frac{I_{D\beta}}{I_D}\right] I_D + \rho\frac{1-\cos\beta}{2}\,(I_B + I_D) \tag{3.8}$$

being

$$\frac{I_{D\beta}}{I_D} = \frac{1+cos\,\beta}{2} + \frac{2b_M}{\pi(3+2b_M)}\left(sin\beta - \beta cos\beta - \pi sin^2\left(\frac{\beta}{2}\right)\right) \tag{3.9}$$

g. Pérez model [79]

$$I = \frac{cos\,\theta}{cos\,\theta_z}\,I_B + \left[(1-F_1)\frac{1+cos\,\beta}{2} + F_1\frac{a}{b} + F_2 sin\beta\right] I_D + \rho\frac{1-cos\,\beta}{2}\,(I_B + I_D) \tag{3.10}$$

For the application of Eq. (3.10), the model uses F_1 and F_2, coefficients expressing the degree of circumsolar and horizon/zenith anisotropy respectively, as well as the parameters a_P and b_P defined by the authors as expressed in Eqs. (3.11) and (3.12) [79].

$$a_P = max(cos\,\theta\,;0) \tag{3.11}$$

$$b_P = max(cos\,85º; cos\theta_z) \tag{3.12}$$

For the right choice of solar tracking equations, it is necessary to know the function of usable irradiance I. It is considered in this study that I can be given by any of the Eqs. (3.2), (3.3), (3.4), (3.5), (3.7), (3.8) or (3.10). Given that, this paper follows a vectorial approach, the following parameters will be considered:

$$cos\beta = \vec{k} \cdot \vec{n} \tag{3.13}$$

$$cos\theta = \vec{s} \cdot \vec{n} \tag{3.14}$$

$$cos\theta_z = \vec{s} \cdot \vec{k} \tag{3.15}$$

Eqs. (3.2), (3.3), (3.5), (3.7), (3.8), (3.9) and (3.10) can be expressed according to the unit vectors, being respectively Eqs. (3.16), (3.17), (3.18), (3.19), (3.20), (3.21) or (3.22). It must be highlighted the vectorial dependence of $\vec{s} \cdot \vec{n}$ and $\vec{k} \cdot \vec{n}$ for these equations with respect to the orientation of the collector plane.

$$I = \frac{\vec{s} \cdot \vec{n}}{\vec{s} \cdot \vec{k}} I_B \tag{3.16}$$

$$I = \frac{\vec{s} \cdot \vec{n}}{\vec{s} \cdot \vec{k}} I_B + \frac{1 + \vec{k} \cdot \vec{n}}{2} I_D + \rho \frac{1 - \vec{k} \cdot \vec{n}}{2} (I_B + I_D) \tag{3.17}$$

$$I = \frac{\vec{s} \cdot \vec{n}}{\vec{s} \cdot \vec{k}} I_B + \left[\frac{\vec{s} \cdot \vec{n}}{\vec{s} \cdot \vec{k}} \frac{I_B}{I_{OH}} + \left(1 - \frac{I_B}{I_{OH}}\right) \frac{1 + \vec{k} \cdot \vec{n}}{2} \right] I_D + \rho \frac{1 - \vec{k} \cdot \vec{n}}{2} (I_B + I_D) \tag{3.18}$$

$$I = \frac{\vec{s} \cdot \vec{n}}{\vec{s} \cdot \vec{k}} I_B + \frac{1 + \vec{k} \cdot \vec{n}}{2} \left(1 + F \left(\frac{1 - \vec{k} \cdot \vec{n}}{2} \right)^{3/2} \right) \left(1 + F (\vec{s} \cdot \vec{n})^2 \left[1 - \left(\vec{s} \cdot \vec{k} \right)^2 \right]^{3/2} \right) I_D + \rho \frac{1 - \vec{k} \cdot \vec{n}}{2} (I_B + I_D) \tag{3.19}$$

$$I = \frac{\vec{s} \cdot \vec{n}}{\vec{s} \cdot \vec{k}} I_B + \left[\frac{\vec{s} \cdot \vec{n}}{\vec{s} \cdot \vec{k}} \frac{I_B}{I_{OH}} + \left(1 - \frac{I_B}{I_{OH}}\right) \frac{1 + \vec{k} \cdot \vec{n}}{2} \left(1 + \sqrt{\frac{I_B}{I_B + I_D}} \left(\frac{1 - \vec{k} \cdot \vec{n}}{2} \right)^{3/2} \right) \right] I_D + \rho \frac{1 - \vec{k} \cdot \vec{n}}{2} (I_B + I_D) \tag{3.20}$$

$$I = \frac{\vec{s} \cdot \vec{n}}{\vec{s} \cdot \vec{k}} I_B + \left[\frac{\vec{s} \cdot \vec{n}}{\vec{s} \cdot \vec{k}} \frac{I_B}{I_{OH}} + \left(1 - \frac{I_B}{I_{OH}}\right) \frac{I_{D\beta}}{I_D} \right] I_D + \rho \frac{1 - \vec{k} \cdot \vec{n}}{2} (I_B + I_D) \tag{3.21}$$

$$\frac{I_{D\beta}}{I_D} = \left(\frac{1 + \vec{k} \cdot \vec{n}}{2} \right) + \frac{2 b_M}{\pi (3 + 2 b_M)} \left(\sqrt{1 - \left(\vec{k} \cdot \vec{n} \right)^2} - \left(\vec{k} \cdot \vec{n} \right) arc\ cos\left(\vec{k} \cdot \vec{n} \right) - \pi \left(\frac{1 - \vec{k} \cdot \vec{n}}{2} \right) \right) \tag{3.22}$$

$$I = \frac{\vec{s} \cdot \vec{n}}{\vec{s} \cdot \vec{k}} I_B + \left[(1 - F_1) \frac{1 + \vec{k} \cdot \vec{n}}{2} + F_1 \frac{\vec{s} \cdot \vec{n}}{b_P} + F_2 \sqrt{1 - \left(\vec{k} \cdot \vec{n} \right)^2} \right] I_D + \rho \frac{1 - \vec{k} \cdot \vec{n}}{2} (I_B + I_D) \tag{3.23}$$

3.2.3. Mathematical approach to single-axis trackers.

This paper uses the unit vector $\vec{e}$ to describe the generic movement of any single-axis tracking system. This is a fixed unit vector included in the rotation axis of the collector plane. Given that the collector surface – and thus $\vec{n}$ – can only rotate about $\vec{e}$, Eq. (3.24) must always be satisfied:

$$\vec{e} \cdot \vec{n} = cos\chi \tag{3.24}$$

Being χ the constant angle formed by $\vec{e}$ and $\vec{n}$.

Table 3.1 shows the characteristic values of χ for the main single-axis trackers described in the literature.

Table 3.1. Values of χ for the main single-axis trackers.

Type	$\vec{e}$	χ
Vertical axis	$0\vec{\imath} + 0\vec{\jmath}+1\vec{k}$	β
E-W horizontal axis	$1\vec{\imath} + 0\vec{\jmath}+0\vec{k}$	$\pi/2$
N-S horizontal axis	$0\vec{\imath} + 1\vec{\jmath}+0\vec{k}$	$\pi/2$
N-S inclined axis	$0\vec{\imath} - sin\tau\vec{\jmath}+cos\tau\vec{k}$	$\pi/2$
Polar	$0\vec{\imath} - sin\varphi\vec{\jmath}+cos\varphi\vec{k}$	$\pi/2$

This paper proposes the use of a cylindrical chart for the solar position in order to show graphically the possibilities of movement of single-axis trackers. In this chart, the line to describe the celestial sphere, to the point in which $\vec{n}$ is oriented is overlapped. Figure 3.2, then, shows the family of curves of the pointing points of the tracking systems from Table 3.1 in the cylindrical chart.

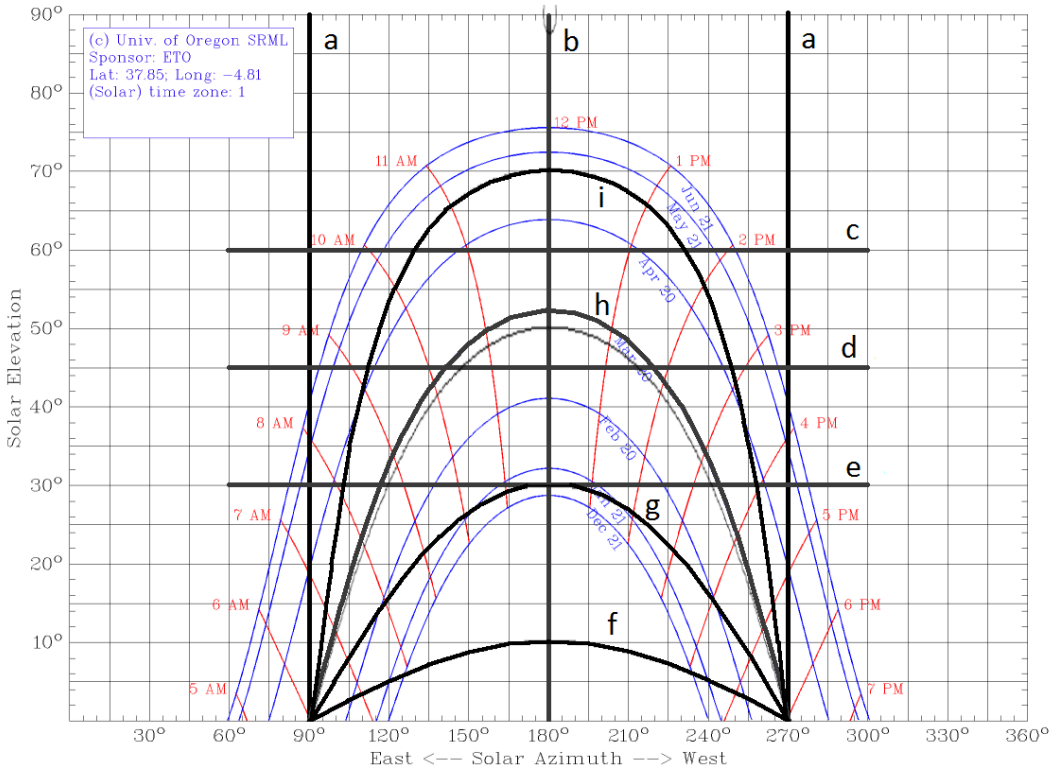

Figure 3.2. Cylindrical chart for Córdoba, Spain, (φ=37,85º N) with the pointing paths of the main single-axis. a) N-S horizontal axis. b) E-W horizontal axis. c) β=30º Vertical axis. d) β=45º Vertical axis. e) β=60º Vertical axis. f) N-S inclined axis τ = 10º. g) N-S inclined axis τ = 30º. h) N-S polar axis. i) N-S inclined axis τ = 70º (the figure was adapted from the software at the University of Oregon Solar Radiation Monitoring Laboratory (http://solardat.uoregon.edu/SunChartProgram.php).

This paper considers movement equations that allow the maximization of irradiance on the collector plane. Mathematically, this equates to find the vector $\vec{n}$ to maximize function shown in Eq. (3.25) according to the conditions given by Eqs. (3.24), (3.26) and (3.27).

$$I = I\left(\vec{s}\cdot\vec{n}, \vec{k}\cdot\vec{n}\right) \tag{3.24}$$

$$\vec{n}\cdot\vec{n} = 1 \tag{3.25}$$

$$\vec{e}\cdot\vec{n} = cos\chi \tag{3.26}$$

$$\vec{e}\cdot\vec{e} = 1 \tag{3.27}$$

For this purpose, the method of Lagrange multipliers is used, as it conducts to the maximum or minimum of a multivariable function when there are some constraints between the input values [99]. As a consequence, it is proposed function Φ with independent variables $\vec{n}, \lambda, \mu$ and ν, where the new variables or Lagrange multipliers λ, μ and ν are methodically introduced.

$$\Phi(\vec{n}, \lambda, \mu, \nu) = I\left(\vec{s}\cdot\vec{n}, \vec{k}\cdot\vec{n}\right) + \lambda(1 - \vec{n}\cdot\vec{n}) + \mu(cos\chi - \vec{e}\cdot\vec{n}) + \nu(1 - \vec{e}\cdot\vec{e}) \tag{3.28}$$

The differentiation with respect to $\vec{n}$ arises:

$$d\Phi = \left[\frac{\partial I}{\partial(\vec{s}\cdot\vec{n})}\vec{s} + \frac{\partial I}{\partial(\vec{k}\cdot\vec{n})}\vec{k} - 2\lambda\vec{n} - \mu\vec{e}\right]d\vec{n} + [1-\vec{n}\cdot\vec{n}]d\lambda + [cos\chi - \vec{e}\cdot\vec{n}]d\mu + [1-\vec{e}\cdot\vec{e}]dv \quad (3.29)$$

Following Lagrange methods implies equating to zero the brackets in Eq. (3.29), obtaining Eqs. (3.30), (3.26), (3.24) and (3.27). The resolution of these gives the values of $\vec{n}$.

$$\frac{\partial I}{\partial(\vec{s}\cdot\vec{n})}\vec{s} + \frac{\partial I}{\partial(\vec{k}\cdot\vec{n})}\vec{k} - 2\lambda\vec{n} - \mu\vec{e} = 0 \quad (3.30)$$

In the resolution of the equation systems is used the auxiliary vector $\vec{u}$, defined by

$$\vec{u} = \frac{\partial I}{\partial(\vec{s}\cdot\vec{n})}\vec{s} + \frac{\partial I}{\partial(\vec{k}\cdot\vec{n})}\vec{k} \quad (3.31)$$

Eq. (3.30) establishes that $\vec{u}, \vec{e}, \vec{n}$ are coplanar, so it represents that there is a linear combination of these, which is equal to zero. If a unit vector $\vec{p}$ is defined – also coplanar with $\vec{u}, \vec{e}$, and perpendicular to $\vec{e}$– the Eq. (3.32) can be found for $\vec{p}$.

$$\vec{p} = \frac{\vec{u} - (\vec{u}\cdot\vec{e})\vec{e}}{|\vec{u} - (\vec{u}\cdot\vec{e})\vec{e}|} = \frac{\vec{u} - (\vec{u}\cdot\vec{e})\vec{e}}{\sqrt{u^2 - (\vec{u}\cdot\vec{e})^2}} \quad (3.32)$$

Figure 3.3 shows a scheme of the coplanar vector $\vec{e}, \vec{u}, \vec{p}$ and $\vec{n}$. This figure shows that $\vec{e}$ and $\vec{p}$ are unit and perpendicular vectors. Consequently, they create an orthogonal basis on which $\vec{n}$ can be expressed from the angle formed with one of them.

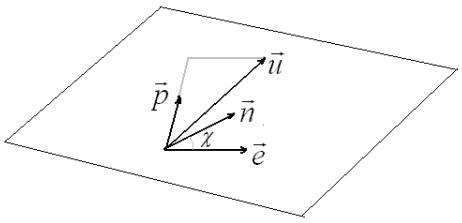

Figure 3.3. Graphic representation of coplanar vectors $\vec{e}, \vec{u}, \vec{p}$ and $\vec{n}$

This way, the expression of $\vec{n}$ solving the system given by Eqs. (3.39), (3.26), (3.24) and (3.27) can be found in Eq. (3.33).

$$\vec{n} = cos\chi\vec{e} + sin\chi\vec{p} \quad (3.33)$$

This equation can be expressed in terms of $\vec{u}$.

$$\vec{n} = cos\chi\vec{e} + sin\chi\frac{\vec{u} - (\vec{u}\cdot\vec{e})\vec{e}}{\sqrt{u^2 - (\vec{u}\cdot\vec{e})^2}} = \left(cos\chi - \frac{(\vec{u}\cdot\vec{e})sin\chi}{\sqrt{u^2 - (\vec{u}\cdot\vec{e})^2}}\right)\vec{e} + \left(\frac{sin\chi}{\sqrt{u^2 - (\vec{u}\cdot\vec{e})^2}}\right)\vec{u} \tag{3.34}$$

$$\begin{aligned}\vec{n} = &\left(cos\,\chi - \frac{\left(\frac{\partial I}{\partial(\vec{s}\cdot\vec{n})}\vec{s}\cdot\vec{e} + \frac{\partial I}{\partial(\vec{k}\cdot\vec{n})}\vec{k}\cdot\vec{e}\right)sin\,\chi}{\sqrt{\left(\frac{\partial I}{\partial(\vec{s}\cdot\vec{n})}\right)^2 + \left(\frac{\partial I}{\partial(\vec{k}\cdot\vec{n})}\right)^2 + 2\left(\frac{\partial I}{\partial(\vec{s}\cdot\vec{n})}\right)\left(\frac{\partial I}{\partial(\vec{k}\cdot\vec{n})}\right)\vec{s}\cdot\vec{k} - \left(\frac{\partial I}{\partial(\vec{s}\cdot\vec{n})}\vec{s}\cdot\vec{e} + \frac{\partial I}{\partial(\vec{k}\cdot\vec{n})}\vec{k}\cdot\vec{e}\right)^2}}\right)\vec{e} \\ &+ \left(\frac{sin\,\chi\,\frac{\partial I}{\partial(\vec{s}\cdot\vec{n})}}{\sqrt{\left(\frac{\partial I}{\partial(\vec{s}\cdot\vec{n})}\right)^2 + \left(\frac{\partial I}{\partial(\vec{k}\cdot\vec{n})}\right)^2 + 2\left(\frac{\partial I}{\partial(\vec{s}\cdot\vec{n})}\right)\left(\frac{\partial I}{\partial(\vec{k}\cdot\vec{n})}\right)\vec{s}\cdot\vec{k} - \left(\frac{\partial I}{\partial(\vec{s}\cdot\vec{n})}\vec{s}\cdot\vec{e} + \frac{\partial I}{\partial(\vec{k}\cdot\vec{n})}\vec{k}\cdot\vec{e}\right)^2}}\right)\vec{s} \\ &+ \left(\frac{sin\,\chi\,\frac{\partial I}{\partial(\vec{k}\cdot\vec{n})}}{\sqrt{\left(\frac{\partial I}{\partial(\vec{s}\cdot\vec{n})}\right)^2 + \left(\frac{\partial I}{\partial(\vec{k}\cdot\vec{n})}\right)^2 + 2\left(\frac{\partial I}{\partial(\vec{s}\cdot\vec{n})}\right)\left(\frac{\partial I}{\partial(\vec{k}\cdot\vec{n})}\right)\vec{s}\cdot\vec{k} - \left(\frac{\partial I}{\partial(\vec{s}\cdot\vec{n})}\vec{s}\cdot\vec{e} + \frac{\partial I}{\partial(\vec{k}\cdot\vec{n})}\vec{k}\cdot\vec{e}\right)^2}}\right)\vec{k}\end{aligned} \tag{3.35}$$

This paper suggests Eq. (3.35) as a unified expression for all the cases of single-axis trackers.

Example 1. N-S horizontal single-axis tracker with concentration. This is the case of multiple installations of parabolic-cylinder concentration tracking systems. Considering that the only usable component of the irradiance is the direct irradiance, Eq. (3.16) is considered for its determination, which implies Eqs. (3.36) and (3.37).

$$\frac{\partial I}{\partial(\vec{s}\cdot\vec{n})} = I_{DN} \tag{3.36}$$

$$\frac{\partial I}{\partial(\vec{k}\cdot\vec{n})} = 0 \tag{3.37}$$

Considering the values of $\vec{e}$ and χ in Table 3.1, applying Eq. (3.35) we obtain Eq. (3.38).

$$\vec{n} = \left(-\frac{I_{DN}s_y}{\sqrt{I_{DN}^2 - (I_{DN}s_y)^2}}\right)\vec{j} + \left(\frac{I_{DN}}{\sqrt{I_{DN}^2 - (I_{DN}s_y)^2}}\right)\vec{s} + \left(\frac{0}{\sqrt{I_{DN}^2 - (I_{DN}s_y)^2}}\right)\vec{k} \tag{3.38}$$

Simplifying, Eq. (3.39) is obtained.

It is easy to see, when substituting in Eq. (3.39) the values given in Eq. (3.1), the coincidence with the equations previously published for this case.

$$\vec{n} = \left(-\frac{s_y}{\sqrt{1-s_y^2}}\right)\vec{j} + \left(\frac{1}{\sqrt{1-s_y^2}}\right)\vec{s} = \left(\frac{s_x}{\sqrt{1-s_y^2}}\right)\vec{\imath} + \left(\frac{s_x}{\sqrt{1-s_y^2}}\right)\vec{k} \tag{3.39}$$

Example 2. Obtaining the optimal position vector for the collector plane located on a polar tracker with $\chi = 90º$, and considering the irradiance model given by Eq. (3.17) as the most appropriate. Considering that these collectors are proposed for photovoltaic collectors, which use the three components of irradiance, as well as the irradiance model proposed in Eq. (3.17) to be adequate, we obtain:

$$\frac{\partial I}{\partial(\vec{s}\cdot\vec{n}\,)} = I_{DN} \tag{3.40}$$

$$\frac{\partial I}{\partial(\vec{k}\cdot\vec{n}\,)} = \frac{I_D}{2} - \frac{\rho I_G}{2} \tag{3.41}$$

Given that Eq. (3.35) is applied where $\vec{k}\cdot\vec{e}$ and $\vec{s}\cdot\vec{e}$ intervene, we get the following values for Eqs. (3.42) and (3.43)

$$\vec{k}\cdot\vec{e} = cos\,\varphi \tag{3.42}$$

$$\begin{aligned}\vec{s}\cdot\vec{e} = {} & (cos\,\Omega t\,cos\,\delta\,sin\,\varphi - sin\,\delta\,cos\,\varphi)(-cos\,\varphi) + (cos\,\Omega t\,cos\,\delta\,cos\,\varphi - sin\,\delta\,sin\,\varphi) \\ & = sin\,\delta\end{aligned} \tag{3.43}$$

Applying Eq. (3.35), we obtain Eq. (3.44):

$$\begin{aligned}\vec{n} = {} & \left(\frac{-I_{DN}sin\delta + \left(\frac{I_D}{2} - \frac{\rho I_G}{2}\right)cos\varphi}{\sqrt{I_{DN}^2 cos^2\delta + \left(\frac{I_D}{2} - \frac{\rho I_G}{2}\right)^2 sin^2\varphi + 2I_{DN}\left(\frac{I_D}{2} - \frac{\rho I_G}{2}\right)(s_z - sin\delta\,cos\varphi)}}\right)\vec{e} \\ & + \left(\frac{I_{DN}}{\sqrt{I_{DN}^2 cos^2\delta + \left(\frac{I_D}{2} - \frac{\rho I_G}{2}\right)^2 sin^2\varphi + 2I_{DN}\left(\frac{I_D}{2} - \frac{\rho I_G}{2}\right)(s_z - sin\delta\,cos\varphi)}}\right)\vec{s} \\ & + \left(\frac{\left(\frac{I_d}{2} - \frac{\rho I_G}{2}\right)}{\sqrt{I_{DN}^2 cos^2\delta + \left(\frac{I_D}{2} - \frac{\rho I_G}{2}\right)^2 sin^2\varphi + 2I_{DN}\left(\frac{I_D}{2} - \frac{\rho I_G}{2}\right)(s_z - sin\delta\,cos\varphi)}}\right)\vec{k}\end{aligned} \tag{3.44}$$

Simplifying Eq. (3.44), we get Eqs. (3.45) and (3.46)

$$\vec{n} = \left(\frac{-I_{DN} sin\delta + \left(\frac{I_D}{2} - \frac{\rho I_G}{2}\right) cos\varphi}{\sqrt{I_{DN}^2 cos^2\delta + \left(\frac{I_D}{2} - \frac{\rho I_G}{2}\right)^2 sin^2\varphi + 2I_{DN}\left(\frac{I_D}{2} - \frac{\rho I_G}{2}\right)(s_z - sin\delta\, cos\varphi)}} \right) \left(0\,\vec{\imath} - sin\varphi\,\vec{\jmath} + cos\varphi\,\vec{k}\right)$$

$$+ \left(\frac{I_{DN}}{\sqrt{I_{DN}^2 cos^2\delta + \left(\frac{I_D}{2} - \frac{\rho I_G}{2}\right)^2 sin^2\varphi + 2I_{DN}\left(\frac{I_D}{2} - \frac{\rho I_G}{2}\right)(s_z - sin\delta\, cos\varphi)}} \right) \left(s_x\,\vec{\imath} + s_y\,\vec{\jmath} + s_z\,\vec{k}\right) \quad (3.45)$$

$$+ \left(\frac{\left(\frac{I_D}{2} - \frac{\rho I_G}{2}\right)}{\sqrt{I_{DN}^2 cos^2\delta + \left(\frac{I_D}{2} - \frac{\rho I_G}{2}\right)^2 sin^2\varphi + 2I_{DN}\left(\frac{I_D}{2} - \frac{\rho I_G}{2}\right)(s_z - sin\delta\, cos\varphi)}} \right) \vec{k}$$

$$\vec{n} = \left(\frac{I_{DN} s_x}{\sqrt{I_{DN}^2 cos^2\delta + \left(\frac{I_D}{2} - \frac{\rho I_G}{2}\right)^2 sin^2\varphi + 2I_{DN}\left(\frac{I_D}{2} - \frac{\rho I_G}{2}\right)(s_z - sin\delta\, cos\varphi)}} \right) \vec{\imath}$$

$$+ \left(\frac{I_{DN}\left(s_y + sin\delta\, sin\varphi\right) + \left(\frac{I_D}{2} - \frac{\rho I_G}{2}\right) cos\varphi\, sin\varphi}{\sqrt{I_{DN}^2 cos^2\delta + \left(\frac{I_D}{2} - \frac{\rho I_G}{2}\right)^2 sin^2\varphi + 2I_{DN}\left(\frac{I_D}{2} - \frac{\rho I_G}{2}\right)(s_z - sin\delta\, cos\varphi)}} \right) \vec{\jmath} \quad (3.46)$$

$$+ \left(\frac{I_{DN}\left(s_y + sin\delta\, sin\varphi\right) + \left(\frac{I_D}{2} - \frac{\rho I_G}{2}\right) cos\varphi\, sin\varphi}{\sqrt{I_{DN}^2 cos^2\delta + \left(\frac{I_D}{2} - \frac{\rho I_G}{2}\right)^2 sin^2\varphi + 2I_{DN}\left(\frac{I_D}{2} - \frac{\rho I_G}{2}\right)(s_z - sin\delta\, cos\varphi)}} \right) \vec{\jmath}$$

3.2.4. Two-axis tracking.

The function to maximize in two-axis tracking is the expressed in Eq. (3.25), with the single restriction imposed by Eq. (3.26). The Lagrange function is given by the Eq. (3.47).

$$\Phi(\vec{n}, \lambda) = I\left(\vec{s}\cdot\vec{n}, \vec{k}\cdot\vec{n}\right) + \lambda(1 - \vec{n}\cdot\vec{n}) \quad (3.47)$$

The differentiation respect to $\vec{n}$ and λ gives:

$$d\Phi = \left[\frac{\partial I}{\partial(\vec{s}\cdot\vec{n})}\vec{s} + \frac{\partial I}{\partial(\vec{k}\cdot\vec{n})}\vec{k} - 2\lambda\vec{n}\right] d\vec{n} + [1 - \vec{n}\cdot\vec{n}]d\lambda \quad (3.48)$$

Equating to zero the brackets in Eq. (3.48), Eqs. (3.49) and (3.26) are obtained, whose resolution gives the value of $\vec{n}$ expressed in Eq. (3.50).

$$\frac{\partial I}{\partial(\vec{s}\cdot\vec{n})}\vec{s}+\frac{\partial I}{\partial(\vec{k}\cdot\vec{n})}\vec{k}-2\lambda\vec{n}=0 \tag{3.49}$$

$$\vec{n}=\frac{\frac{\partial I}{\partial(\vec{s}\cdot\vec{n})}\vec{s}+\frac{\partial I}{\partial(\vec{k}\cdot\vec{n})}\vec{k}}{\sqrt{\left(\frac{\partial I}{\partial(\vec{k}\cdot\vec{n})}\right)^2+\left(\frac{\partial I}{\partial(\vec{k}\cdot\vec{n})}\right)^2+2\left(\frac{\partial I}{\partial(\vec{s}\cdot\vec{n})}\right)\left(\frac{\partial I}{\partial(\vec{k}\cdot\vec{n})}\right)\vec{s}\cdot\vec{k}}} \tag{3.50}$$

Example 3. Two-axis tracker with concentration. This is the case of parabolic discs. Considering that the only usable component of the irradiance is the direct irradiance, Eq. (3.16) is considered, thus:

$$\frac{\partial I}{\partial(\vec{s}\cdot\vec{n}\,)}=I_{DN} \tag{3.36}$$

$$\frac{\partial I}{\partial(\vec{k}\cdot\vec{n}\,)}=0 \tag{3.37}$$

It is easy to observe here that Eq. (3.50) leads to Eq. (3.51).

$$\vec{n}=\vec{s} \tag{3.51}$$

Example 4. Two-axis tracker for PV modules that use the three components of irradiance. Considering the irradiance model suggested in Eq. (3.17) to be adequate, Eqs. (3.40) and (3.41) are obtained.

$$\frac{\partial I}{\partial(\vec{s}\cdot\vec{n}\,)}=I_{DN} \tag{3.40}$$

$$\frac{\partial I}{\partial(\vec{k}\cdot\vec{n}\,)}=\frac{I_D}{2}-\frac{\rho I_G}{2} \tag{3.41}$$

Applying Eq. (3.50), we get Eq. (3.52)

$$\vec{n}=\frac{I_{DN}\vec{s}+\left(\frac{I_D}{2}-\frac{\rho I_G}{2}\right)\vec{k}}{\sqrt{I_{DN}^2+\left(\frac{I_D}{2}-\frac{\rho I_G}{2}\right)^2+I_{DN}(I_D-\rho I_G)s_z}} \tag{3.52}$$

In Eq. (3.52), it can be observed that always that $\left(\frac{I_D}{2}-\frac{\rho I_G}{2}\right)$ is positive, the normal vector in this tracking mode would have a higher elevation than in the case of astronomical tracking.

A cylindrical chart is normally used to represent the solar position and path on the celestial vault. Nevertheless, it can also be used to represent other movements or trajectories [98]. In this paper, the cylindrical chart is used to represent the movement of any planar collector over a solar tracker by representing on the chart the set of directions pointed by vector $\vec{n}$. The daily movement of the tracker hence corresponds to a trajectory over the chart.

Figure 3.4 shows, on a cylindrical chart, the recommended tracking paths for the representative values of winter and spring according to the hypothesis of isotropic sky given by Eq. (3.52). When comparing these paths to the solar paths (typical from the astronomical tracking), it can be observed how Eq. (3.52) recommends a higher elevation of $\vec{n}$ with respect to $\vec{s}$ for all cases. The model proposed here shows a quite different behavior from the astronomical one during the sunrise and the sunset on those days with low radiation levels, as it recommends completely horizontal positions for a better collection of diffuse radiation.

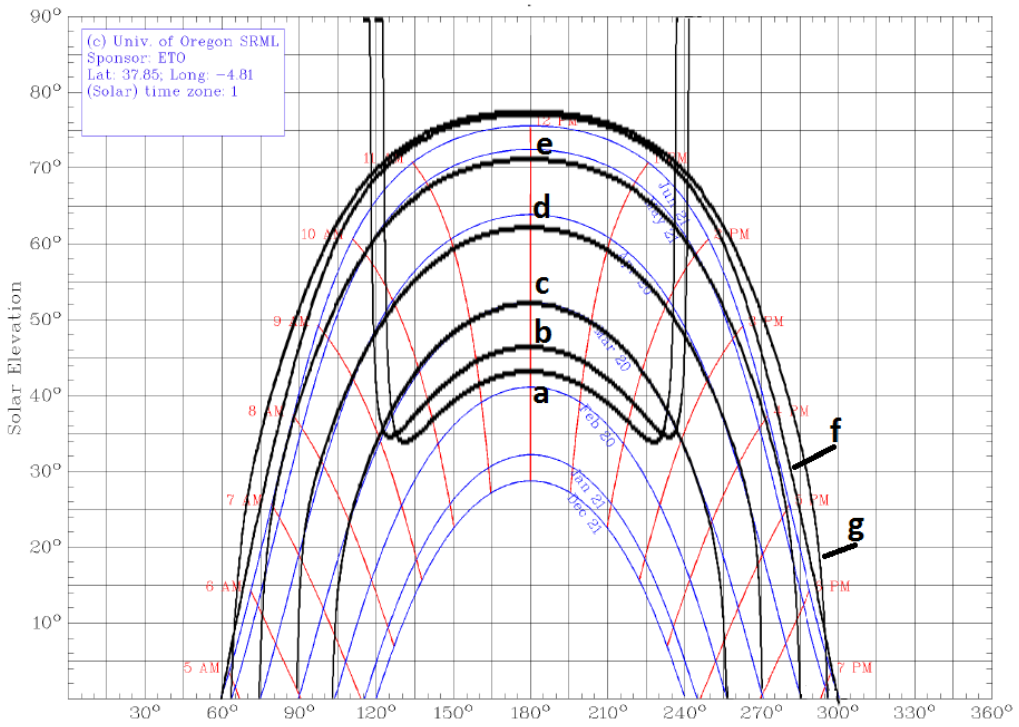

Figure 3.4. Cylindrical chart for Córdoba, Spain (φ =37,85ºN) with the pointing paths of the two-axis tracker under the hypothesis of isotropic sky for the days in half of the months: a) December; b) January; c) February; d) March; e) April; f) May; g) June.

3.3. Results.

Eqs. (3.35) and (3.50) are themselves results of this paper. It is convenient, however, to calculate energy collection in the collector plane of a tracker when irradiance follows any of the functions given by Eqs. (3.16), (3.17), (3.18), (3.19), (3.20), (3.21) and (3.23), and the tracking vector is the optimal vector generated by Eqs. (3.35) or (3.50). Furthermore, it is also useful to compare this collection to the values calculated for an astronomical tracking system.

These comparisons have been developed for a wide set of European locations with latitude greater than 40° N. The models show similar behavior in all cases. Therefore, the case of Paris, France, (*φ =48,73ºN*) has been selected to be shown as representative.

Table 3.2 shows the considered daily horizontal radiation for representative days in each month. Table 3.3 is obtained for a horizontal N-S single-axis tracking system comparing tracking criteria and irradiance models.

Table 3.2. Global radiation values per month measured in Paris, France.

Month	H (MJ/m2day)
Jan	2.73
Feb	5.17
Mar	8.80
Apr	13.57
May	17.04
Jun	19.63
Jul	17.64
Aug	16.18
Sep	11.36
Oct	6.41
Nov	3.03
Dec	2.01

Table 3.3 shows a systematic improvement in the collection when the position of the collector is determined by Eq. (3.35). In the months with a higher proportion of diffuse irradiance, increases over 10% are observed; moreover, an increase of about 1% is obtained in those months of high radiation.

Table 3.3. Results of the simulation of solar radiation with a horizontal N-S single-axis tracking system and different tracking criteria and irradiance model

Month	Isotropic sky			Hay-Davies Model			Klucher Model			Reindl Model			Muneer Model			Perez Model		
	(a)	(b)	(c)	(d)	(e)	(f)	(g)	(h)	(i)	(j)	(k)	(l)	(m)	(n)	(o)	(p)	(q)	(r)
	H(MJ/m²day)	H(MJ/m²day)	%	H(MJ/m²day)	H(MJ/m²day)	%	H(MJ/m²day)	(MJ/m²day)	%	H(MJ/m²day)	H(MJ/m²day)	%	H(MJ/m²day)	H(MJ/m²day)	%	H(MJ/m²day)	H(MJ/m²day)	%
Jan	2.44	2.70	10.7	2.46	2.72	10.2	2.52	2.76	9.4	2.49	2.72	8.9	2.35	2.70	15.1	2.49	2.70	8.4
Feb	4.79	5.18	8.3	4.84	5.22	7.8	5.06	5.41	6.8	4.90	5.23	6.6	4.65	5.19	11.6	4.97	5.22	5.0
Mar	8.43	8.93	5.9	8.57	9.02	5.3	9.16	9.56	4.4	8.68	9.04	4.2	8.28	8.94	8.1	8.78	9.05	3.0
Apr	13.70	14.14	3.2	13.98	14.35	2.7	15.09	15.43	2.2	14.17	14.42	1.8	13.60	14.19	4.3	14.17	14.43	1.8
May	17.76	18.16	2.2	18.15	18.47	1.7	19.49	19.78	1.5	18.39	18.58	1.0	17.72	18.24	2.9	18.26	18.52	1.4
Jun	21.32	21.62	1.4	21.86	22.08	1.0	23.38	23.59	0.9	22.14	22.25	0.5	21.42	21.79	1.7	21.79	22.01	1.0
Jul	18.36	18.78	2.3	18.76	19.09	1.8	20.06	20.36	1.5	19.00	19.19	1.0	18.31	18.86	3.0	18.85	19.11	1.4
Aug	17.31	17.61	1.7	17.75	17.97	1.2	19.20	19.42	1.1	17.99	18.11	0.6	17.36	17.73	2.1	17.77	17.98	1.2
Sep	11.47	11.85	3.3	11.71	12.04	2.8	12.68	12.97	2.3	11.88	12.10	1.8	11.39	11.89	4.4	11.89	12.12	1.9
Oct	6.00	6.45	7.5	6.08	6.50	6.9	6.42	6.80	5.9	6.16	6.51	5.7	5.85	6.46	10.4	6.24	6.50	4.2
Nov	2.70	3.01	11.5	2.72	3.02	11.1	2.79	3.08	10.3	2.75	3.02	10.0	2.59	3.01	16.3	2.74	3.00	9.4
Dec	1.76	1.98	12.4	1.77	1.98	12.0	1.80	2.00	11.3	1.79	1.98	10.9	1.68	1.98	17.6	1.76	1.97	12.0
Year	10.53	10.89	3.5	10.75	11.07	2.9	11.50	11.79	2.5	10.89	11.12	2.1	10.46	10.94	4.6	10.84	11.08	2.2

(a) Radiation on a surface on a N-S single-axis tracking system with movement based on the solar position with irradiance described by Eq. (17).
(b) Radiation on a surface on a N-S single-axis tracking system with movement based on Eq. (34) with irradiance described by Eq. (17).
(c) Percentage increase of (b) with respect to (a).
(d) Radiation on a surface on a N-S single-axis tracking system with movement based on the solar position with irradiance described by Eq. (18).
(e) Radiation on a surface on a N-S single-axis tracking system with movement based on Eq. (34) with irradiance described by Eq. (18).
(f) Percentage increase of (e) with respect to (d).
(g) Radiation on a surface on a N-S single-axis tracking system with movement based on the solar position with irradiance described by Eq. (19).
(h) Radiation on a surface on a N-S single-axis tracking system with movement based on Eq. (34) with irradiance described by Eq. (19).
(i) Percentage increase of (h) with respect to (g).
(j) Radiation on a surface on a N-S single-axis tracking system with movement based on the solar position with irradiance described by Eq. (20).
(k) Radiation on a surface on a N-S single-axis tracking system with movement based on Eq. (34) with irradiance described by Eq. (20).
(l) Percentage increase of (k) with respect to (j).
(m) Radiation on a surface on a N-S single-axis tracking system with movement based on the solar position with irradiance described by Eq. (22).
(n) Radiation on a surface on a N-S single-axis tracking system with movement based on Eq. (34) with irradiance described by Eq. (22).
(o) Percentage increase of (n) with respect to (m).
(p) Radiation on a surface on a N-S single-axis tracking system with movement based on the solar position with irradiance described by Eq. (23).
(q) Radiation on a surface on a N-S single-axis tracking system with movement based on Eq. (34) with irradiance described by Eq. (23).
(r) Percentage increase of (q) with respect to (p).

3.4. Conclusions.

This paper shows the deduction of general equations that optimize the energy radiation of collectors installed on single-axis Eq. (3.35) and two-axis Eq. (3.50) tracking systems. The equations proposed are generic for any continuous tracking system, and the symmetry in the positions of the tracker with respect to the meridian plane are not required. Astronomical tracking, proposed by numerous authors as the optimal tracking system, should be checked for each case (type of usability and validated model that satisfactorily explains irradiance). Consequently, it should not be considered a priori as the most adequate system in all cases. In fact, the cases studied here enable us to observe how the astronomical movement may provide energy collections inferior to the data determined when the values of $\vec{n}$ given by Eqs. (3.35) or (3.50) are used.

The equations proposed here include the astronomical tracking model if the value given by Eq. (3.16) is considered as usable irradiance. Other models that consider the diffuse component of the irradiance make that vector $\vec{n}$ includes a component in direction $\vec{k}$ with respect to the astronomical model. This means that these models predict that the collector plane should be more horizontal than the astronomical model.

In the simplest models of irradiance Eqs. (3.16), (3.17) and (3.18), the partial derivatives with respect to $\vec{s} \cdot \vec{n}$ and $\vec{n} \cdot \vec{k}$ give constant values. In these cases, Eqs. (3.35) and (3.50) directly provide the value of $\vec{n}$ for the optimal collection situation. However, when the partial derivatives depend on $\vec{n}$, Eqs. (3.35) and (3.50) become solvable equations where the components of $\vec{n}$ can be solved. It is recommended for these cases the numerical method of iteration. The authors have been able to check experimentally that replacing the values of an approach $\vec{n}^{\,(i)}$ of $\vec{n}$ in the second member of Eqs. (3.35) and (3.50), the member of the right $\vec{n}^{\,(i+1)}$ is obtained, being $\vec{n}^{\,(i+1)}$ a better approach than $\vec{n}^{\,(i)}$. It is advisable to start the iterations from $\vec{n}^{\,(i)} = \vec{s}$. In all the cases, the convergence allows to finish the process with less than twenty iterations.

Capítulo 4 . A novel backtracking approach for two-axis solar PV tracking plant

A NOVEL BACKTRACKING APPROACH FOR TWO-AXIS SOLAR PV TRACKING PLANTS

Renewable Energy, Volume 145, January 2020, Pages 1214-1221

L.M. Fernández-Ahumada[1], J. Ramírez-Faz[2], R. López-Luque[3], M. Varo-Martínez[3,*], I.M. Moreno-García[4], F. Casares de la Torre[2]

[1] Computing and Numeric Analysis. University of Cordoba. Campus of Rabanales, 14071 Cordoba, Spain.

[2] Electrical Engineering. University of Cordoba. Campus of Rabanales, 14071 Cordoba, Spain.

[3] Applied Physics. University of Cordoba. Campus of Rabanales, 14071 Cordoba, Spain.

[4] Electronic and Computers Engineering. University of Cordoba. Campus of Rabanales, 14071 Cordoba, Spain.

*Corresponding Author: Phone: + 34957218602 Fax: + 34957212068 e-mail address: fa2vamam@uco.es

ABSTRACT

Solar tracking is a technique required to increase energy production in multiple photovoltaic (PV) facilities. In these plants, during low-elevation solar angle hours, shadows appear between the collectors causing a dramatic decrease in production. This paper presents a novel optimal tracking strategy to prevent the creation of these shadows. The presented method determines whether or not there is shading between collectors. Thus, when the collectors are not shaded, a tracking trajectory for maximum irradiance on the collectors is suggested. However, when the collectors are shaded, backtracking is proposed. Therefore, energy production in plants with this novel tracking method can be 1.31 % higher than that in PV installations with astronomical tracking. Moreover, this method allows the study of PV facilities for which there have been no published approaches, such as plants with non-rectangular collectors or those located on topographically heterogeneous surfaces.

KEYWORDS: PV Solar Plants, Two-axis Solar Tracker, Power Losses by Shading in PV Plants, Backtracking.

4.1. Introduction

Technologies based on the use of solar energy have recently received more attention, and their development aims to respond to the growing need for renewable energy. In this context, scientific advances in the field of photovoltaics (PV) are allowing this technology to become an alternative sustainable energy source [10,11]. However, these advances are not always properly applied to PV plant design and/or operation, and, consequently, the optimal development that these advances require for PV plants has not yet been achieved.

This is evident in the case of using solar tracking to increase the ability of PV plants to harness solar resources. Solar trackers can be classified as one- or two-axis trackers. In one-axis trackers, the collector's surface rotates around a fixed axis, while the surface moves around two fixed axes in two-axis trackers, which allows the collector plane to orientate towards any direction of the celestial sphere [12]. In this research area, authors [13–15] have analysed the effects of the type of tracking on energy production at different latitudes, and their results show that, in any case, the higher the latitude, the more effective the tracking, with differences reaching 57% [17].

In solar tracking PV plants, the collector's orientation is commonly governed by equations based on the astronomical movement of the Sun, which can predict the position of the Sun in the celestial sphere with an accuracy of an order of mrad [20,21,23]. In this field, mathematical equations based on applying spherical trigonometry to solar movement have been developed to calculate the elevation and azimuth position for one- and two-axis trackers for each moment [22,23,27,28,32,72] Recently, in contrast to this method, it is possible to deduce all of the astronomical factors governing the movement of the Sun and the orientation of solar tracking systems from the definition of 'solar vector' (unit vector along the direction towards the centre of the solar disk) and applying vector algebra [69–71,86,100].

Applying the astronomical model to solar tracking means that the angle formed between the direct solar rays and the normal angle to the collector's surface ϑ must be as low as possible. With astronomical tracking, the value of the direct irradiance component is maximized, which is appropriate for applications focused on this component (such as concentration technologies). However, in PV, all irradiance components (direct, diffuse, and reflected irradiance) are usable. Therefore, this type of tracking is not the most suitable. As Duffie and Beckman [22] and Mousazadeh et al. [11] noted, on cloudy days, when the solar disk is not visible and direct radiation does not reach the collectors, collectors located on a fixed horizontal position would collect more energy than those with astronomical tracking. Despite this, no work has been conducted to determine the appropriate equations for optimising solar tracking on cloudy days.

Thus, it is necessary to study the influence of diffuse and reflected components on solar tracking in greater depth to determine the equations that can allow maximum radiative capture.

Additionally, one of the most important aspects to consider in plants with astronomical solar tracking is shading between the modules, which mainly occurs during the first and last hours of the day and causes production losses, as well as the appearance of hot spots in the modules [17].

To characterise and optimise the design of tracking plants, Diaz-Dorado et al. [20-21] developed a model that considers the arrangement of the cells within the photovoltaic modules, as well as the exact position of each module within the tracking surface, to determine the shading effects for all cells in the tracker. In this model, shading is characterised following a conventional tracking strategy to achieve perpendicularity between the direct solar rays and the collector's surface [20-21].

To estimate power losses caused by shading, Martinez-Moreno et al. [35] have proposed a predictive model that does not require any specific information regarding the connections between the cells and modules. This model has been validated by different authors [36,37] who have developed more extensive models based on Martinez-Moreno's model to determine the productivity of PV plants. Similarly, Perpiñan [38] developed a method for estimating and optimising energy costs based on plant design parameters, specifically the ground cover ratio (GCR, which is the ratio between the PV module area and the terrain occupied by the PV plant). For this, the method uses Gordon and Wenger's hypothesis [39] when determining energy losses due to shading, which considers the losses proportional to the percentage of the shaded area. Narvarte and Lorenzo [26] studied the productivity of a PV plant considering different types of solar tracking and three simple hypotheses for estimating losses by shading.

Panico et al. [40] proposed backtracking as an approach to minimise the effects of shading. This technique involves deviating the direction of the solar trackers from the solar position to avoid shading between the collectors when necessary. Different authors [17,40,41] have demonstrated the advantages of backtracking, as follows:

A. Advantages of land use: By avoiding the effects of shading, the distances between trackers can be reduced, resulting in greater GCR.
B. Operating advantages: The work conducted by Lorenzo and Narvarte [17] indicates that, in all cases, energy balance is more favourable in plants with backtracking than in those allowing shading between collectors.

C. Design advantages: The absence of shading and, therefore, of hot spots, suggests lower maintenance costs.

Therefore, the reliability of plants with backtracking is greater than that in plants that allow shading [17,41]. Consequently, many technological solutions to implement backtracking are being developed [101–103].

To determine the orientation of the collectors during backtracking, different methods based on the geometric determination of shadows between polygons have been proposed [13,42,72]. However, these methods are often limited to simple geometric situations such as:

i. Exclusively rectangular collectors.
ii. Regular ground layouts where only the shading between contiguous collectors is considered.
iii. Flat topographic surfaces.
iv. Horizontal topographic surfaces.
v. Movement around the azimuthal and elevational axes without considering other combinations of axes that entail the rotation of the collector around the normal axis to the collector's surface.

Considering the aforementioned limitations, this study presents a simple and more generic backtracking method to avoid shadows and optimise solar energy collection. The method is based on the vector treatment of the geometry of the Sun-Earth position, as well as the implicit geometry of solar tracking plants. Furthermore, this method does not *a priori* assume the astronomical tracking hypothesis commonly assumed in the literature, which aims to maintain the position of the collector's surface perpendicular to the direct solar rays [100]. Thus, the proposed method allows the following, which are novelties in comparison to conventional methodologies:

1. The study of plants with non-rectangular surface collectors.
2. The analysis of facilities where collectors are not necessarily located at the regular nodes of a geometric grid.
3. The determination and comparison of the effects of different tracking modes.
4. The consideration of plants located on real topographical surfaces, and not only flat or horizontal surfaces.
5. The consideration of global irradiance on collectors, instead of being limited to direct irradiance (typical for astronomical tracking).

Therefore, the method presented here will be useful for optimising the design of new photovoltaic two-axis tracker plants, as well as for controlling the movement of current plants by improving and optimising their electrical production.

4.2.Materials and methods

4.2.1. Astronomical and Vector Fundamentals

To optimise the trajectory of solar trackers in PV plants, this work is based on the definition of the solar vector $\vec{s}$ in an Earth reference system, where the Ox axis is oriented to the West, the Oy axis is oriented to the South, and the Oz axis is oriented to the zenithal direction, with $\vec{i}$, $\vec{j}$, and $\vec{k}$ the respective unit vectors (Figure 4.1). The solar vector is given by Eq. (4.1), where δ is the solar declination [86], φ the latitude and Ωt is the hourly angle, which is defined as the product of the Earth's rotation speed ($\Omega = 2\pi/24\ rad/h$) and the time elapsed since the solar noon.

$$\vec{s} = s_x\,\vec{\imath} + s_y\,\vec{\jmath} + s_z\,\vec{k} = sin\Omega t\ cos\,\delta\,\vec{\imath} + (cos\,\Omega t\ cos\,\delta\ sin\,\varphi - sin\,\delta\ cos\,\varphi)\vec{\jmath} + \\ +(cos\,\Omega t\ cos\,\delta\ cos\,\varphi + sin\,\delta\ sin\,\varphi)\vec{k} \tag{4.1}$$

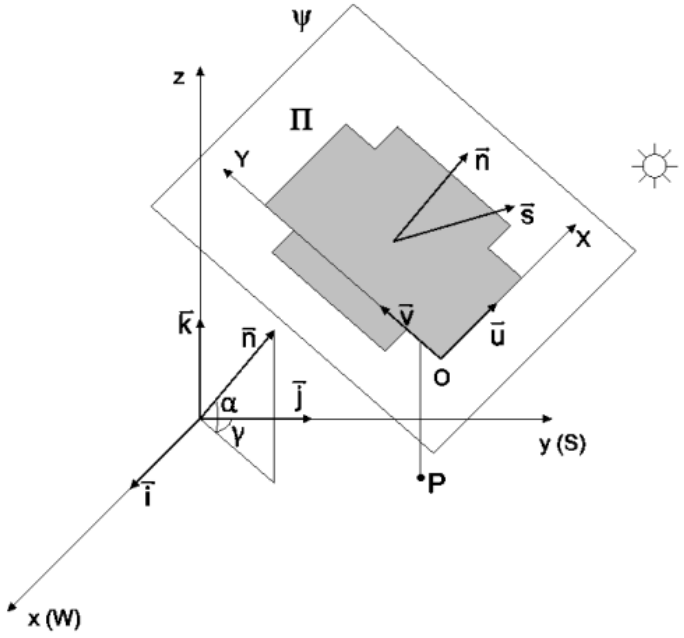

Figure 4.1. Representation of the collector's surface in the Earth reference system

Figure 4.1 also shows the polygon Π, which represents the perimeter of the collector's surface, and the vector normal to that surface, $\vec{n}$. The components of the vector $\vec{n}$ in the Earth reference

system, depending on the azimuth *(γ)* and elevation *(α)* angles of the collectors, are given by Eq. (4.2).

$$\vec{n} = cos\,\alpha \cdot sin\,\gamma\vec{\imath} + cos\,\alpha \cdot cos\,\gamma\,\vec{\jmath} + sin\,\alpha\,\vec{k} \tag{4.2}$$

Additionally, the projection plane is considered as the plane that contains the collector's surface. A flat coordinate system associated with this plane is defined (OXY) with unit vectors $\vec{u}_f$ and $\vec{v}_f$. During tracking, the system will move while rigidly attached to the collector polygon. As a result, the mathematical expressions for $\vec{u}_f$ and $\vec{v}_f$ will depend on the collector's orientation at every moment, given by *α* and *γ*, and be conditioned by the type of tracking. Eqs. (4.3)-(4.16) present the expressions for the most frequent tracking typologies (shown in Figure 4.2).

- Azimuth-elevation tracking (A-E)

$$\vec{u}_f = -cos\,\gamma\,\vec{\imath} + sin\,\gamma\,\vec{\jmath} \tag{4.3}$$

$$\vec{v}_f = sin\,\alpha \cdot cos\,\gamma\vec{\imath} - sin\,\alpha \cdot cos\,\gamma\,\vec{\jmath} + cos\,\alpha\,\vec{k} \tag{4.4}$$

- Equatorial tracking (EQ)

$$\vec{u}_f = -cos\,\theta_1\,\vec{\imath} + sin\,\theta_1 \cdot cos\,\varphi\,\vec{\jmath} + sin\,\theta_1 \cdot sin\,\varphi\,\vec{k} \tag{4.5}$$

$$\vec{v}_f = -sin\theta_2 \cdot sin\theta_1\vec{\imath} - (cos\theta_1 \cdot sin\,\theta_2 \cdot cos\varphi + cos\,\theta_2 \cdot sin\varphi)\vec{\jmath} - (cos\theta_1 \cdot sin\,\theta_2 \cdot sin\varphi - cos\,\theta_2 \cdot sin\theta_1)\vec{k} \tag{4.6}$$

where

$$\theta_1 = tan^{-1}\left(\frac{cos\alpha \cdot sin\gamma}{cos\alpha \cdot cos\gamma \cdot cos\varphi - sin\alpha \cdot sin\varphi}\right) \tag{4.7}$$

$$\theta_2 = sin^{-1}(\,cos\alpha \cdot cos\gamma \cdot sin\varphi + sin\alpha \cdot cos\varphi) \tag{4.8}$$

- Elevation-Rolling tracking (E-R)

$$\vec{u}_f = -cos\,\theta_2\,\vec{\imath} + sin\theta_1 \cdot sin\,\theta_2\,\vec{\jmath} + cos\theta_1 \cdot sin\theta_2\vec{k} \tag{4.9}$$

$$\vec{v}_f = -cos\,\theta_1\,\vec{\jmath} + sin\,\theta_1\vec{k} \tag{4.10}$$

where

$$\theta_1 = tan^{-1}(cos\gamma \cdot cotan\alpha) \tag{4.11}$$

$$\theta_2 = sin^{-1}(cos\alpha \cdot sin\gamma) \tag{4.12}$$

- Rolling-Elevation tracking (R-E)

$$\vec{u}_f = -cos\theta_1\vec{\imath} + sin\theta_1\vec{k} \tag{4.13}$$

$$\vec{v}_f = sin\theta_1 \cdot cos\theta_2\vec{\imath} + sin\theta_2\vec{\jmath} + cos\theta_1 \cdot cos\theta_2\vec{k} \tag{4.14}$$

where

$$\theta_1 = tan^{-1}(sin\gamma \cdot cos\alpha) \tag{4.15}$$

$$\theta_2 = cos^{-1}(cos\gamma \cdot cos\alpha) \tag{4.16}$$

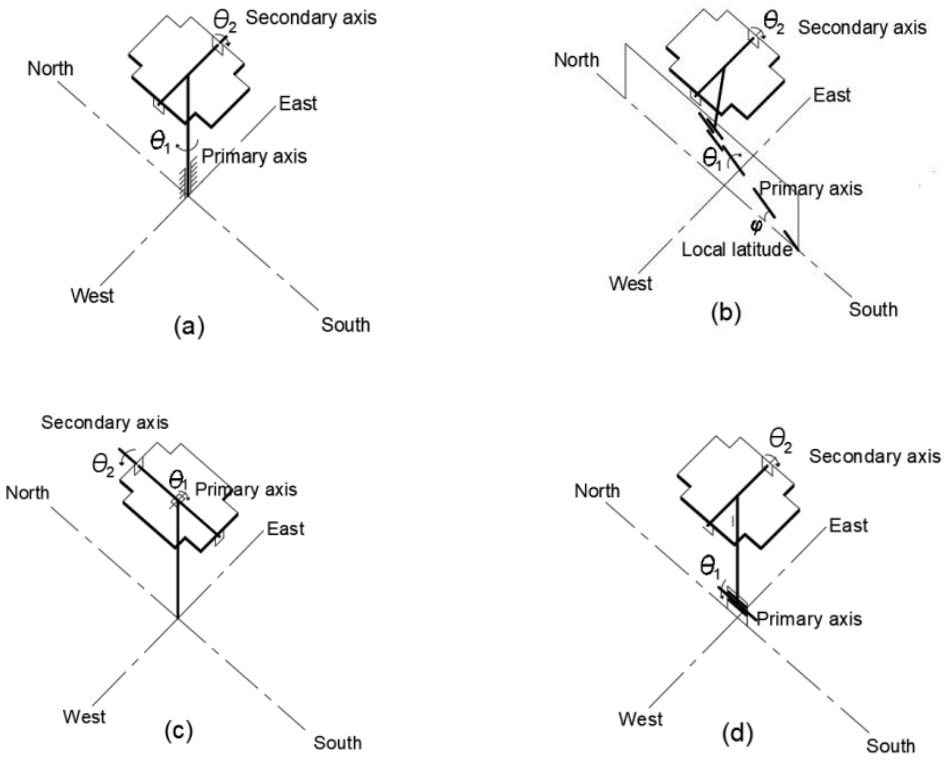

Figure 4.2. Common tracking strategies: a) Azimuth-elevation tracking (A-E), b) Equatorial tracking (EQ), c) Elevation-Rolling tracking (E-R), and d) Rolling-Elevation tracking (R-E)

4.2.2. Geometrical Methodology

Based on the geometric fundamentals defined in the previous section, this work studies shadows to dichotomously determine whether there is an intersection between the PV collectors at a specific time, rather than to quantify the shape and size of the shaded polygons. Therefore, by calculating the irradiance received by the collector's surfaces for a given hour at different positions when there is no shading, the maximum irradiance position can be

elucidated. Moreover, by conducting this study over a certain period, it is possible to define the trajectory of the collectors that optimises energy capture by a PV plant for each day of the year.

In this study, it is considered that all collectors have the same geometric shape and move in the same manner. Considering this, it can be stated that the planes that contain the collector surfaces are always parallel. Therefore, regardless of the solar position with respect to the collectors, the solar projection Π'_i of any collector Π_i on plane Ψ containing the reference tracker Π_0 will produce a polygon with the same shape and dimensions as the collector polygon i (Figure 4.3). From this projection, it can be concluded that Π_i shades Π_0 if polygons Π_0 and Π'_i intersect.

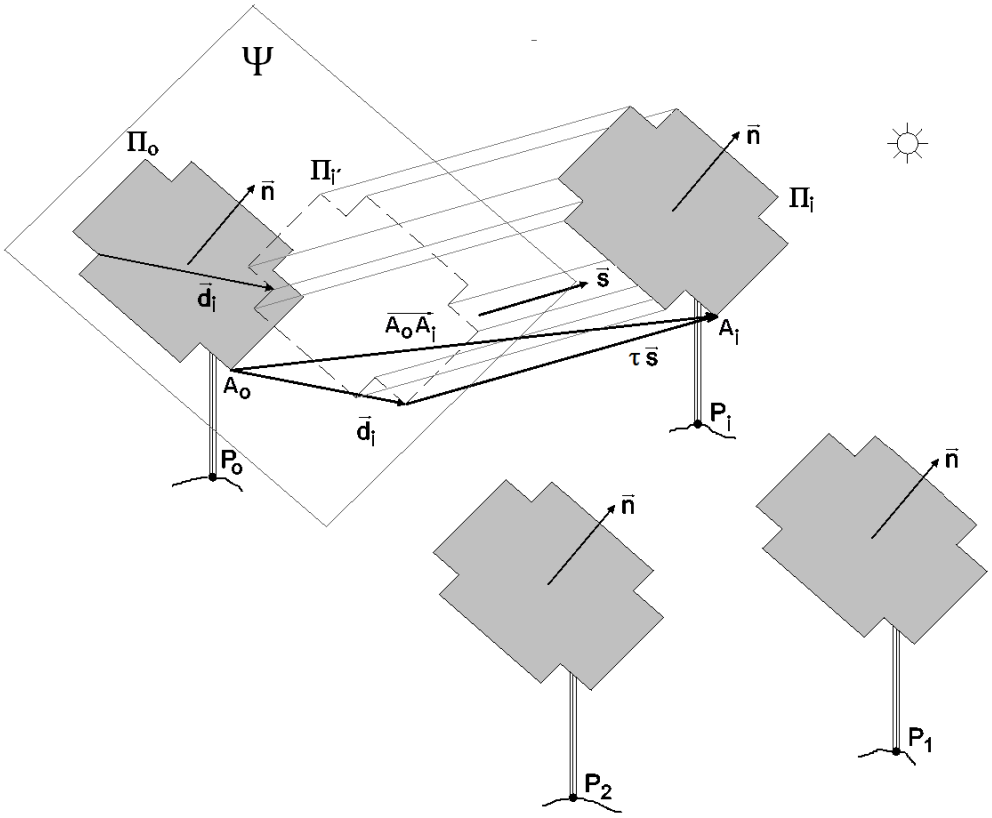

Figure 4.3. Geometry of the set of trackers

As all collectors are considered equal and the perimeters of the projected collectors in the solar direction maintain their geometry, polygon Π'_i could be considered as a translation of the reference collector Π_0 contained on plane Ψ, with $\vec{d}_i$ as the translation vector. Similarly, as the collectors remain parallel, the distance between any two equivalent points (A_i and A_0) of collectors Π_i and Π_0 is constant. That is, $\overrightarrow{A_0A_i} = \overrightarrow{P_oP_i}$. Consequently, to determine $\vec{d}_i$, the

parallelogram rule is applied to the vectors involved in the described geometric problem (Figure 4.3), which produces Eq. (4.17).

$$\overrightarrow{P_oP_\iota} = \overrightarrow{a_0a_\iota} = \overrightarrow{d_\iota} + \tau_{ap} \cdot \vec{s} \tag{4.17}$$

Furthermore, to determine τ_{ap}, the scalar product between Eq. (4.17) and the vector normal to plane Ψ, $\vec{n}$, is calculated, which produces Eq. (4.18), where $\vec{n}\cdot\overrightarrow{d_i}$ is zero as both vectors are perpendicular.

$$\vec{n} \cdot \overrightarrow{P_oP_\iota} = \overrightarrow{a_0a_\iota} = \overrightarrow{d_\iota} + \tau_{ap} \cdot \vec{s} \tag{4.18}$$

Consequently, scalar τ_{ap} is given by Eq. (4.19).

$$\tau_{ap} = \frac{\overrightarrow{P_oP_\iota} \cdot \vec{n}}{\vec{s} \cdot \vec{n}} \tag{4.19}$$

Substituting (4.19) into (4.17), the translation vector of projection Π'_i with respect to reference collector Π_0 on plane Ψ, $\overrightarrow{d_i}$, can be obtained (Eq. 4.20).

$$\overrightarrow{d_\iota} = \overrightarrow{P_oP_\iota} - \frac{\overrightarrow{P_oP_\iota} \cdot \vec{n}}{\vec{s} \cdot \vec{n}} \cdot \vec{s} \tag{4.20}$$

Thus, expression (4.20) allows the components of $\overrightarrow{d_i}$ in Earth reference system Oxyz to be calculated. However, as $\overrightarrow{d_i}$ belongs to the OXY plane, the Cartesian components in the collector plane can be determined by Eqs. (4.21) and (4.22).

$$d_X = \overrightarrow{d} \cdot \vec{u}_f \tag{4.21}$$

$$d_Y = \vec{d} \cdot \vec{v}_f \tag{4.22}$$

Once the projections have been obtained, a test based on Minkowski algebra [69–71] is conducted to determine whether the polygons intersect and, therefore, whether there would be shading. For this, all the feasible polygons on Ψ resulting from moving Π_0 are drawn so that any point on its perimeter matches the origin of the 0XY reference system associated with plane Ψ (Figure 4.4). Polygon Σ is defined as the envelope of this family of polygons. Therefore, it is possible to affirm that Π_0 and Π'_i intersect if the representation of the corresponding $\overrightarrow{d_i}$, vector moved to the origin of the 0XY reference system, is fully included in Σ (Figure 4.4).

To ensure that reference collector Π_0 is not shaded at a given time, it is necessary to check that it is not shaded by any other collector in the PV plant. Given that envelope Σ is the same for any pair of collectors as they all exhibit the same geometry and remain parallel, it would be sufficient to determine whether the $\vec{d_i}$ vectors (for *i*=1, N-1, with N being the number of PV panels in the plant) linked to each pair of collector surfaces, Π_0-Π_i, are included in envelope Σ for cases that meet the following conditions:

I. Collector Π_i is visible from the reference collector Π_0: $\overrightarrow{P_0P_i} \cdot \vec{n} > 0$.
II. The sun does not irradiate the rear side of the collectors: $\vec{s} \cdot \vec{n} > 0$.
III. It is a specific moment of the solar day: $\vec{s} \cdot \vec{k} > 0$.

Under these conditions, a single $\vec{d_i}$ included in the Σ envelope will indicate that the studied collector is shaded.

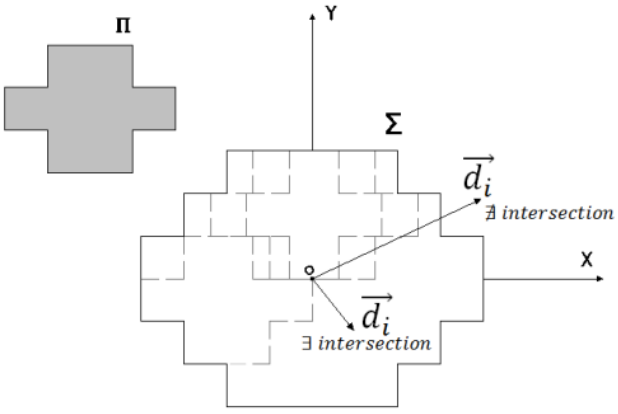

Figure 4.4. Obtaining enveloping polygon Σ from Π

4.2.3. Optimisation of the Collector Position under the no Shading Hypothesis

According to the described method, for each moment in time, whether the reference collector is shaded or not for different collector orientations (given by its azimuth, γ, and elevation, α) can be analysed. Based on this analysis, for any specific moment in time, it is also possible to represent the delimitation of the two regions in a cylindrical chart (γ, α): one corresponding to shaded collectors and another corresponding to non-shaded collectors. In addition, as will be demonstrated in the application, the irradiance received by the collectors at each orientation can be also represented on the same chart using irradiance isovalue curves. From these two delimited areas and using the irradiance isovalue curves, the point with maximum irradiance for each moment in time, and, consequently, the optimum orientation of the solar trackers, can be

selected. Repeating this process for different moments in time the same day can allow the optimal tracking trajectory (with maximum irradiance and without shading) to be defined.

4.3. Results and Discussion

Once the proposed methodology has been described, the optimal trajectories for tracking and backtracking at the "El Molino" PV solar plant located in Cordoba, Spain, are obtained (latitude=37.75492°N; longitude=5.04548°W). This plant is an Azimuth Elevation tracker plant arranged in a rectangular grid with an east-west distance (d_{EW}) of 20 m and north-south distance (d_{NS}) of 14 m (Figure 4.5).

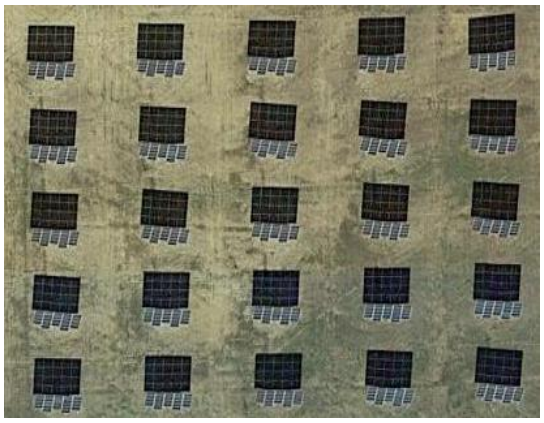

Figure 4.5. Application example: Spatial distribution of the collectors of the El Molino PV plant (Cordoba, Spain).

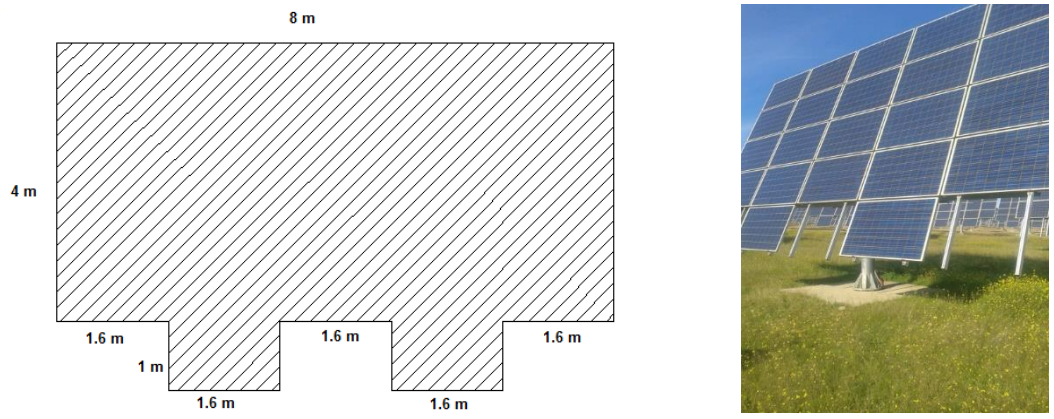

(a) (b)

Figure 4.6. Application example: Shape and dimensions of the photovoltaic collectors in the El Molino PV plant (Cordoba, Spain).

Based on the geometry of the collectors (Figure 4.6), Figure 4.7 shows the envelope Σ for the collectors' surface. In practice, the polygons constituting the collectors (Figure 4.6a) only have right angles. Therefore, the surrounding polygon Σ has only right angles (Figure 4.7), simplifying

the test to determine whether the $\vec{d_i}$ vectors are included in Σ. Therefore, in this example, each $\vec{d_i}$ is included in the Σ envelope if condition (4.23) or (4.24) is verified.

$$|d_{iX}| < 8\ m\ and \cdot |d_{iY}| < 4\ m \tag{4.23}$$

$$|d_{iX}| < 6.4\ m\ and \cdot |d_{iY}| < 5\ m \tag{4.24}$$

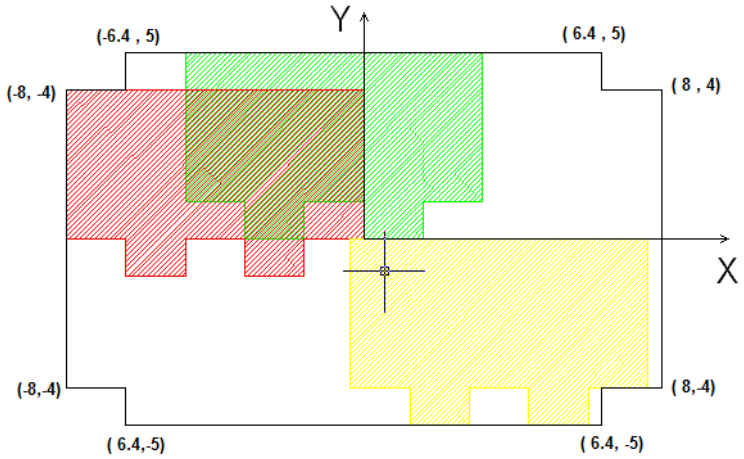

Figure 4.7. Application example: Shape and dimensions of polygon Σ enveloping the set of polygons generated by sliding Π_0 onto the origin of the coordinates (values in metres).

The analysis method proposed here was applied every five minutes for one astronomical year. As this methodology involves a dichotomous test to establish whether or not there is shading at a specific collector orientation defined by its azimuth *(γ)* and elevation *(α)*, a binary search for the elevation limit between the shaded and non-shaded areas has been programmed for fixed azimuth values. It has been verified that eight iterations are sufficient for estimating this limit with an error below 0.3 deg.

For Julian Day 349 at 8:20 (true solar time; TST), Figure 4.8 shows a cylindrical chart representing the boundary between the shaded (grey region, corresponding to the cases for which at least one $\vec{d_i}$ is included in Σ) and not-shaded (blue region, corresponding to the cases for which all vectors $\vec{d_i}$ are not included in Σ) areas. Moreover, the irradiance isolines were included in the non-shaded area. As the proposed methodology only considers the collector positions at which there would be no shading, a single irradiance model is assumed. Therefore, Liu-Jordan's equation [73] (Eq. (4.25)) was considered as it was used by Fernandez-Ahumada et al. [100], where I_B and I_D are direct and diffuse irradiances, respectively, and ρ is the albedo. In this

study, ρ*=0.2* is considered following [73]. Therefore, it is possible to determine the solar irradiance captured by the collectors for each orientation without shading using Eq. (4.25).

$$I = \frac{cos\,\theta}{cos\,\theta_z}\,I_B + \frac{1+cos\,\beta}{2}\,I_D + \rho\frac{1-cos\,\beta}{2}\,(I_B + I_D) \tag{4.25}$$

Similarly, Figure 4.8 presents the collector orientation for three different tracking strategies:

a. Astronomical tracking with no shading (ATNS, represented by a green circle): tracking governed by an astronomic equation for an ideal PV plant where the distances between the collectors are sufficiently large to avoid shading.
b. Maximum irradiance tracking with no shading (MITNS, represented by a red circle): the optimal tracking strategy proposed by Fernandez-Ahumada et al.[100], which seeks maximum irradiance levels on an ideal isolated collector that is not affected by shadows from adjoining collectors.
c. Maximum irradiance backtracking (MIBT, represented by a blue cross): tracking strategy proposed in this study, which seeks maximum irradiance levels while avoiding shading between the collectors by backtracking when necessary.

Therefore, for this day and time, this novel backtracking approach proposes that the tracker should point towards the maximum irradiance direction within the non-shaded region (blue cross in Figure 4.8). Figure 4.8 also shows that the orientations corresponding to ATNS and MITNS are within the region where there are shadows between the collectors and, consequently, the irradiance captured by the PV modules is reduced. However, it should be noted that, in this case, the minimum and maximum limits of the azimuth or elevation are not considered. Consequently, if these constructive limits exist, they should also be represented as additional restrictions in the cylindrical charts.

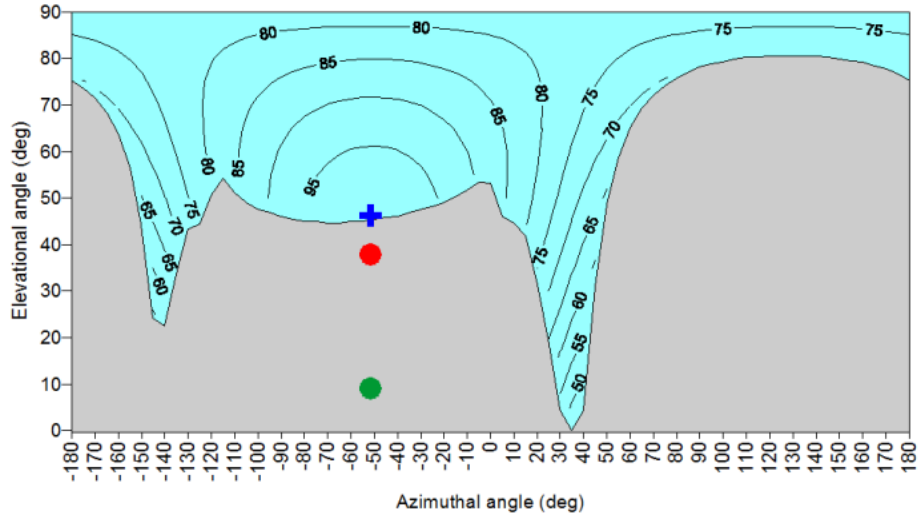

Figure 4.8. Application example: Splitting of the spatial directions and selection of the angles (γ, α) that optimise irradiance (W/m2) for the reference collector in the El Molino PV plant (Cordoba, Spain) on Julian day 349 at 8:20 TST.

Moreover, based on the method outlined above, the path to be tracked by the collector for the day of study can be proposed. Therefore, Figure 4.9 shows the trajectories corresponding to the three different analysed tracking strategies: ATNS (green line), MITNS (red line), and MIBT (blue line). As shown, the proposed MIBT trajectory (blue curve) exhibits sections where it does not coincide with the MITNS trajectory (red curve) corresponding to the maximum solar irradiance collection under an ideal situation with no shading. For these periods, backtracking is proposed as the movement that optimises energy collection by the plant, as it considers the real shadows between the collectors, which reduce the levels of irradiance from their optimal values considered by MITNS.

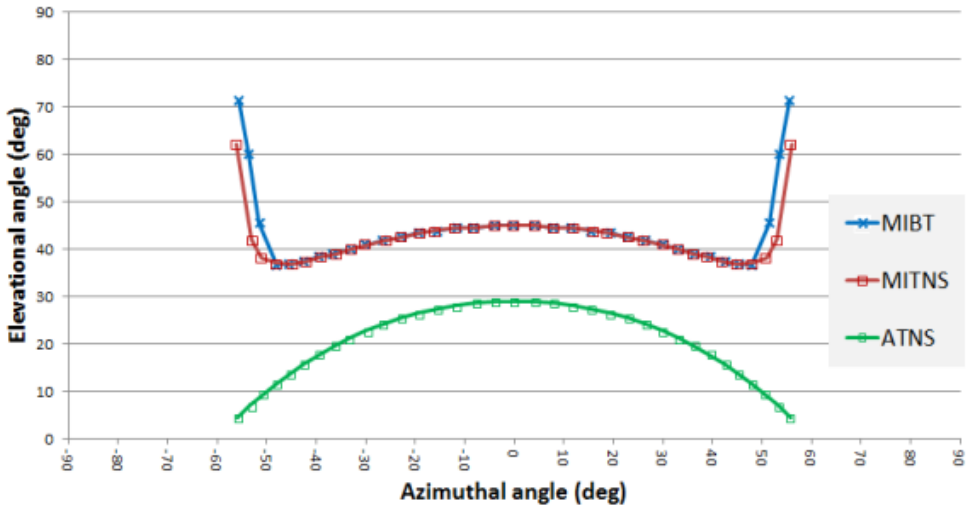

Figure 4.9. Application example: Potential collector pointing trajectories of the PV plant "El Molino" (Cordoba, Spain) on the Julian day=349

Finally, the daily radiation was determined for each approach to compare energy production under the three potential strategies (ATNS, MITNS, and MIBT). The values for the three cases were obtained by integrating Eq. (4.25) on representative days. Therefore, although the three tracking strategies imply no shading between collectors, in contrast to MIBT, ATNS and MITNS are only valid for isolated trackers and not for plants with many PV modules. Accordingly, the simulated energy production of these two ideal tracking strategies can be considered as maximum potential values and should be used as a reference to evaluate the improvements made by the proposed tracking method.

Table 4.1 shows the simulated energy production (kWh) values for each month against the peak power (kWp) of the collectors. In line with Fernandez-Ahumada's results [100], energy production under MITNS is higher than that under ATNS. Similarly, it has been verified that, for several months, energy production by solar plants under MIBT reaches values between the optimal values of MITNS and ATNS. Production by MIBT solar plants is 0.89% lower than that by MINTS plants, but 1.31% higher than that by ATNS plants.

Table 4.1. Comparative analysis of the energy production levels of PV solar plants with different tracking strategies.

Month	**MIBT (kWh/kWp)**	**MITNS (kWh/kWp)**	**ATNS (kWh/kWp)**	**Decrease in MIBT vs. MITNS (%)**	**Increase in MIBT vs. ATNS (%)**
January	82.4	84.2	83.7	2.16	-1.51
February	114.7	116.0	114.0	1.09	0.59
March	144.3	146.3	144.4	1.36	-0.11
April	160.8	163.0	161.4	1.35	-0.39
May	177.1	179.6	178.4	1.41	-0.76
June	250.5	251.1	244.5	0.24	2.44
July	291.0	291.3	280.7	0.08	3.68
August	269.3	269.6	259.0	0.09	4.01
September	197.7	198.4	192.1	0.34	2.93
October	125.4	127.3	125.9	1.49	-0.35
November	86.6	88.5	88.0	2.11	-1.52
December	65.0	67.4	67.4	3.54	-3.49
Year	**1965.0**	**1982.7**	**1939.5**	**0.89**	**1.31**

The proposed method improves the results obtained by Narvarte and Lorenzo [26] in their characterisation of the energy losses due to shading in plants with different astronomical tracking typologies (one and two-axis). They demonstrated that, in all cases, energy production losses increase with GCR. Therefore, in comparison to the ideal astronomical tracking, they estimated that the uncertainty of energy production is within 2% for GCR=0.09. These results are similar to those published by Panico [40], even though this study is restricted to one-axis trackers. Specifically, Panico found that the losses due to shading in installations with GCR=0.09 compared to astronomical tracking are 2.5% [40]. These values are also within the intervals proposed by Gordon and Wenger [39], who demonstrated that energy losses by shading in plants with GCR=0.09 depend on the collectors' geometry and spatial layout.

Consequently, all published studies indicate that shading causes energy losses in comparison to energy generation under ideal astronomical tracking. Therefore, this study shows that solar energy collection by plants with the proposed tracking strategy, MIBT, is better than that by plants with astronomical tracking and only 0.98% lower than that by plants with the ideal MITNS tracking. However, owing to the scarcity of publications in this area, the authors of this paper consider that it is necessary to continue studying the influence of design parameters on energy collection by plants with MIBT, as well as to implement this novel tracking strategy in actual PV installations to evaluate its development.

4.4. Conclusions

In this study, a new methodology for defining the optimal tracking strategy without shading of sets of two-axis motion PV tracker collectors is proposed. In contrast to astronomical tracking, the proposed method indicates that collectors do not have to be constantly perpendicular to the direct solar rays, as it considers the diffuse and reflected irradiance, as well as the direct irradiance, reaching PV collectors. Therefore, when collectors are not shaded, a tracking trajectory seeking maximum irradiance on the collectors is suggested. However, when the collectors are shaded, backtracking is proposed. Therefore, based on the concepts of solar vectors and vector algebra, this method analyses shading between the collectors. However, the proposed technique is not based on the calculation of the area of polygon intersections; rather, it is based on whether or not such intersections are present. Consequently, in contrast with other tracking strategies found in previous studies, this novel method is based on algorithms that are significantly simpler and faster. Thus, owing to its novelties and advantages, this method is easier to be used to simulate energy production with different radiative models and is applicable to situations for which no published generic methods can be found, such as PV plants:

i. with non-rectangular surface collectors
ii. with collectors that are not located on the regular nodes of a geometric mesh
iii. with different tracking modes
iv. with trackers located on real topographical surfaces

The energy production by PV plants with this new tracking strategy, called MIBT, has been analysed and compared to two ideal tracking strategies:

1) ATNS: Astronomical tracking in an ideal PV plant where the distances between the collectors are large enough to avoid shading.
2) MITNS: optimal tracking that seeks the maximum irradiance levels on an ideal isolated collector not affected by potential shadows from adjoining collectors [15].

The results show that MIBT improves the energy collection by 1.31% in comparison to ATNS, and the energy collection is only 0.89% lower than that by MITNS plants. Therefore, considering these results and the advantages of this method, the authors consider that this method will not only be useful for designing new facilities, but could also help to improve the productivity and management of many PV plants by redefining tracking strategies.

ACKNOWLEDGEMENTS

This research is partially supported by the CLARA Project, which has received funding from the European Union's Horizon 2020 research and innovation programme under Grant Agreement No 730482. The authors thank Magtel Operaciones SL for their collaboration in this research.

Capítulo 5 . A methodology for buildings access to solar radiation in sustainable cities

A METHODOLOGY FOR BUILDINGS ACCESS TO SOLAR RADIATION IN SUSTAINABLE CITIES

Sustainability 2019, 11(23), 6596; 22 Nov 2019

L.M. Fernández-Ahumada [1], J. Ramírez-Faz [2], R. López-Luque [3], A. Márquez-García [4] and M. Varo-Martínez [3,*]

[1] Computing and Numeric Analysis. University of Cordoba. Campus of Rabanales, 14071 Cordoba, Spain; lmfernandez@uco.es

[2] Electrical Engineering. University of Cordoba. Campus of Rabanales, 14071 Cordoba, Spain; jramirez@uco.es

[3] Applied Physics. University of Cordoba. Campus of Rabanales, 14071 Cordoba, Spain; fa1lolur@uco.es

[4] Research Group Physics for Renewable Energies. University of Cordoba. Campus of Rabanales, 14071 Cordoba, Spain; alvaromarquezugr@gmail.com

***** Correspondence: fa2vamam@uco.es; Tel.: +34-957-218602

Received: date; Accepted: date; Published: date

Abstract: The growing need to improve the environmental and energy sustainability of buildings involves the use of solar radiation incident on their surfaces. However, in cities this task is complicated due to the constructive geometry that leads to shading between buildings. In this context, this work presents a study of solar access to the façades of buildings in cities. The methodology is based on the determination of the incident annual solar radiation in 121 significant points of each façade considering the twelve representative days of the year. To characterize the influence of the different city typologies on solar access, the urban solar coefficient is proposed. A study in two neighborhoods in Cordoba (Spain) with different urban settings have been analyzed. Specifically, two typologies of neighborhoods have been compared: one with ”L-shaped” and “U-shaped blocks” and another with “Grouped blocks”. For both, the Urban Solar Coefficient has been calculated, obtaining a higher mean value for the neighborhood with ”L-shaped” and “U-shaped blocks” (0.317) than for the one with “Grouped blocks” (0.260). Accordingly, the results show that urban morphology can influence the Urban Solar Coefficient and solar access. Finally, a regression model for each neighborhood has been obtained in order to determine the dependence of the Urban Solar Coefficient on neighborhood geometry factors.

Keywords: Sustainable Cities; Solar Access; Solar Radiation on Buildings.

5.1. Introduction

Cities in developed countries are undergoing fast growth due to different factors such as the increase in global population [2] or migration from rural environment and underdeveloped countries, among others [104,105]. In fact, more than half of the world's population now lives in cities and this number is expected to reach 66% by 2050 [106,107]. As a result of this urban population increase, major problems related to the sustainability of cities are emerging, such as the worsening of air quality as a consequence of the use of fossil fuels for transportation or heating of buildings [105,107–109]. Specifically, in terms of energy supply, it is estimated that 75% of total energy is consumed in cities [105] and that this consumption will double over the next three decades [110,111]. These circumstances, together with the environmental problems associated with fossil fuels [112], have encouraged research and development of renewable energies in order to improve energy efficiency and sustainability in cities [107,111]. Among these renewable energy sources, solar energy stands out as a source of clean energy, abundant and available, to a greater or lesser extent, throughout the Earth [9].

In addition, urban planning has always searched, as a main goal, an ideal integration of living spaces (buildings and squares), communication systems (roads and streets) and land area (topography) [113]. However, the lack of available space in cities has caused the appearance of new neighborhood configurations, which only give importance to the rise of population density [114]. Therefore, nowadays, parameters such as population density, street width and accessibility, determine the typology of new neighborhoods [115]. Nevertheless, despite the harnessing of solar energy in cities becoming an obligation in new dwellings to make them sustainable, solar radiation levels are not frequently considered when making decisions about urban planning.

In fact, to develop energy efficiency measures in new buildings it is necessary to know the levels of solar radiation reaching every piece of the building which could be used to install solar panels or thermal collectors [43,44]. In addition, this information about solar radiation can also be used for the estimation of natural lighting on its windows and, consequently, to guarantee solar rights [45], especially in cities with a great presence of skyscrapers. Daylight also has a positive influence on the health and human behavior of the residents [46,47] and it contributes to improving the indoor climate, increasing thermal comfort, and, consequently, reducing the energy demand of a dwelling [47–52]. For all these reasons, an in-depth knowledge of the level of available solar radiation on the façades of buildings in cities is necessary [53].

Furthermore, a complete knowledge of the solar radiation on façades in complex cities also allows developing new passive solar building designs [54], making it easier to choose the ideal materials for windows (transparent or translucent polymer) and their layout in each case [55]. These techniques turn out to be especially interesting in areas where the heating loads in buildings represent an important part of the electricity bill. With this in mind, Building Performance Simulation (BPS) tools compare different design alternatives related to the efficiency and energy consumption in buildings, providing useful and quick information to the technicians [56]. Owing to the importance of the level of solar irradiance on façades and roofs [57,58], architects should consider it during the early phases of their projects. In this line of work, Tang Minfang [59] studied the effect of the azimuth angle and the height of the main façades of a building on the available solar radiation and Salazar Trujillo [60] described the influence of solar radiation on the temperatures inside the rooms in order to improve energy efficiency.

However, in cities, this analysis can prove complex [51], due to several interactions existing, including those with neighboring buildings or the effect of the trees [61] and the fact that each neighborhood must be studied independently [62].

Geographic Information System (GIS) techniques allow representing complex cities and can be used for the estimation of the most appropriate parts of a building for the installation of PV panels [63] or identifying the zones of optimal solar energy potential [64]. Besides, using these techniques, the results may be scalable and automated, in comparison with points-based methods [65]. A good example of a methodology based in GIS is the Solar Energy Planning (SEP) developed by Gadsden et al. [66], which not only can predict the energy consumed by dwellings, but also the achievable power saving when using PV systems, solar assisted hot water or passive solar design.

Several software applications have been developed to study the distribution of solar radiation in complex cities. One of the most important is Heliodon. This tool, designed by Benoit Beckers and Luc Masset, graphically represents the solar irradiance reaching building façades. However, to minimize the computation time, it only considers the direct component of solar radiation [67]. Additionally, Solene software, designed by the Centre de Recherche Méthodologique d'Architecture (CERMA) analyzes sunlight in cities [68]. It allows determining shadows between buildings as well as daylight both inside and outside a building. Accordingly, it is quite useful as a tool for architects who can easily simulate daylight when deciding window distribution on façades and roofs.

In this paper a new characterization of the solar radiation reaching the building façades of neighborhoods of different typologies is presented. As an innovation, it considers not only direct solar radiation but also the diffuse and reflected components. In that way, a new framework for characterizing solar radiation reaching building façades in urban environments is provided. This framework is applied in two neighborhoods with different typologies in Cordoba (Spain) in order to determine the influence of the neighborhood morphology on solar access. Finally, a new correlation to estimate the solar radiation on the façades of the buildings of each neighborhood has been determined.

5.2. Data: neighborhoods selected

In this paper, two different neighborhoods of Cordoba (Spain) have been analyzed. Cordoba is made up of different typologies of neighborhoods. Specifically, the oldest ones, located near the center, present irregular net. However, since the middle of the 20th century, the growth of the city has been planned in advance in order to design a street layout capable of distributing the traffic flow through the neighborhoods and to improve accessibility to buildings In addition, due to the high temperatures registered in summer in Cordoba, recent buildings have recreational spaces such as swimming pools, areas of play, etc.

5.2.1. Case A. U-shaped blocks and L-shaped blocks neighborhood

In this first case, a neighborhood made up of “U-shaped” and “L-shaped” blocks (Figure 5.1) is studied. This building structure is nowadays the most common solution for the growth of the city selected, Cordoba. This urban development planning is conceived for a horizontal growth of the city and the roads and the blocks of the neighborhood maintain an “orthogonal urban net”. These neighborhoods are characterized by low population density, high accessibility and extensive recreational spaces among buildings [116,117].

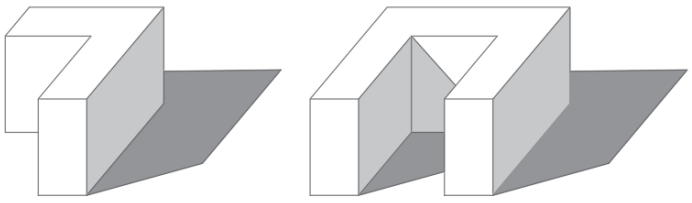

Figure 5.1. L-Shaped and U-Shaped blocks

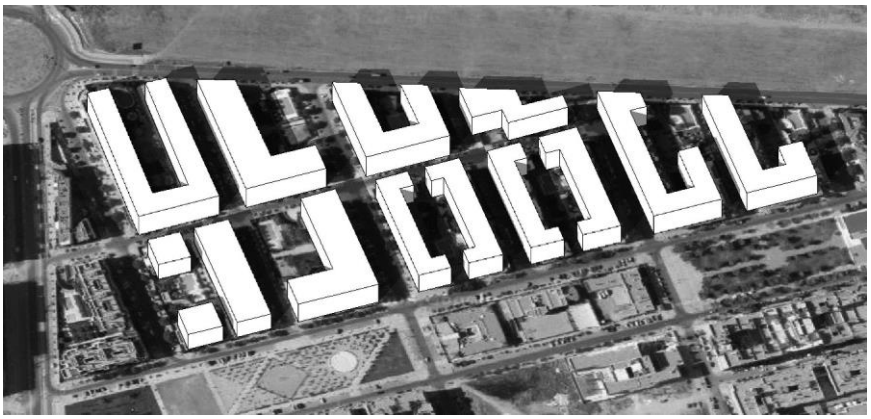

Figure 5.2. 3D view of a U-shaped and L-shaped neighborhood (Case A) of Cordoba (Spain).

For this first study, the neighborhood selected, which will be denoted by the letter A, is located in the north of Cordoba (37°53'50.0"N 4°47'50.6"W) and was built in 2007 (Figure 5.2). Since it is a real neighborhood, it is made up of different kinds of buildings. However, most of them are U-shaped and L-shaped blocks or have a similar structure with two-by-two parallel façades. Accordingly, it will be considered as a U-shaped and L-shaped block neighborhood.

Figure 5.3 shows the perimeter and the height of all the buildings of neighborhood A. Specifically, the buildings of neighborhood A have an average height of 17 meters [116].

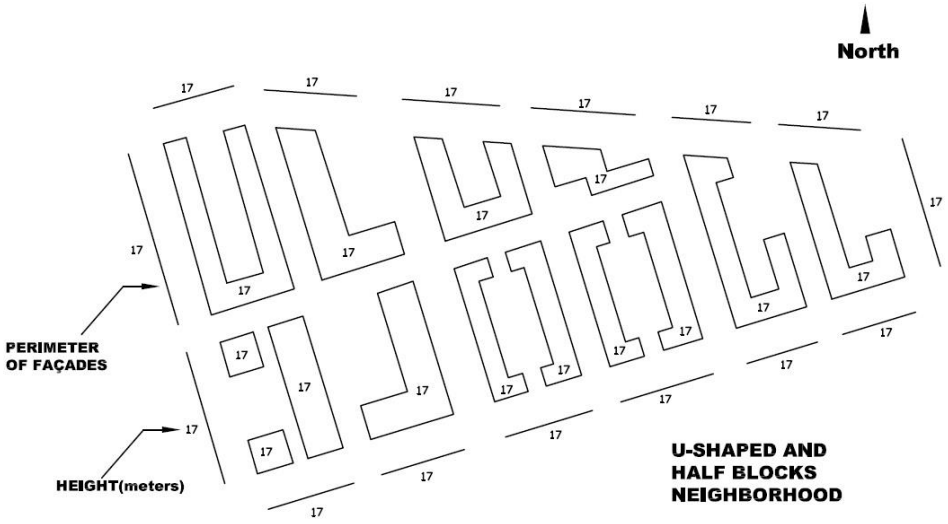

Figure 5.3. Perimeter and heights of the buildings of a U-shaped and L-shaped block neighborhood (Case A) of Cordoba (Spain).

5.2.2. Case B. Grouped blocks neighborhood

Secondly, a neighborhood made up of “grouped blocks” (Figure 5.4) is considered. This typology of urban planning is often used when the available space is reduced. This usually happens when an old block located in the center of a city is pulled down and a new one is rebuilt in its place. In this context, the roads and the street layout cannot be modified so that the number of dwellings planned will determine the height of the building and its population density.

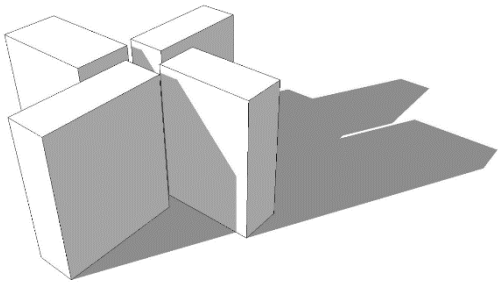

Figure 5.4. Grouped blocks

In this case, the neighborhood selected, B (Figure 5.5), is situated in a consolidated area of the city of Cordoba (37°52'57.7"N 4°47'48.3"W) and it was built in the sixties. The buildings have the maximum height allowed in Cordoba, that is, 7 floors and, consequently, their average height is 25 meters [116].

The building configuration used in this neighborhood is the “grouped blocks” with a distribution of attached buildings in which most of the façades are external. The available space between the blocks is used for recreational uses, gardens, etc. This is a common case of vertical growth of the city. Figure 5.6 shows the perimeter and the height of all the buildings of the neighborhood B studied.

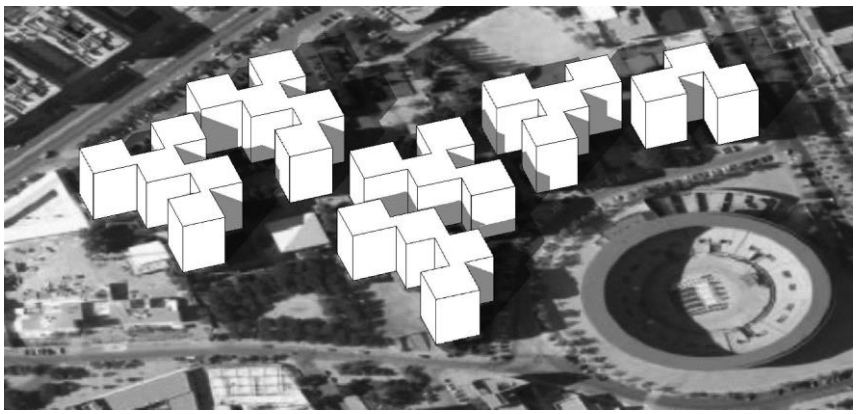

Figure 5.5. 3D view of a grouped block neighborhood (Case B) of Cordoba (Spain)

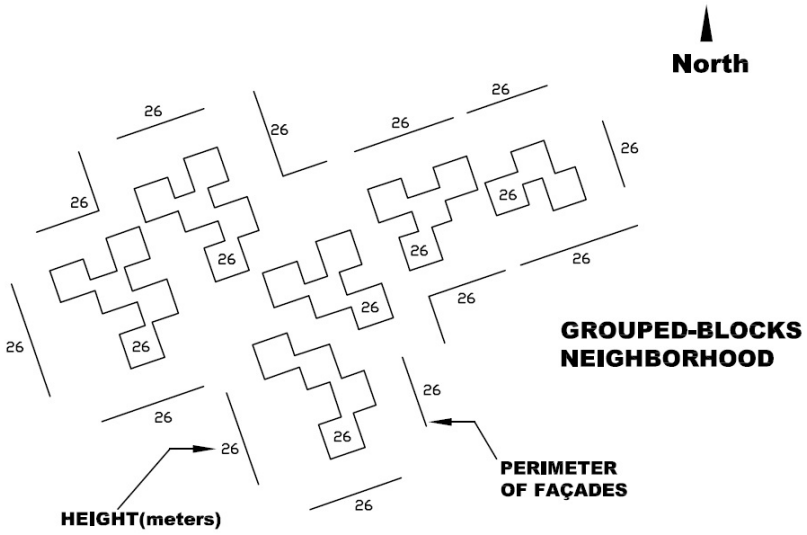

Figure 5.6. Perimeter and heights of the buildings of a grouped block neighborhood (Case B) of Cordoba (Spain)

5.3. Methodology

To describe the solar radiation reaching the building façades of a neighborhood and its dependence on the neighborhood typologies, firstly, the level of solar radiation received on different points of the façades of the buildings of each selected neighborhood is determined. For this purpose, a dimensionless factor called "Urban Solar Coefficient" (USC) is proposed (Eq. (5.1)). This factor is defined as the proportion between the annual average solar radiation reaching a particular point of a façade of a neighborhood, $\overline{H_{g,a,p}}$ (in kWh/m^2), and the annual average horizontal solar radiation in the neighborhood, $\overline{H_{g,a}}$ (in kWh/m^2). Thus, the parameter USC represents a measure of the capacity of an urban environment to access the solar resource.

$$USC = \frac{\overline{H_{g,a,p}}}{\overline{H_{g,a}}} \tag{5.1}$$

This dimensionless parameter is exclusive for each point of a façade and it represents its solar capacity. Due to the effect of the shadows of neighboring buildings, the level of solar radiation reaching a specific point of a building façade depends on the geometry of the neighborhood (height of the point studied, distance to other façades and so on). Once the USC of each point of each façade has been computed, a statistical analysis of the USC values obtained is developed. From the USC data for the façades of all the buildings of each neighborhood, different regression models have been estimated to determine the dependence of USC on the neighborhood geometry factors. According to this, a simple and accurate empirical mathematical expression for the dependence of USC on the geometry for each neighborhood has been proposed (Eq. (5.2)):

$$USC\ (H, D, \theta) = c_1 + c_2 \cdot H + c_3 \cdot D + c_4 \cdot \sin \theta_{ff} + c_5 \cdot cos\theta_{ff} \quad (5.2)$$

where:

H: Height of the studied point (in meters)

D: Distance between the façade studied and the closest one (in meters)

θ_{ff}: Façade facing (in degrees)

c_1, c_2, c_3, c_4, c_5: Correlation coefficients. They may be estimated for each neighborhood typology.

5.3.1. Solar radiation model

In order to obtain the existing correlation, for each typology of neighborhood, between the different variables and the Urban Solar Coefficient (USC) on every point of the façades, the proposed tool uses a specific solar radiation model that considers the three components of the global solar irradiance received on a façade, that is, direct, diffuse and reflected irradiance. Among these three components, global solar irradiance depends mainly on direct irradiance which comes straight from the sun without being scattered. Diffuse irradiance is the solar irradiance reaching the façade after having been scattered from the direct solar beam. Finally, in cities, reflected irradiance, that is, the irradiance reflected by any other surface or façade, must also be considered. Its intensity depends on the reflection coefficient or albedo of other surfaces. Thus, the global solar irradiance received on a façade is given by Eq. (5.3).

$$I = \frac{\vec{n} \cdot \vec{s}}{\vec{k} \cdot \vec{s}} \cdot I_b + \frac{l + \vec{n} \cdot \vec{k}}{2} \cdot I_d + \frac{l - \vec{n} \cdot \vec{k}}{2} \cdot \rho \cdot (I_b + I_d) \quad (5.3)$$

where:

$\vec{n}$: Normal vector to the external surface of the façade of the building

$\vec{s}$: Solar vector

$\vec{k}$: Normal vector of the tangent plane of the location considered

ρ: Albedo

I_b: Direct irradiance on horizontal surface

I_d: Diffuse irradiance on horizontal surface

In this solar radiation model, the direct (I_b) and diffuse (I_d) irradiances on horizontal surface have been estimated from synthetic series of data of horizontal global radiation. These series are based on 10-year daily measurements. Thus, global solar radiation for a specific period of time can be determined by integrating, over the time, the global irradiance (I) on a point given by Eq. (5.3).

However, Eq. (5.3) shows poor results when estimating solar radiation on façades since it does not consider the influence of the height on the diffuse and reflected irradiance. In order to improve this method, a new expression has been developed considering that diffuse and reflected irradiance depend on the portion of sky seen from the studied point. That is, a point with a great height will see a bigger portion of the sky vault and it will receive more diffuse irradiance. On the other hand, a point located close to the floor will see a greater portion of the neighboring buildings so that irradiance reflected from them will be greater. To quantify this behavior, a dimensionless term, called Sky View Factor (SVF) has been defined. It estimates the portion of the celestial vault seen from a specific point [118].

Accordingly, SVF will determine whether the most important component of the global solar irradiance reaching a specific point of a façade will be the diffuse or reflected irradiance (Eq. (5.4))[100].

$$I = \frac{\vec{n} \cdot \vec{s}}{\vec{k} \cdot \vec{s}} \cdot I_b + SFV \cdot I_d + (1 - SFV) \cdot \rho \cdot (I_b + I_d) \quad (5.4)$$

5.3.2. Software application for the analysis

In this paper, the average annual solar radiation on the building façades of two different neighborhoods has been studied. For this purpose, using Eq. (5.4), it is necessary to estimate the solar irradiance received on different points of each façade for all the buildings and both neighborhoods. Specifically, in each façade, 121 points are considered. In addition, each neighborhood is made up of more than 100 façades. Due to the great amount of points to analyze, different functions and subroutines in Visual Basic environment have been developed to automatize the calculation. Table 5.1 lists these subroutines.

Table 5.1. Summary of Subroutines developed

Name of Subroutine	Features
Shadow	It takes the value 0 if the point is Shaded and 1 if it is lighted
Sky View Factor	Portion of the sky seen from the point [0-0.5]
Daily Radiation	Energy in kWh/ m2 with a 6 minutes integration interval
Irradiance	Measure of the irradiance in W/m2 on the point

5.3.2.1. Shadow subroutine

This function determines whether a specific point on the façade of a building is shaded or not. The result will be 0 if the point is shaded and 1 if not.

In order to locate this point, each façade is represented in a local reference system of two orthogonal axis ρ and μ whose values range from 0 to 1 in steps of 0.1 (Figure 5.7). Thus, in each façade 121 different points can be studied.

Accordingly, the shadow function uses as input parameters the selected façade and two parameters which indicate the specific point of the façade to be studied. Additionally, other input parameters are the Julian day, the solar time and the latitude of the location of the neighborhood.

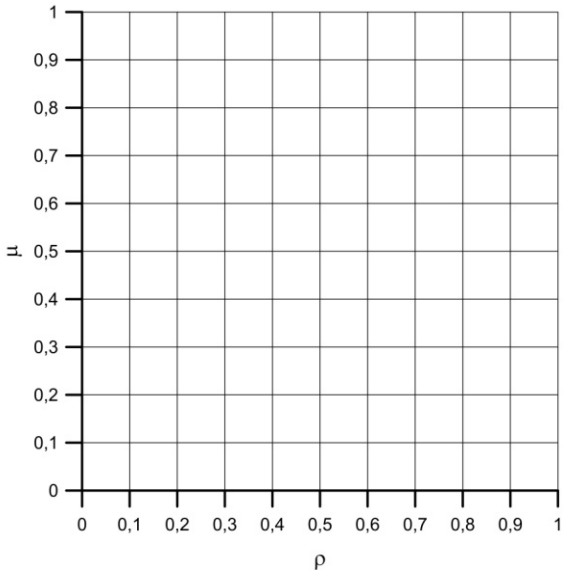

Figure 5.7. Grid façade representation

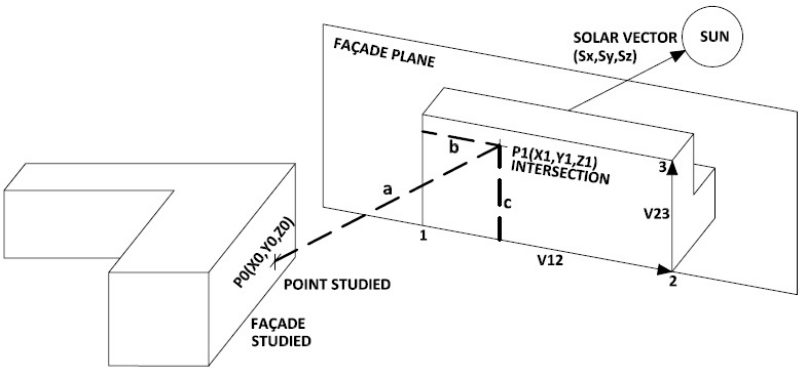

Figure 5.8. Representation of the geometric problem

To determine whether the point is shaded or lighted, first, its Cartesian coordinates are defined in the global reference system of the city. Then, for the Julian day, latitude and solar time selected, the subroutine will estimate the position of the sun and the straight line from the sun

to the façade point of study. After that, the intersections between this line and the planes representing the neighboring façades will be calculated (Figure 5.8) by solving the equation system given by Eq. (5.5). Thus, the selected façade point will be shaded if the following conditions are satisfied: a>1, 0<b<1 and 0<c<1.

$$\begin{pmatrix} X_0 \\ Y_0 \\ Z_0 \end{pmatrix} + a \begin{pmatrix} S_x \\ S_y \\ S_z \end{pmatrix} = \begin{pmatrix} X_1 \\ Y_1 \\ Z_1 \end{pmatrix} + b \begin{pmatrix} V_{12x} \\ V_{12y} \\ V_{12z} \end{pmatrix} + c \begin{pmatrix} V_{23x} \\ V_{23y} \\ V_{23z} \end{pmatrix} \quad (5.5)$$

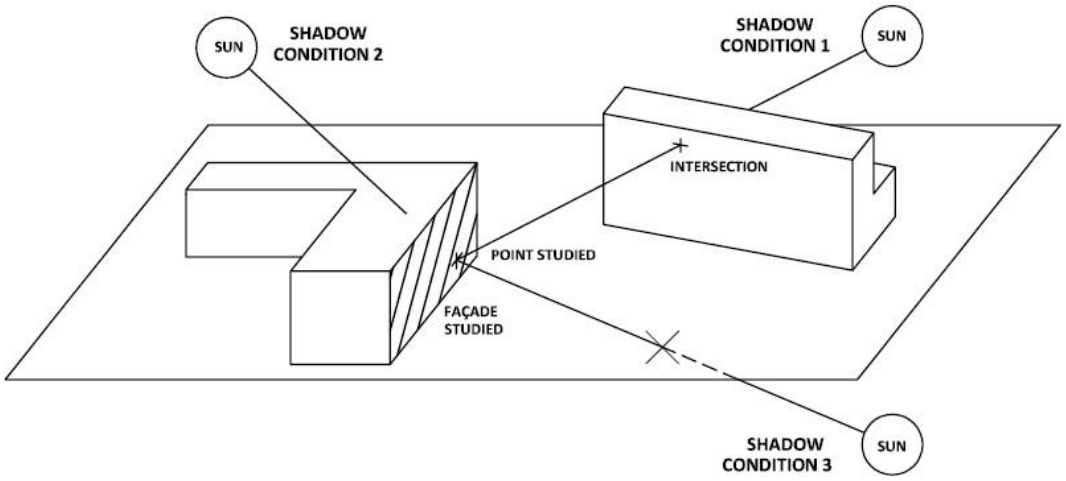

Figure 5.9. Representation of the shading conditions

Figure 5.9 shows the different situations that must be discussed when studying whether the selected point is shaded or not. The output given by the shadow subroutine will be 0 (shadowed point) when there is one intersection point on the façade of an adjacent building (condition 1), when the angle between the normal vector of the external surface of the façade and the solar vector is greater than π/2 rad (condition 2) or when the moment of time considered is before sunrise or after sunset (condition 3). In any other case, the studied point will be lighted and, consequently, the output of the Shadow Function will be 1.

5.3.2.2. Sky View Factor subroutine

A shadowed point of a façade will not receive direct solar irradiance, but diffuse or reflected irradiance could reach it. Specifically, the higher the point considered, the greater the portion of the celestial vault seen from it. Thus, the higher points of the façade receive more diffuse irradiance than the lower ones, which will receive more reflected radiation from nearby façades. Since the diffuse component of the solar radiation is greater than the reflected one, the higher points of the façade will receive higher radiation levels.

A new subroutine, called Sky View Factor (SVF), has been developed to simulate this phenomenon. Specifically, for each one of the 121 points considered on a façade, 1012 rays in different directions are generated (Figure 5.10). For each of them, it determines whether the ray points to the celestial vault or, on the contrary, it reaches the ground or a surrounding building (applying conditions defined in Figure 5.9). From that analysis, the Sky View Factor (SVF) is defined as the ratio between the number of rays pointing the celestial vault and the total amount of rays generated. Accordingly, this parameter does not depend on the time but only on the point under consideration and the geometry of the neighborhood selected. In that way, the SVF and its complementary value make it possible to calculate more realistically the diffuse and reflected solar radiation that reaches a point on the façade of a building in a neighborhood considering the obstacles posed by the buildings that surround it.

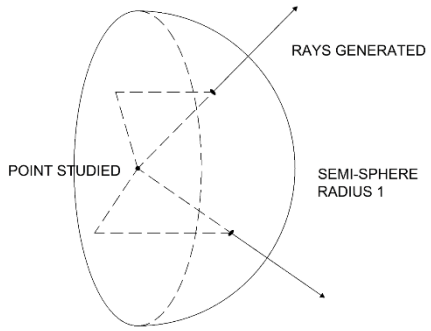

Figure 5.10. Generation of the rays on the selected point. Adapted from [119]

5.3.2.3. Instantaneous Irradiance Subroutine

This subroutine estimates the irradiance (W/ m^2) reaching a specific point of a façade at a solar time using Eq. (5.4) and considering as input data: the façade selected and the coordinates of the point under study in the local reference system, the latitude, the Julian day, the solar time, the albedo and the solar radiation on a horizontal plane at this latitude and moment of time. Specifically, to simplify the calculation, for the albedo, a mean value of 0.2 has been considered [22].

5.3.2.4. Daily Solar Radiation Subroutine

From the result of the Instantaneous Irradiance subroutine, this function calculates the daily solar radiation (kWh/m^2) for each point of the façade under study and a Julian day. Specifically, it calculates the irradiance every 6 minutes throughout each complete day, multiplies the result by 0.1 hour and adds all the values of the day obtaining the daily radiation. Accordingly, the

result of this function provides valuable information for evaluating the feasibility of a photovoltaic or thermal installation on the façade of a building.

Figure 5.11 shows the flowchart of the Visual Basic application designed for the calculations.

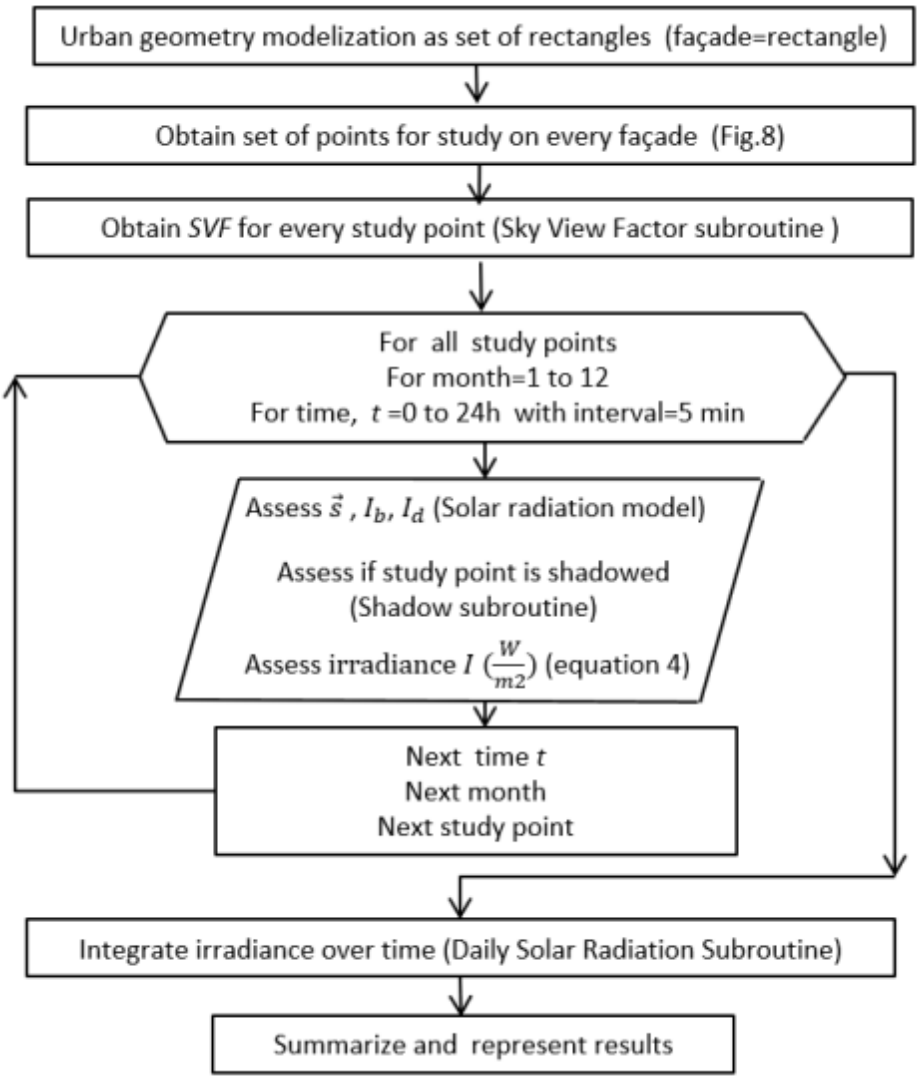

Figure 5.11. Flowchart of the Visual Basic application developed

5.4. Discussion and Regressions

As explained before, the USC value has been calculated for the 121 points considered (Figure 5.7) on each façade of neighborhoods A and B. Specifically, 14036 USC values for neighborhood A and 13673 USC values for neighborhood B have been obtained. To simplify the graphical representation and visualization of the data, an auxiliary variable, USC_{100}, is defined according to Eq. (5.6).

$$USC_{100} = 100 \cdot USC \tag{5.6}$$

Figure 5.12 shows the USC_{100} absolute frequency histogram for neighborhood A. For this representation, consecutive classes of index i have been defined so that i meets Eq. (5.7).

$$i - 1 < USC_{100} \leq i \tag{5.7}$$

This condition is equivalent to define i according to Eq. (5.8)

$$i = integer(USC_{100}) + 1 \tag{5.8}$$

Thus, as an example, if USC=0.341, it will belong to class *35*.

Similarly, Figure 5.13 shows the USC_{100} absolute frequency histogram for neighborhood B.

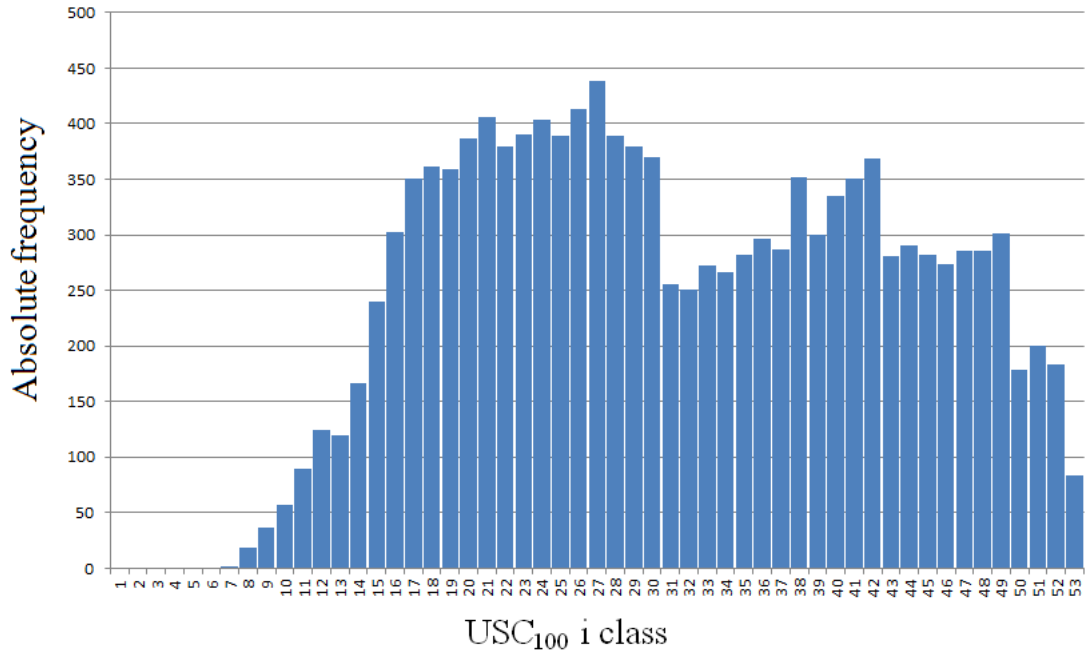

Figure 5.12. USC_{100} histogram for neighborhood A.

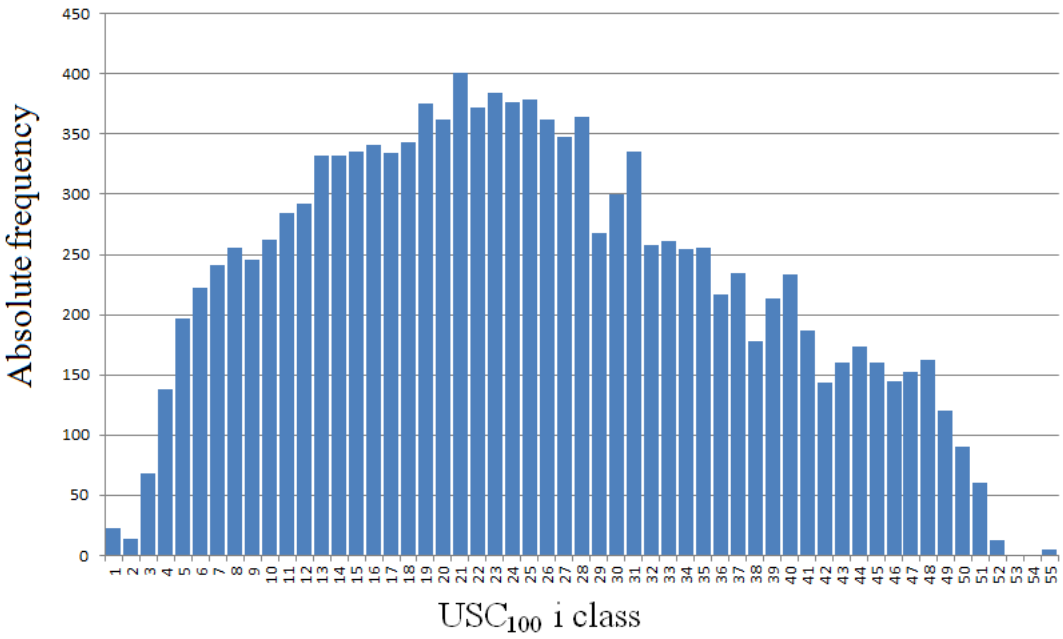

Figure 5.13. USC_{100} histogram for neighborhood B

Figure 5.12 shows a displacement of USC values in neighborhood A with respect to values in neighborhood B (Figure 5.13), which implies better access to solar resources in neighborhood A in general. This effect is linked to the lower height of the buildings in neighborhood A, as well as to the distribution in a simpler geometry. The intertwined geometry of neighborhood B favors the existence of north-facing walls that are also obstructed in all directions. Normally the lowest points of this type of façades are associated with the lowest values of the USC index. In both neighborhoods, as expected, the maximum USC values are reached at the highest points of the façades that are best oriented to the south and have a low level of obstruction. The value of the maximums of USC is slightly higher in neighborhood B, which could be explained by the greater height of the buildings and their better South orientation.

Table 5.2. Descriptive statistic values for USC in both neighborhoods

Descriptive statistic values	Neighborhood A	Neighborhood B
N sample	14036	13673
Minimum	0.063	0.012
Maximum	0.528	0.540
Average	0.317	0.260
Median	0.304	0.249
Variance	0.013	0.017
Standard Deviation	0.116	0.132

Table 5.2 shows the values of the descriptive statistics of USC for both distributions, from which significant differences in the mean and the median have been observed. Both parameters indicate that access to the solar resource is about 20% higher in neighborhood A than in neighborhood B.

The exposed methodology also allows mapping the USC_{100} variable in façades. This enables us to deepen the details of the differences in access to the solar resource at each point of the same façade. Figure 5.14 and Figure 5.15 show the variability of USC_{100} in representative façades of the neighborhoods A and B respectively. They also allow quantifying, in specific façades, the dependence of the USC_{100} gradient on the height. It is worth highlighting that in the façades analyzed, the increase of this gradient is greater on the highest points than on lowest ones. This behavior is more evident as the height of the building increases.

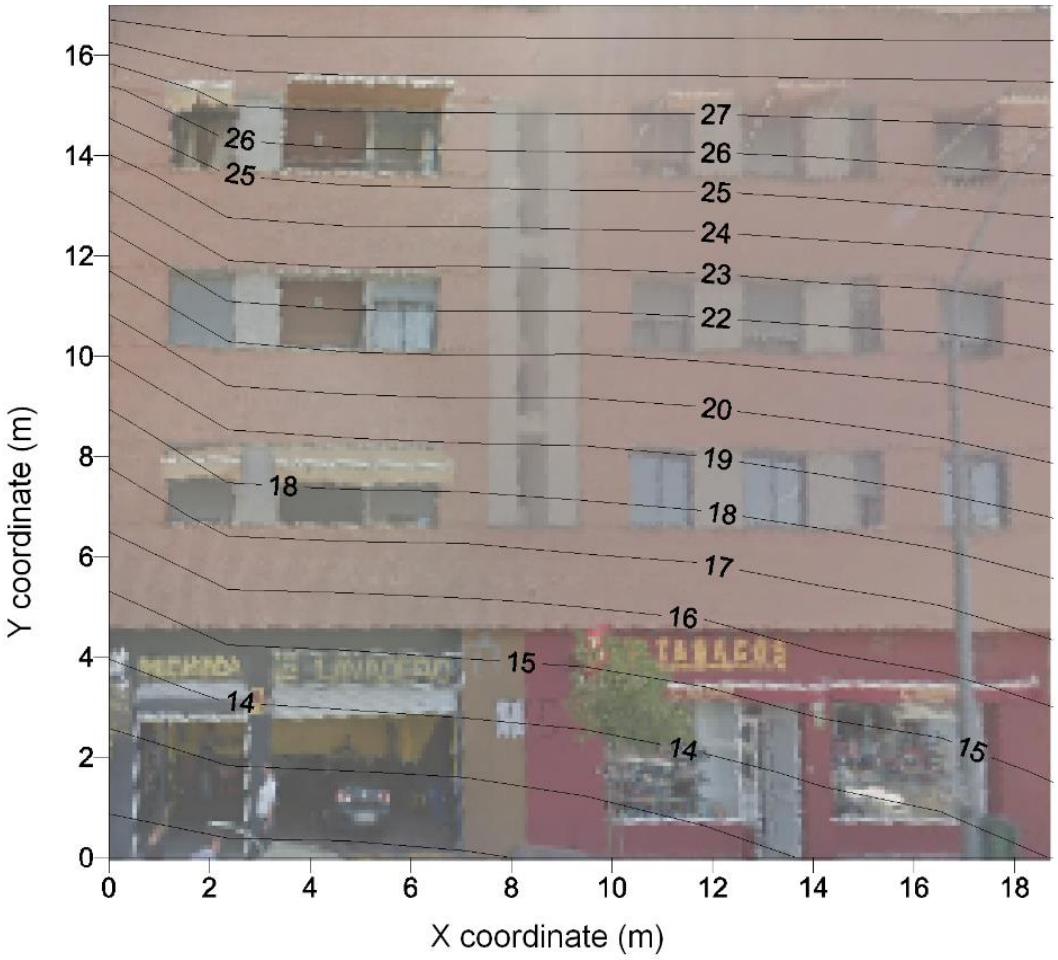

Figure 5.14. USC_{100} map for a representative façade of neighborhood A.

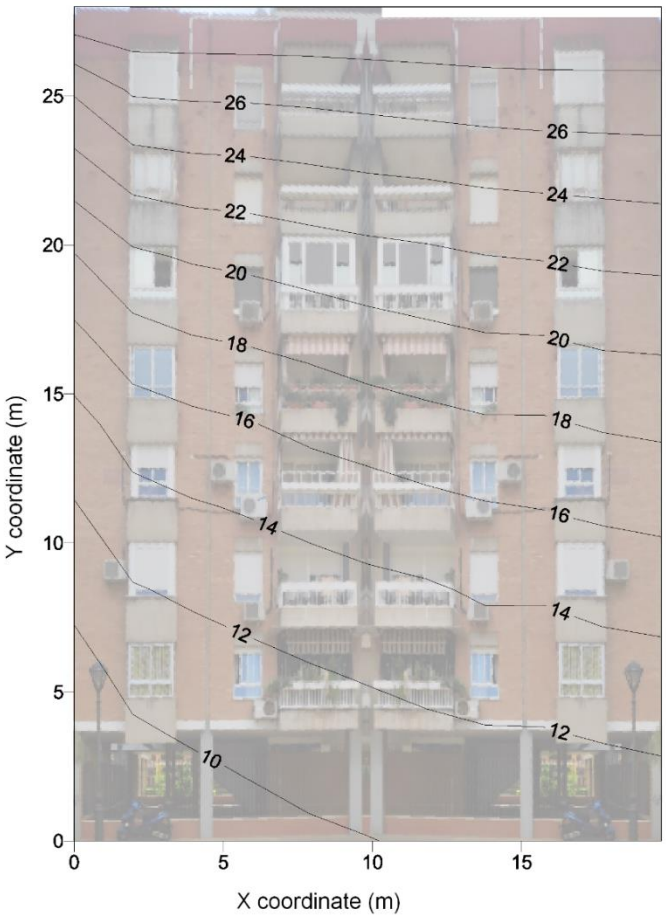

Figure 5.15. USC_{100} map for a representative façade of neighborhood B

Finally, with the USC data of all the façades and buildings, a regression analysis has been performed for each neighborhood in order to analyze the variables with the most significant influence on the USC value.

Studying the influence of façade facing, street width and height of the studied point on the outcome of the USC factor at each point studied, a linear regression is proposed (Eq. (5.9)).

$$USC\left(H,D_s,\theta_{ff}\right)=k_1+k_2\cdot H+k_3\cdot D_s+k_4\cdot cos\theta_{ff} \quad (5.9)$$

where

H: Height of the studied point over the ground (in meters)

D_s: Street width (in meters)

θ_{ff} : Façade facing (in degrees)

k_1, k_2, k_3, k_4: Constants

Eq. (5.10) shows the result of the regression for neighborhood A. It is observed that the height of the studied point over the floor and the street width keep a direct relationship with the USC factor while in the case of the cosine of the orientation of the façade is reversed. Its correlation coefficient has a value of 0.919.

$$USC(H, D_s, \theta_{ff}) = 0.197 + 0.012 \cdot H + 0.001 \cdot D_s - 0.115 \cdot cos\theta_{ff} \quad (5.10)$$

On the other hand, the regression for neighborhood B (Eq. (5.11)) has a correlation value of 0.86 which is lower than the value obtained for neighborhood A. In this case, as in the previous one, the influence of the height of the point considered and the street width is direct and the orientation of the façade reverse.

$$USC(H, D_s, \theta_{ff}) = 0.074 + 0.010 \cdot H + 0.002 \cdot D_s - 0.091 \cdot cos\theta_{ff} \quad (5.11)$$

These regressions allow knowing the value of USC factor, and therefore the annual radiation received at any point on the façade chosen, knowing only the typology of the neighborhood and the annual radiation on a horizontal surface.

5.5. Conclusions

In this paper, a novel model for calculating the solar radiation that reaches the façade of a building in a complex neighborhood is presented. The equation proposed allows obtaining accurate results for the irradiance, considering how the position of the adjacent buildings affects to the diffuse and reflected irradiance received on the façade. For this purpose, the Sky View Factor (SVF) is calculated. Considering the obstacles posed by surrounding buildings, it represents the portion of celestial vault viewed from each point of the façade. Accordingly, the SVF depends on the position of the point on the façade of the building but remains constant as long as the geometry of the neighborhood is not altered.

Four subroutines, programmed in Visual Basic Excel environment, have been developed to solve the problem of shading, the quantification of the obstacles seen, and the radiation received on a complete façade. Therefore, these subroutines allow the calculation of the solar radiation reaching any point of a selected façade of a neighborhood. From it, it is possible to display the results of the radiation on the façade in an intuitive way, through a solar radiation contour map.

The model and the program created have been used to characterize two typologically different neighborhoods through their capacity for the solar energy harnessing. To this aim, the Urban Solar Coefficient (USC) has been defined, relating the annual radiation on horizontal surface of the study area and the annual radiation received at a chosen point on a façade. Calculating this

factor on 121 points on each façade and for all the façades compounding the neighborhood, the distribution of the USC values for each neighborhood and the two different histograms that characterize the radiation according to the urban typology have been obtained. A comparative statistical analysis of the USC data for each neighborhood shows that the maximum values of USC are registered in neighborhood B (0.540) since its buildings are higher than the ones in neighborhood A, with a relative maximum USC value of 0.528. To the contrary, the relative minimum value in neighborhood A (0.063) is higher than in neighborhood B (0.012) due to the fact that the geometry of the neighborhood A is simpler, and its building are lower and more separated which reduces the effect of obstacles. On the whole, the mean value is higher in neighborhood A (0.317) than in neighborhood B (0.260) which implies a best access to solar resources in the first area than in the second one.

Finally, with the results obtained, one regression for each neighborhood has been proposed to determine the dependence of USC on geometry of the buildings. These regressions allow calculating easily the amount of radiation received on the points of the façades, in neighborhoods that meet the characteristics described in this paper. In this way, the methodology and the tool proposed provide the calculation of the solar irradiance incident on any point of the façade of a given neighborhood. However, the tool presents some limitations and it is planned to be improved in upcoming works with the inclusion of a new subroutine that represents in 3D contour maps the values of irradiance in all the facades of the buildings of a certain neighborhood. Likewise, a network of sensors is being designed to automatically monitor the experimental irradiance received on a given façade in order to validate the methodology and tool proposed in this work.

Despite these limitations, the methodology and tool proposed could be very useful, among other applications, to plan urban designs of new neighborhoods that guarantee the solar rights and favor an optimum harnessing of the solar resource, whether for natural lighting or for the generation of energy from renewable sources, which will have a positive impact on the sustainability of cities.

.

Capítulo 6 .
Conclusiones

6.1. Conclusiones del primer artículo

6.2. Conclusiones del segundo artículo

6.3. Conclusiones del tercer artículo

En la tesis presentada se analizan los resultados de la implementación de un estudio matemático de seguidores solares que busca la maximización de la captación energética; de un enfoque novedoso de retroseguimiento ante la problemática del sombreo; y de una metodología que trata de evaluar el acceso solar en edificios urbanos.

Se muestran a continuación las conclusiones de este trabajo distribuidas por cada uno de los artículos académicos que lo conforman.

6.1. Conclusiones del primer artículo

En el primer artículo, se ha obtenido la deducción de las ecuaciones generales que optimizan captación energética de la radiación de los colectores instalados en sistemas de seguimiento de un eje, Ecuación (3.35), y de dos ejes, Ecuación (3.50).

$$\vec{n} = \left(cos\,\chi - \frac{\left(\frac{\partial I}{\partial(\vec{s}\cdot\vec{n})}\vec{s}\cdot\vec{e} + \frac{\partial I}{\partial(\vec{k}\cdot\vec{n})}\vec{k}\cdot\vec{e}\right) sin\,\chi}{\sqrt{\left(\frac{\partial I}{\partial(\vec{s}\cdot\vec{n})}\right)^2 + \left(\frac{\partial I}{\partial(\vec{k}\cdot\vec{n})}\right)^2 + 2\left(\frac{\partial I}{\partial(\vec{s}\cdot\vec{n})}\right)\left(\frac{\partial I}{\partial(\vec{k}\cdot\vec{n})}\right)\vec{s}\cdot\vec{k} - \left(\frac{\partial I}{\partial(\vec{s}\cdot\vec{n})}\vec{s}\cdot\vec{e} + \frac{\partial I}{\partial(\vec{k}\cdot\vec{n})}\vec{k}\cdot\vec{e}\right)^2}} \right)\vec{e}$$

$$+ \left(\frac{sin\,\chi\,\frac{\partial I}{\partial(\vec{s}\cdot\vec{n})}}{\sqrt{\left(\frac{\partial I}{\partial(\vec{s}\cdot\vec{n})}\right)^2 + \left(\frac{\partial I}{\partial(\vec{k}\cdot\vec{n})}\right)^2 + 2\left(\frac{\partial I}{\partial(\vec{s}\cdot\vec{n})}\right)\left(\frac{\partial I}{\partial(\vec{k}\cdot\vec{n})}\right)\vec{s}\cdot\vec{k} - \left(\frac{\partial I}{\partial(\vec{s}\cdot\vec{n})}\vec{s}\cdot\vec{e} + \frac{\partial I}{\partial(\vec{k}\cdot\vec{n})}\vec{k}\cdot\vec{e}\right)^2}} \right)\vec{s} \qquad (3.35)$$

$$+ \left(\frac{sin\,\chi\,\frac{\partial I}{\partial(\vec{k}\cdot\vec{n})}}{\sqrt{\left(\frac{\partial I}{\partial(\vec{s}\cdot\vec{n})}\right)^2 + \left(\frac{\partial I}{\partial(\vec{k}\cdot\vec{n})}\right)^2 + 2\left(\frac{\partial I}{\partial(\vec{s}\cdot\vec{n})}\right)\left(\frac{\partial I}{\partial(\vec{k}\cdot\vec{n})}\right)\vec{s}\cdot\vec{k} - \left(\frac{\partial I}{\partial(\vec{s}\cdot\vec{n})}\vec{s}\cdot\vec{e} + \frac{\partial I}{\partial(\vec{k}\cdot\vec{n})}\vec{k}\cdot\vec{e}\right)^2}} \right)\vec{k}$$

$$\vec{n} = \frac{\frac{\partial I}{\partial(\vec{s}\cdot\vec{n})}\vec{s} + \frac{\partial I}{\partial(\vec{k}\cdot\vec{n})}\vec{k}}{\sqrt{\left(\frac{\partial I}{\partial(\vec{k}\cdot\vec{n})}\right)^2 + \left(\frac{\partial I}{\partial(\vec{k}\cdot\vec{n})}\right)^2 + 2\left(\frac{\partial I}{\partial(\vec{s}\cdot\vec{n})}\right)\left(\frac{\partial I}{\partial(\vec{k}\cdot\vec{n})}\right)\vec{s}\cdot\vec{k}}} \qquad (3.50)$$

Las ecuaciones (3.35) y (3.50) son genéricas para cualquier sistema de seguimiento continuo, no siendo necesaria la simetría en las posiciones del seguidor respecto al plano meridiano. El seguimiento astronómico, propuesto por numerosos autores como el sistema de seguimiento óptimo, debe ser comprobado en cada caso (tipo de aprovechamiento y modelo validado que

explique satisfactoriamente la irradiancia). En consecuencia, no debe considerarse a priori como el sistema más adecuado en todos los casos.

Los casos estudiados permiten observar cómo el movimiento astronómico puede proporcionar captaciones energéticas inferiores a las determinadas cuando se utilizan los valores de $\vec{n}$ dados por las ecuaciones (3.35) o (3.50).

Las ecuaciones propuestas incluyen al modelo de seguimiento astronómico si se considera como irradiancia útil la dada por la ecuación (3.16). Otros modelos que dan peso a la componente difusa de la irradiancia hacen que el vector $\vec{n}$ incorpore una componente en dirección $\vec{k}$ respecto al modelo astronómico. Esto es, predicen que el plano colector debe estar más horizontal que en el modelo astronómico.

En los modelos más sencillos de irradiancia, las ecuaciones (3.16), (3.17) y (3.18), las derivadas parciales con respecto a $\vec{s} \cdot \vec{n}$ y $\vec{n} \cdot \vec{k}$, dan lugar a expresiones matemáticas independientes de $\vec{n}$. En estos casos, las ecuaciones (3.35) y (3.50) proporcionan directamente el valor de $\vec{n}$ para una situación de captación óptima. Cuando las derivadas parciales dependen de $\vec{n}$, las ecuaciones (3.35) y (3.50) también pueden ser resueltas. Para estos casos, se recomienda el método numérico de iteración. Se ha podido comprobar experimentalmente que, sustituyendo en el segundo miembro de las ecuaciones (3.35) y (3.50), los valores de una aproximación $\vec{n}^{(i)}$ de $\vec{n}$, se obtiene en el miembro de la izquierda $\vec{n}^{(i+1)}$. Siendo $\vec{n}^{(i+1)}$una aproximación mejor que $\vec{n}^{(i)}$. Se recomienda iniciar las iteraciones a partir de $\overrightarrow{n}^{(0)} = \vec{s}$. En todos los casos, la convergencia permite finalizar con menos de veinte iteraciones.

Una reflexión sobre el movimiento de los seguidores solares basados en sensores -que buscan permanentemente la posición del plano colector que optimiza la irradiancia interceptada- hace pensar que este movimiento es más aproximado al calculado con las ecuaciones (3.35) y (3.50) (utilizando el modelo de irradiancia adecuado) que al astronómico. Bajo esta perspectiva, se deduce que las ecuaciones (3.35) y (3.50) predicen el movimiento de seguidores basados en sensores que optimizan la irradiancia en el plano colector.

6.2. Conclusiones del segundo artículo

En el segundo artículo, se propone una nueva metodología para definir la estrategia de seguimiento óptima sin sombreo en conjuntos de seguidores fotovoltaicos. En contraste con el seguimiento astronómico, el método propuesto indica que los colectores no tienen que estar constantemente perpendiculares a los rayos solares directos, ya que considera todas las componentes de la irradiancia (la directa pero también la difusa y la reflejada) que llegan a los colectores fotovoltaicos.

De esta manera, cuando los colectores no están sombreados, se propone una trayectoria de seguimiento que busque la máxima irradiancia en los colectores. Sin embargo, cuando la estrategia anterior genera a sombreo entre colectores, se propone el retroseguimiento. Este método analiza el sombreado entre los colectores basándose en los conceptos de vectores solares y álgebra vectorial. La técnica propuesta se basa en la existencia o no de intersecciones de polígonos frente a la habitual basada en el cálculo del área de intersecciones de dichos polígonos. En consecuencia, a diferencia de otras estrategias de seguimiento encontradas en estudios revisados, este novedoso método se basa en algoritmos que son significativamente más simples y rápidos. Así, por sus novedades y ventajas, este método es más fácil de utilizar para simular la producción de energía con diferentes modelos radiativos. Igualmente, es aplicable a situaciones en las que no se pueden encontrar métodos genéricos publicados, como en el caso de las plantas fotovoltaicas:

i. con colectores de superficie no rectangular

ii. con colectores que no están ubicados en los nodos regulares de un mallado geométrico

iii. con diferentes modos de seguimiento

iv. con seguidores situados en superficies topográficas reales

La producción de energía de las plantas fotovoltaicas con esta nueva estrategia de seguimiento, denominada MIBT (seguimiento de Máxima Irradiancia con BackTracking), ha sido analizada y comparada con dos estrategias de seguimiento ideales:

1) ATNS (seguimiento astronómico sin sombreo): Seguimiento astronómico en una planta fotovoltaica ideal donde las distancias entre los colectores son lo suficientemente grandes como para evitar sombras.

2) MITNS (seguimiento de máxima irradiancia sin sombreo): seguimiento óptimo que busca los máximos niveles de irradiancia en un colector aislado ideal no afectado por las sombras potenciales de colectores contiguos [15]. Este sería el método propuesto el primer artículo de la tesis. Este tipo de seguimiento daría lugar a una producción teórica máxima potencial, inalcanzable en instalaciones con múltiples colectores.

Los resultados muestran que el MIBT mejora la captación de energía en un 1,31% en comparación con el ATNS, y que la captación de energía es sólo un 0,89% inferior a la de las instalaciones del MITNS. Por lo tanto, considerando estos resultados y las ventajas de este método, se considera que

este no solo será útil para el diseño de nuevas instalaciones, sino que también podría ayudar a mejorar la productividad y la gestión de múltiples plantas fotovoltaicas mediante la redefinición de las estrategias de seguimiento.

6.3. Conclusiones del tercer artículo

En el tercer artículo, se presenta un novedoso modelo para el cálculo de la radiación solar que llega a la fachada de un edificio en un conjunto urbano arquitectónicamente complejo. La ecuación (5.4) propuesta permite obtener resultados precisos de la irradiancia considerando cómo la posición de los edificios adyacentes afecta a la irradiancia difusa y reflejada recibida en la fachada. Para este propósito, se calcula el Factor de Visión del Cielo (SVF). Considerando los obstáculos que plantean los edificios circundantes, el SVF representa la parte eficaz la bóveda celeste visible desde cada punto de la fachada. En consecuencia, el SVF depende de la posición del punto en la fachada del edificio y de los edificios circundantes.

$$I = \frac{\vec{n} \cdot \vec{s}}{\vec{k} \cdot \vec{s}} \cdot I_b + SFV \cdot I_d + (1 - SFV) \cdot \rho \cdot (I_b + I_d) \tag{5.4}$$

donde:

$\vec{n}$: vector normal a la superficie externa de la fachada del edificio

$\vec{s}$: vector solar

$\vec{k}$: vector normal del plano tangente de la localización considerada

ρ: Albedo

I_b: irradiancia directa sobre la superficie

I_d: irradiancia difusa sobre superficie horizontal

Se han desarrollado cuatro subrutinas, programadas en el entorno Visual Basic Excel, para resolver el problema del sombreado, la cuantificación de los obstáculos vistos y la radiación recibida en una fachada completa. Por lo tanto, estas subrutinas permiten calcular la radiación solar que llega a cualquier punto de una fachada seleccionada de un barrio. Partiendo de estas subrutinas, es posible visualizar los resultados de la radiación en la fachada de forma intuitiva, a través de mapas de contorno de radiación solar.

El modelo y el programa creado han servido para caracterizar la capacidad para el aprovechamiento de la energía solar de dos barrios de tipología constructiva. Para ello, se ha definido el Coeficiente Solar Urbano (USC), que relaciona la radiación anual recibida en un punto elegido de una fachada y la radiación anual sobre la superficie horizontal del área de estudio. Calculando este factor en 121

puntos de cada fachada (ejemplo en la Figura 5.14), y para todas las fachadas representativas de los barrios elegidos, se han obtenido la distribución de los valores de USC para cada barrio y los dos histogramas que caracterizan la radiación según la tipología urbana.

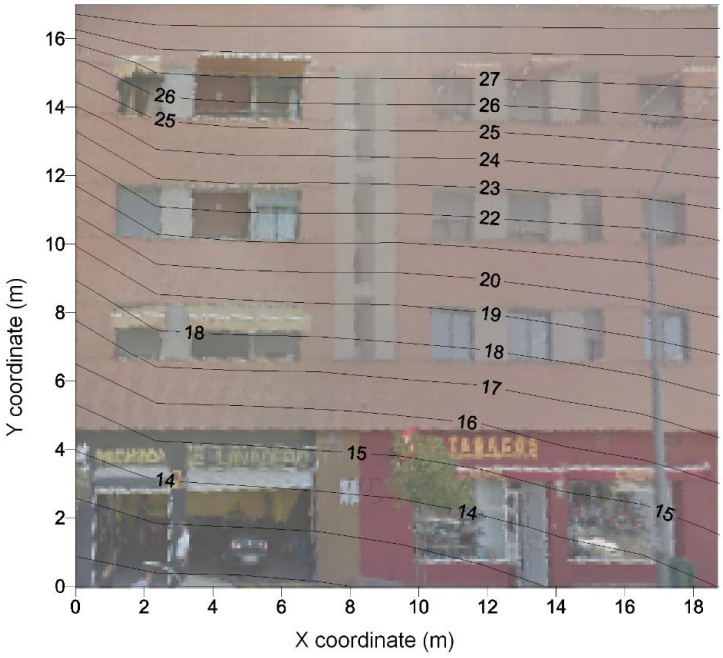

Figura 5.14. Mapa USC_{100} para la fachada de un edificio representativo del barrio A

Un análisis estadístico comparativo de los datos de USC para cada barrio muestra que los valores máximos de este coeficiente se registran en el barrio B (0,540) ya que sus edificios son más altos que los del barrio A, con un valor máximo relativo de USC de 0,528. Por el contrario, el valor mínimo relativo en el barrio A (0,063) es mayor que en el barrio B (0,012) debido a que la geometría del barrio A es más simple y sus construcciones más bajas y dispersas, lo que reduce el efecto de los obstáculos. En general, el valor medio es mayor en el barrio A (0,317) que en el barrio B (0,260), lo que implica un mejor acceso a los recursos solares en la primera zona que en la segunda.

Finalmente, con los resultados obtenidos, se ha propuesto una regresión en cada barrio para determinar la dependencia de USC respecto a la geometría de los edificios. Estas regresiones, basadas en la ecuación (5.2) permiten calcular fácilmente la cantidad de radiación recibida en los puntos de las fachadas en los barrios que cumplen las características descritas en esta tesis.

$$USC\ (H, D, \theta) = c_1 + c_2 \cdot H + c_3 \cdot D + c_4 \cdot \sin \theta_{ff} + c_5 \cdot cos\theta_{ff} \quad (5.2)$$

donde:

H: es la altura del punto estimado (m)

D: Distancia entre la fachada estudiada y la más próxima (m)

θ_{ff}: Orientación de la fachada (°)

c_1, c_2, c_3, c_4, c_5: Coeficientes de correlación.

Sin embargo, la herramienta presenta algunas limitaciones y está previsto mejorarla en próximos trabajos con la inclusión de una nueva subrutina que represente en los mapas de contorno 3D los valores de irradiancia en todas las fachadas de los edificios de un barrio determinado. Asimismo, se está diseñando una red de sensores para monitorizar automáticamente la irradiancia experimental recibida en una determinada fachada con el fin de validar la metodología y la herramienta propuesta.

Bibliografía

1. IEA *Global Energy & CO2 Status Report: The latest trends in energy and emissions in 2018*; 2019;

2. United Nations *World Population Prospects 2019*; 2019;

3. McLeman, R. Thresholds in climate migration. *Popul. Environ.* **2018**, *39*, 319–338.

4. Lyng, K.-A.; Brekke, A. Environmental Life Cycle Assessment of Biogas as a Fuel for Transport Compared with Alternative Fuels. *Energies* **2019**, *12*, 532.

5. Kinney, P.L. Interactions of Climate Change, Air Pollution, and Human Health. *Curr. Environ. Heal. Reports* **2018**, *5*, 179–186.

6. UNFCCC. Conference of the Parties (COP) ADOPTION OF THE PARIS AGREEMENT - Conference of the Parties COP 21. *Adopt. Paris Agreement. Propos. by Pres.* **2015**.

7. United Nations Transforming our world: the 2030 Agenda for Sustainable Development. United Nations Sustainable knowledge platform. *Sustain. Dev. Goals* **2015**.

8. Drivers of sustainable cleaner production and sustainable energy options. *J. Clean. Prod.* **2016**, *138*, 1–7.

9. Panwar, N.L.; Kaushik, S.C.; Kothari, S. Role of renewable energy sources in environmental protection: A review. *Renew. Sustain. Energy Rev.* 2011, *15*, 1513–1524.

10. Salas, V.; Olias, E. Overview of the photovoltaic technology status and perspective in Spain. *Renew. Sustain. Energy Rev.* **2009**, *13*, 1049–1057.

11. Mousazadeh, H.; Keyhani, A.; Javadi, A.; Mobli, H.; Abrinia, K.; Sharifi, A. A review of principle and sun-tracking methods for maximizing solar systems output. *Renew. Sustain. Energy Rev.* **2009**, *13*, 1800–1818.

12. Lee, C.-Y.; Chou, P.-C.; Chiang, C.-M.; Lin, C.-F. Sun Tracking Systems: A Review. *Sensors (14248220)* **2009**, *9*, 3875–3890.

13. Lorenzo, E.; Pérez, M.; Ezpeleta, A.; Acedo, J. Design of tracking photovoltaic systems with a single vertical axis. *Prog. Photovoltaics Res. Appl.* **2002**, *10*, 533–543.

14. Perpiñan, O.; Lorenzo, E.; Castro, M.A.; Eyras, R. Energy payback time of grid connected PV systems: Comparison between tracking and fixed systems. *Prog. Photovoltaics Res. Appl.* **2009**, *17*, 137–147.

15. Huld, T.; Suri, M.; Dunlop, E.D. Comparison of potential solar electricity output from fixed-inclined and two-axis tracking photovoltaic modules in Europe. *Prog. Photovoltaics Res. Appl.* **2008**, *16*, 47–59.

16. Huld, T.; Cebecauer, T.; Šúri, M.; Dunlop, E.D. Analysis of one-axis tracking strategies for

PV systems in Europe. *Prog. Photovoltaics Res. Appl.* **2010**, *18*, 183–194.

17. Lorenzo, E.; Narvarte, L.; Muñoz, J. *Tracking and back-tracking*; 2011;

18. García, M.; Marroyo, L.; Lorenzo, E.; Pérez, M. Experimental energy yield in 1.5v and 2v PV concentrators with conventional modules. *Prog. Photovoltaics Res. Appl.* **2008**, *16*, 261–270.

19. Grena, R. An algorithm for the computation of the solar position. *Sol. Energy* **2008**, *82*, 462–470.

20. Blanco-Muriel, M.; Alarcón-Padilla, D.C.; López-Moratalla, T.; Lara-Coira, M. Computing the solar vector. *Sol. Energy* **2001**, *70*, 431–441.

21. Reda, I.; Andreas, A. Solar position algorithm for solar radiation applications. *Sol. Energy* **2004**, *76*, 577–589.

22. Duffie, J.A.; Beckman, W.A. *Solar Engineering of Thermal Processes: Fourth Edition*; 2013; ISBN 9780470873663.

23. Braun, J.E.; Mitchell, J.C. Solar geometry for fixed and tracking surfaces. *Sol. Energy* **1983**, *31*, 439–444.

24. Meinel, A.B.; Meinel, M.P. *Applied solar energy*; Applied Energy, 1979;

25. Neville, R.C. Solar energy collector orientation and tracking mode. *Sol. Energy* **1978**, *20*, 7–11.

26. Narvarte, L.; Lorenzo, E. Tracking and ground cover ratio. *Prog. Photovoltaics Res. Appl.* **2008**, *16*, 703–714.

27. Riley, D.; Hansen, C. Sun-Relative Pointing for Dual-Axis Solar Trackers Employing Azimuth and Elevation Rotations. *J. Sol. Energy Eng.* **2014**, *137*, 031008.

28. Jolly, P.G. Derivation of solar angles using vector algebra. *Sol. Energy* **1986**, *37*, 429–430.

29. Sproul, A.B. Derivation of the solar geometric relationships using vector analysis. *Renew. Energy* **2007**, *32*, 1187–1205.

30. Parkin, R.E. Solar angles revisited using a general vector approach. *Sol. Energy* **2010**, *84*, 912–916.

31. Chong, K.K.; Wong, C.W. General formula for on-axis sun-tracking system and its application in improving tracking accuracy of solar collector. *Sol. Energy* **2009**, *83*, 298–305.

32. Rapp-Arrarás, Í.; Domingo-Santos, J.M. Algorithm for the calculation of the horizontal coordinates of the Sun via spatial rotation matrices. *Renew. Energy* **2009**, *34*, 876–882.

33. Díaz-Dorado, E.; Cidrás, J.; Carrillo, C. Discrete I–V model for partially shaded PV-arrays. *Sol. Energy* **2014**, *103*, 96–107.

34. Díaz-Dorado, E.; Cidrás, J.; Carrillo, C. A method to estimate the energy production of photovoltaic trackers under shading conditions. *Energy Convers. Manag.* **2017**, *150*, 433–450.

35. Martínez-Moreno, F.; Muñoz, J.; Lorenzo, E. Experimental model to estimate shading losses on PV arrays. *Sol. Energy Mater. Sol. Cells* **2010**, *94*, 2298–2303.

36. Fartaria, T.O.; Pereira, M.C. Simulation and computation of shadow losses of direct normal, diffuse solar radiation and albedo in a photovoltaic field with multiple 2-axis trackers using ray tracing methods. *Sol. Energy* **2013**, *91*, 93–101.

37. Hu, Y.; Yao, Y. A methodology for calculating photovoltaic field output and effect of solar tracking strategy. *Energy Convers. Manag.* **2016**, *126*, 278–289.

38. Perpiñán, O. Cost of energy and mutual shadows in a two-axis tracking PV system. *Renew. Energy* **2012**, *43*, 331–342.

39. Gordon, J.M.; Wenger, H.J. Central-station solar photovoltaic systems: Field layout, tracker, and array geometry sensitivity studies. *Sol. Energy* **1991**, *46*, 211–217.

40. Panico, D.; Garvison, P.; Wenger, H.; Shugar, D. Backtracking: a novel strategy for tracking PV systems. In Proceedings of the The Conference Record of the Twenty-Second IEEE Photovoltaic Specialists Conference - 1991; IEEE, 1991; pp. 668–673.

41. Pedro, M.C.-R.M. Modelling of shading effects in photovoltaic optimization. **2016**.

42. Schneider, D. Control Algorithms for Large-scale Single-axis Photovoltaic Trackers. *Acta Polytech.* **2012**, *52*.

43. Drif, M.; Pérez, P.J.; Aguilera, J.; Aguilar, J.D. A new estimation method of irradiance on a partially shaded PV generator in grid-connected photovoltaic systems. *Renew. Energy* **2008**.

44. Zhang, X.; Wei, Z. A Hybrid Model Based on Principal Component Analysis, Wavelet Transform, and Extreme Learning Machine Optimized by Bat Algorithm for Daily Solar Radiation Forecasting. *Sustainability* **2019**, *11*, 4138.

45. Alzoubi, H.H.; Alshboul, A.A. Low energy architecture and solar rights: Restructuring urban regulations, view from Jordan. *Renew. Energy* **2010**.

46. Edwards, L.; Torcellini, P. *A Literature Review of the Effects of Natural Light on Building Occupants*; Golden, Colorado, 2002;

47. Calama-González, C.; León-Rodríguez, Á.; Suárez, R. Daylighting and Energy Performance Evaluation of an Egg-Crate Device for Hospital Building Retrofitting in a Mediterranean Climate. *Sustainability* **2018**, *10*, 2714.

48. Ihm, P.; Nemri, A.; Krarti, M. Estimation of lighting energy savings from daylighting. *Build. Environ.* **2009**, *44*, 509–514.

49. Gago, E.J.; Muneer, T.; Knez, M.; Köster, H. Natural light controls and guides in buildings. Energy saving for electrical lighting, reduction of cooling load. *Renew. Sustain. Energy Rev.* **2015**, *41*, 1–13.

50. Torres-Roldán, M.; López-Luque, R.; Varo-Martínez, M. Design of an innovative and simplified polar heliostat for integration in buildings and urban environments. *Sol. Energy* **2015**, *119*, 159–168.

51. Torres-Roldán, M.; López-Luque, R.; Varo-Martínez, M. Assessment of the pointing error of heliostats with a single not polar rotation axis for urban applications. *Sol.*

Energy **2016**, *137*, 281–289.

52. Spacek, A.D.; Neto, J.M.; Biléssimo, L.D.; Junior, O.H.A.; Neto, G.P.D.F.; Giansella, R.D.S.; Santana, M.V.F. De; Malfatti, C.D.F. Proposal for an Experimental Methodology for Evaluation of Natural Lighting Systems Applied in Buildings. *Energies* **2017**, *10*, 1014.

53. Polo, M.-E.; Pozo, M.; Quirós, E. Directional Statistics in Solar Potential of Rooftops at Three Different Neighborhoods of a Medium Size City. *Proceedings* **2018**, *2*, 1275.

54. Gómez-Munoz, V.M.; Porta-Gándara, M.A. General model to build awnings and external walls with optimum shading interaction. *Renew. Energy* **2004**.

55. Smith, G.B. Materials and systems for efficient lighting and delivery of daylight. In Proceedings of the Solar Energy Materials and Solar Cells; 2004.

56. Kanters, J.; Horvat, M.; Dubois, M.C. Tools and methods used by architects for solar design. *Energy Build.* **2014**.

57. Brito, M.C.; Freitas, S.; Guimarães, S.; Catita, C.; Redweik, P. The importance of facades for the solar PV potential of a Mediterranean city using LiDAR data. *Renew. Energy* **2017**.

58. Bayón-Cueli, C.; Barbón, A.; Bayón, L.; Barbón, N. A cost-energy based methodology for small-scale linear Fresnel reflectors on flat roofs of urban buildings. *Renew. Energy* **2020**, *146*, 944–959.

59. Mingfang, T. Solar control for buildings. *Build. Environ.* **2002**.

60. Salazar Trujillo, J.H. Solar Performance and Shadow Behaviour in Buildings. Case Study with Computer Modelling of a Building in Loranca, Spain. *Build. Environ.* **1998**.

61. Gómez-Muñoz, V.M.; Porta-Gándara, M.A.; Fernández, J.L. Effect of tree shades in urban planning in hot-arid climatic regions. *Landsc. Urban Plan.* **2010**.

62. Shao, J. Calculation of sunshine duration and saving of land use in urban building design. *Energy Build.* **1990**.

63. La Gennusa, M.; Lascari, G.; Rizzo, G.; Scaccianoce, G.; Sorrentino, G. A model for predicting the potential diffusion of solar energy systems in complex urban environments. *Energy Policy* **2011**.

64. Abd Alla, S.; Bianco, V.; Tagliafico, L.A.; Scarpa, F. An innovative approach to local solar energy planning in Riva Trigoso, Italy. *J. Build. Eng.* **2020**, *27*, 100968.

65. Mardaljevic, J.; Rylatt, M. Irradiation mapping of complex urban environments: An image-based approach. In Proceedings of the Energy and Buildings; 2003.

66. Gadsden, S.; Rylatt, M.; Lomas, K.; Robinson, D. Predicting the urban solar fraction: A methodology for energy advisers and planners based on GIS. In Proceedings of the Energy and Buildings; 2003.

67. Antaluca, E.; Merino, L.; Beckers, B. Correlation between measured and calculated solar radiation data in Compiègne, France. In Proceedings of the Proceedings of the International Conference on Energy and Environment Technologies and EquipmProceedings of the International Conference on Energy and Environment Technologies and Equipment, EEETE ’10; 2010.

68. Miguet, F. A further step in environment and bioclimatic analysis: The software tool solene. In Proceedings of the IBPSA 2007 - International Building Performance Simulation Association 2007; 2007.

69. Chazelle, B. The polygon containment problem. *Adv. Comput. Res.* **1983**, *1*, 1–33.

70. Lozano-Pérez, T. Spatial Planning: A Configuration Space Approach. *IEEE Trans. Comput.* **1983**.

71. Avnaim, F.; Boissonnat, J.-D. Polygon placement under translation and rotation. *RAIRO - Theor. Informatics Appl.* **1989**, *23*, 5–28.

72. Lorenzo, E.; Narvarte, L.; Muñoz, J. Tracking and back-tracking. *Prog. Photovoltaics Res. Appl.* **2011**, *19*, 747–753.

73. Liu, B.Y.H.; Jordan, R.C. A Rational Procedure for Predicting The Long-Term Average Performance of Flat-Plate Solar-Energy Collectors. *Sol. Energy* **1963**, *7*, 53–74.

74. Hay, J.E. Calculating solar radiation for inclined surfaces: Practical approaches. *Renew. Energy* **1993**, *3*, 373–380.

75. Klucher, T.M. Evaluation of models to predict insolation on tilted surfaces. *Sol. Energy* **1979**, *23*, 111–114.

76. Reindl, D.T.; Beckman, W.A.; Duffie, J.A. Evaluation of hourly tilted surface radiation models. *Sol. Energy* **1990**, *45*, 9–17.

77. Usher, J.R.; Muneer, T. Case studies in solar radiation modelling. *Math. Comput. Model.* **1989**, *12*, 1155–1165.

78. Skartveit, A.; Asle Olseth, J. Modelling slope irradiance at high latitudes. *Sol. Energy* **1986**, *36*, 333–344.

79. Perez, R.; Ineichen, P.; Seals, R.; Michalsky, J.; Stewart, R. Modeling daylight availability and irradiance components from direct and global irradiance. *Sol. Energy* **1990**, *44*, 271–289.

80. Gueymard, C. An anisotropic solar irradiance model for tilted surfaces and its comparison with selected engineering algorithms. *Sol. Energy* **1987**, *38*, 367–386.

81. Loutzenhiser, P.G.; Manz, H.; Felsmann, C.; Strachan, P.A.; Frank, T.; Maxwell, G.M. Empirical validation of models to compute solar irradiance on inclined surfaces for building energy simulation. *Sol. Energy* **2007**, *81*, 254–267.

82. Yoon, K.; Yun, G.; Jeon, J.; Kim, K.S. Evaluation of hourly solar radiation on inclined surfaces at Seoul by Photographical Method. *Sol. Energy* **2014**, *100*, 203–216.

83. Yadav, A.K.; Chandel, S.S. Tilt angle optimization to maximize incident solar radiation: A review. *Renew. Sustain. Energy Rev.* **2013**, *23*, 503–513.

84. Ahmad, M.J.; Tiwari, G.N. Optimization of Tilt Angle for Solar Collector to Receive Maximum Radiation. *Open Renew. Energy J.* **2009**, *2*, 19–24.

85. Tsalides, P.; Thanailakis, A. Direct computation of the array optimum tilt angle in constant-tilt photovoltaic systems. *Sol. Cells* **1985**, *14*, 83–94.

86. Evseev, E.G.; Kudish, A.I. The assessment of different models to predict the global solar radiation on a surface tilted to the south. *Sol. Energy* **2009**, *83*, 377–388.

87. Khorasanizadeh, H.; Mohammadi, K.; Mostafaeipour, A. Establishing a diffuse solar radiation model for determining the optimum tilt angle of solar surfaces in Tabass, Iran. *Energy Convers. Manag.* **2014**, *78*, 805–814.

88. Stanciu, C.; Stanciu, D. Optimum tilt angle for flat plate collectors all over the World – A declination dependence formula and comparisons of three solar radiation models. *Energy Convers. Manag.* **2014**, *81*, 133–143.

89. Bakirci, K. General models for optimum tilt angles of solar panels: Turkey case study. *Renew. Sustain. Energy Rev.* **2012**, *16*, 6149–6159.

90. Baltas, P.; Tortoreli, M.; Russell, P.E. Evaluation of power output for fixed and step tracking photovoltaic arrays. *Sol. Energy* **1986**, *37*, 147–163.

91. Martin, N.; Ruiz, J.M. Calculation of the PV modules angular losses under field conditions by means of an analytical model. *Sol. Energy Mater. Sol. Cells* **2001**, *70*, 25–38.

92. Drago, P. A simulated comparison of the useful energy gain in a fixed and a fully tracking flat plate collector. *Sol. Energy* **1978**, *20*, 419–423.

93. Cruz-Peragón, F.; Casanova-Peláez, P.J.; Díaz, F.A.; López-García, R.; Palomar, J.M. An approach to evaluate the energy advantage of two axes solar tracking systems in Spain. *Appl. Energy* **2011**, *88*, 5131–5142.

94. Chang, T.P. Output energy of a photovoltaic module mounted on a single-axis tracking system. *Appl. Energy* **2009**, *86*, 2071–2078.

95. Huang, B.J.; Sun, F.S. Feasibility study of one axis three positions tracking solar PV with low concentration ratio reflector. *Energy Convers. Manag.* **2007**, *48*, 1273–1280.

96. Li, Z.; Liu, X.; Tang, R. Optical performance of vertical single-axis tracked solar panels. *Renew. Energy* **2011**, *36*, 64–68.

97. Chang, T.P. Performance analysis of tracked panel according to predicted global radiation. *Energy Convers. Manag.* **2009**, *50*, 2029–2034.

98. Ramírez-Faz, J.; López-Luque, R. Development of a methodology for quantifying insolation variables in windows and building openings. *Renew. Energy* **2012**, *37*, 426–433.

99. Zill, D.; Wright, W. *Multivariable Calculus*; 4th ed.; Jones and Bartlett Publishers, 2011; ISBN 9780763749668.

100. Fernández-Ahumada, L.M.; Casares, F.J.; Ramírez-Faz, J.; López-Luque, R. Mathematical study of the movement of solar tracking systems based on rational models. *Sol. Energy* **2017**, *150*, 20–29.

101. Control Seguimiento Solar, Sun tracker control, solar nachführung - Suntrack Available online: http://www.suntrack.es/english/aplicaciones1.html (accessed on Dec 3, 2018).

102. Solar production machines - Machinery and Plant Construction - Siemens Global Website Available online:

https://new.siemens.com/global/en/markets/machinebuilding/solar-production-machines/solar-tracking.html (accessed on Dec 3, 2018).

103. Lauritzen Solutions Available online: http://www.lauritzen.biz/products.html (accessed on Dec 3, 2018).

104. Eremia, M.; Toma, L.; Sanduleac, M. The Smart City Concept in the 21st Century. *Procedia Eng.* **2017**, *181*, 12–19.

105. Milošević, M.R.; Milošević, D.M.; Stević, D.M.; Stanojević, A.D. Smart City: Modeling Key Indicators in Serbia Using IT2FS. *Sustainability* **2019**, *11*, 3536.

106. UNITED NATIONS *World Urbanization Prospects 2018*; 2018;

107. Sandman, H.; Levänen, J.; Savela, N. Using Empathic Design as a Tool for Urban Sustainability in Low-Resource Settings. *Sustainability* **2018**, *10*, 2493.

108. Martos, A.; Pacheco-Torres, R.; Ordóñez, J.; Jadraque-Gago, E. Towards successful environmental performance of sustainable cities: Intervening sectors. A review. *Renew. Sustain. Energy Rev.* **2016**, *57*, 479–495.

109. Lindfors, A.; Feiz, R.; Eklund, M.; Ammenberg, J. Assessing the Potential, Performance and Feasibility of Urban Solutions: Methodological Considerations and Learnings from Biogas Solutions. *Sustainability* **2019**, *11*, 3756.

110. Alamdari, P.; Nematollahi, O.; Alemrajabi, A.A. Solar energy potentials in Iran: A review. *Renew. Sustain. Energy Rev.* **2013**, *21*, 778–788.

111. Mardonova, M.; Choi, Y. Assessment of Photovoltaic Potential of Mining Sites in Uzbekistan. *Sustainability* **2019**, *11*, 2988.

112. Østergaard, P.A.; Duic, N.; Noorollahi, Y.; Mikulcic, H.; Kalogirou, S. Sustainable development using renewable energy technology. *Renew. Energy* **2020**, *146*, 2430–2437.

113. Belakehal, A.; Tabet Aoul, K.; Bennadji, A. Sunlighting and daylighting strategies in the traditional urban spaces and buildings of the hot arid regions. *Renew. Energy* **2004**.

114. Glaeser, E.L.; Kahn, M.E. Sprawl and Urban Growth. *Handb. Reg. Urban Econ.* **2004**, *4*, 2481–2527.

115. Van Esch, M.M.E.; Looman, R.H.J.; De Bruin-Hordijk, G.J. The effects of urban and building design parameters on solar access to the urban canyon and the potential for direct passive solar heating strategies. *Energy Build.* **2012**.

116. Ayuntamiento de Córdoba (Spain) Plan General de Ordenación Urbanística (PGOU) Available online: http://www.gmucordoba.es/urbanismo/plan-general-de-ordenacion-urbanistica-pgou (accessed on Nov 7, 2019).

117. Instituto de Estadística y Cartografía de Andalucía. Distribución Espacial de la Población en Andalucía Available online: http://www.juntadeandalucia.es/institutodeestadisticaycartografia/distribucionpob/index.htm (accessed on Nov 7, 2019).

118. Ramírez-Faz, J.; López-Luque, R.; Casares, F.J. Development of synthetic hemispheric projections suitable for assessing the sky view factor on vertical planes. *Renew. Energy*

2015, *74*, 279–286.

119. Márquez-García, A.; Varo-Martínez, M.; López-Luque, R. *Solar Energy in Urban Environments: A New Solar Radiation Model for the Analysis of Energy on Façades*; LAP Lambert Academic Publishing: Germany, 2013; ISBN 10: 3659495859.

Anexo I

Primer artículo del compendio: “Estudio matemático del movimiento de seguidores solares basado en modelos racionales”.

Publicado en la revista Solar Energy, editorial Elsevier.

Enviado el 5 de septiembre de 2016, aceptado el 4 de abril de 2017.

Factor de impacto en 2017: 4,374.

Solar Energy 150 (2017) 20–29

Contents lists available at ScienceDirect

Solar Energy

journal homepage: www.elsevier.com/locate/solener

Mathematical study of the movement of solar tracking systems based on rational models

L.M. Fernández-Ahumada [a], F.J. Casares [b], J. Ramírez-Faz [b,*], R. López-Luque [c]

[a] Computing and Numeric Analysis, University of Córdoba, Campus de Rabanales, 14071 Córdoba, Spain
[b] Electrical Engineering, University of Córdoba, Campus de Rabanales, 14071 Córdoba, Spain
[c] Applied Physics, University of Córdoba, Campus de Rabanales, 14071 Córdoba, Spain

ARTICLE INFO

Article history:
Received 5 September 2016
Received in revised form 19 January 2017
Accepted 4 April 2017
Available online 21 April 2017

Keywords:
Solar tracking
Photovoltaic
Equations

ABSTRACT

This paper presents the analytical deduction of generic and unified equations of the movement of solar tracking systems. These equations reproduce published equations, which only consider the sun position, or the equations of the astronomical movement. As a novelty, these equations are more generic, thus allowing the optimization of the positioning of PV installations where diffuse and reflected irradiance are usable. The analysis of the results obtained criticizes the axiomatic idea – widely considered by numerous authors – establishing that the ideal tracking system in PV installations is that tracker providing the best possible alignment with direct sunbeams.

1. Introduction

The use of renewable energy sources is one of the main problems of humanity in the short term. This situation entails that different technologies associated to the use of solar energy are experiencing a dramatic increase. This is the case of the photovoltaic sector, where scientific and industrial progress are creating a sustainable energy alternative (Salas and Olias, 2009; Mousazadeh et al., 2009). These improvements, however, do not always have adequate design practices and proper installation management. As a consequence, they may hinder the progress of PV technology not allowing the optimal use of the installation. This paper presents that equations for astronomical tracking, generally recommended, may be unsuitable since they limit production in percentages even over 10%. This criticism arises from the analysis of the equations also included in this paper, and is deducted to perform an optimal solar tracking.

Solar tracking systems, in general, are classified into two categories: (i) single-axis tracking systems, where a mobile element adopts its position by rotating about a fixed axis; and (ii) two-axis tracking systems, where the collector plane rotates about two fixed axes, allowing the orientation towards any direction of the celestial sphere (Lee et al., 2009). In cases, the movement in azimuth and the elevation of the collector surface could be predetermined by a set of equations (open-loop control) or permanently recalculated from the reading of the radiation sensors (closed-loop control). Lorenzo et al. (2002), Perpiñan et al. (2009), Huld et al. (2008) and Huld et al. (2010) present the productive increases according to the types of tracking systems for different latitudes and technologies, showing that the tracking process is more effective as the latitude is higher. The biggest increases are of the order of 57% (Mousazadeh et al., 2009). Tracking is compulsory in those applications where solar radiation is concentrated (García et al., 2008).

The equations included in the references to determine the orientation of the tracking systems are exclusively based on the astronomical movement of the sun. The development of astronomical equations enables the prediction of the solar position on the celestial sphere with a precision of the order of milliradian (Grena, 2008; Blanco-Muriel et al., 2001; Reda and Andreas, 2004). According to this, Duffie and Beckman (2013), Braun and Mitchell (1983), Meinel and Meinel (1979), Neville (1978), Narvarte and Lorenzo (2008) and Riley and Hansen (2014) present the equations for both single-axis and two-axis trackers obtained by the application of the spherical trigonometry to the solar movement. More recently, papers including Jolly (1986), Sproul (2007), Parkin (2010), Chong and Wong (2009), Rapp-Arrarás and Domingo-Santos (2009) have opened a new line to describe the solar movement, as well as solar tracking systems, thanks to the application of vectorial algebra. The solar vector $\vec{s}$ thus is defined as the unit vector directed to the center of the solar disc. All the astronomical relations are deducted when changes of coordinated systems are made

* Corresponding author.
E-mail address: jramirez@uco.es (J. Ramírez-Faz).

http://dx.doi.org/10.1016/j.solener.2017.04.006
0038-092X/

Glossary

a_P, b_P, F_1, F_2	Perez model parameters
b_M	Muneer parameter
$\vec{e}$	unit vector of the rotation axis
F	Klucher model parameter
H	daily global radiation
$\vec{i}, \vec{j}, \vec{k}$	unit vectors associated to a local cartesian system
I	global solar irradiance on the tilted collector
I_B	direct solar irradiance on horizontal plane
I_D	diffuse solar irradiance
I_{DN}	direct normal irradiance
$I_{D\beta}$	diffuse solar irradiance on the tilted plane
I_G	global solar irradiance ($I_B + I_D$)
I_{0H}	extraterrestrial irradiance
$\vec{n}$	normal vector to the surface
$\vec{p}$	unit vector, coplanar with $\vec{u}, \vec{e}$ and perpendicular to $\vec{e}$
u	irradiance gradient
$\vec{s}$	solar vector
s_x, s_y, s_z	components of solar vector

Greek letters

β	inclination angle of the collector
δ	solar declination
θ	angle of incidence of sunbeams on the inclined plane
θ_z	solar zenith angle
λ, μ, ν	Lagrange multipliers
τ	generic angle in single-axis tracker between horizontal plane and rotation axis
Φ	Lagrange function
φ	latitude
ρ	albedo
χ	angle between $\vec{n}$ and $\vec{e}$
Ω	Earth's rotation speed

by using matricial algebra, or by applying the definitions of the dot and cross product.

The application of the astronomical model to the solar tracking is materialized thanks to the condition of minimizing the incidence angle θ that sunbeams create with the normal of the collector surface. In terms of solar irradiance, it is a tracking system that only considers the maximization of the direct component (Huld et al., 2010). Consequently, it is appropriate for applications that can only use this component (usually applications with concentration). This movement of tracker planes is not the most adequate for PV, where all the radiation components are usable. This effect is especially evident on those days when direct radiation does not reach the collectors and the solar disc is not visible. An astronomical tracking of the sun involves a lower energy collection at all moments of the day compared to the energy obtained in a fixed horizontal plane. Duffie and Beckman (2013) and Mousazadeh et al. (2009) show this effect on days with a low incidence of direct radiation. Literature, however, does not include papers oriented towards the development of solar tracking equations for those days. This way, there is a need to study the effect of the diffuse and reflected components on the solar tracking in order to obtain the equations for the maximum radiation collection.

The characterization of solar radiation on tilted collector planes has been studied by numerous authors, who have proposed several semi-empirical approaches (Liu and Jordan, 1963; Hay, 1993; Klucher, 1979; Reindl et al., 1990; Usher and Muneer, 1989; Skartveit and Asle Olseth, 1986; Perez et al., 1990; Gueymard, 1987). Klucher (1979), Loutzenhiser et al. (2007) and Yoon et al. (2014) compare the irradiance models with a series of measures recorded in different localities for the most explanatory irradiance model. Yadav and Chandel (2013), Ahmad and Tiwari (2009), Tsalides and Thanailakis (1985), Evseev and Kudish (2009), Khorasanizadeh et al. (2014), Stanciu and Stanciu (2014) and Bakirci (2012) have used these models to determine the optimal inclination of collectors in different localities. These authors consider that the optimal inclination allows to collect the maximum radiation, ignoring other factors like collector temperature, dust or Fresnel reflection losses. In this light, Baltas et al. (1986) and Martin and Ruiz (2001) propose models to consider these effects on static collectors. These losses should be insignificant for collectors on solar trackers as they are only significant for high incidence values (Baltas et al., 1986; Martin and Ruiz, 2001). The absence of papers about the problem to obtain the optimal position of tracking collectors from the irradiance models has also been observed when analyzing the studies by authors like Drago (1978), Cruz-Peragón et al. (2011), Chang (2009a), Huang and Sun (2007), Li et al. (2011) and Chang (2009b). Focusing on the purpose of knowing the maximum energy available for PV installations, they integrate the incident modelled irradiance on collectors with astronomical movement. Nevertheless, they ignore the fact that all irradiance models implicitly entail the optimal position where the tracker should be located.

This paper presents a rational model to study the movement equations of solar tracking systems using vectorial algebra and differential calculus. It is aimed that this model is unified, valid for all types of solar tracking systems, including all the rational equations currently described in the literature. It is also aimed that this model includes explicitly actually usable irradiance models. The proposed methods are based on the mathematical maximization of the usable irradiance on the collector plane.

2. Proposal of the model

2.1. Astronomical bases of solar tracking

This paper departs from the description of the solar vector $\vec{s}$ in a local system of axes, following the represented in Fig. 1.

Fig. 1(a) shows the solar vector on an equatorial reference system with the origin in the center of the Earth, the $Ox'y'$ plane coinciding with the equator plane. Therefore, the Oz' axis is parallel to the Earth's rotational axis, and the $Oz'y'$ plane coincides with the plane of the local meridian (Torres-Roldán et al., 2015). In this coordinate system the hour angle, given by the product of the rotation speed $\Omega = 2\pi/24$ rad/h) by the time elapsed after the solar midday, and declination δ can be represented as the angle φ. Figs. 1(a) and (b) show the terrestrial reference system, where the following axes are used: Ox: direction to the West; Oy: direction to the South; and Oz: zenithal direction; in which $\vec{i}, \vec{j}, \vec{k}$ are the respective unit vectors. The solar vector, thus, is given by Eq. (1) as shown in Ramírez-Faz and López-Luque (2012).

$$\begin{aligned}\vec{s} &= s_x\vec{i} + s_y\vec{j} + s_z\vec{k} \\ &= \sin\Omega t\cos\delta\,\vec{i} + (\cos\Omega t\cos\delta\sin\varphi - \sin\delta\cos\varphi) \\ &\quad \times \vec{j} + (\cos\Omega t\cos\delta\cos\varphi + \sin\delta\sin\varphi)\vec{k}\end{aligned} \tag{1}$$

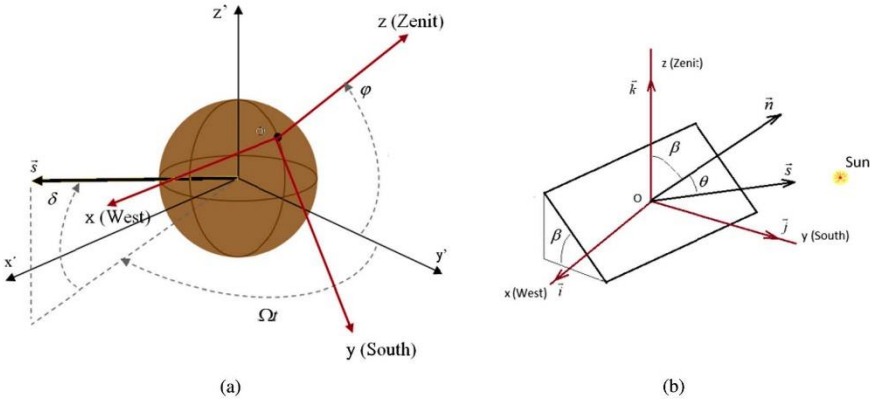

Fig. 1. Earth reference system.

Fig. 1(b) also represents the unit vector $\vec{n}$, orthogonal to the collector plane and representative of the spatial position of the collector. The angle between vector $\vec{n}$ and vector $\vec{s}$ is θ, while the angle between $\vec{n}$ and $\vec{k}$ is β.

2.2. Models to calculate usable irradiance

In general, the direct, diffuse and reflected components can be distinguished in the solar irradiance incidental on a plane. Direct irradiance is closely related to Sun-Earth geometry, as the electromagnetic rays of this component come directly from the positional direction of the Sun Studies of direct shadowing are actually geometric studies based on the astronomical movement, which enable the characterization of the effect of obstructions on the collector plane. The diffuse component is formed by all rays incoming from all directions of celestial vault, except the Earth-Sun direction. The atmospheric scattering and the reflection of the solar radiation entail greater difficulties for its characterization. Models normally consider diffuse irradiance as climatic variable obtained from measurements of multiple years (Duffie and Beckman, 2013).

As several empirical models are available to describe the diffuse irradiance, it is necessary to select the most adequate for each location. Calibration of parameters and statistical comparison between models are the main steps to choose the most adequate model (Gueymard, 1987).

We present below six models of proven validity. The first can be applied regardless of climate, as long as direct irradiance is usable. If it is an application that uses all the components, a model (like one of the five suggested here) should be validated.

The models proposed in this paper are:

a. Direct irradiance model. Eq. (2) describes the irradiance to be considered on the collector plane in all cases where only direct irradiance is usable. This is the case of solar concentration.

$$I = \frac{\cos\theta}{\cos\theta_z} I_B \tag{2}$$

b. Isotropic sky model. Described by Duffie and Beckman (2013) and Liu and Jordan (1963), this model assumes that diffuse radiation is isotropically distributed in the sky dome. This model establishes Eq. (3).

$$I = \frac{\cos\theta}{\cos\theta_z} I_B + \frac{1+\cos\beta}{2} I_D + \rho \frac{1-\cos\beta}{2}(I_B + I_D) \tag{3}$$

c. Hay-Davies model (Hay, 1993). This model establishes that a determined fraction I_B/I_{OH} of the diffuse irradiance is directed from the direction of the solar disc.

$$I = \frac{\cos\theta}{\cos\theta_z} I_B + \left[\left(\frac{\cos\theta}{\cos\theta_z}\right)\frac{I_B}{I_{OH}} + \left(1 - \frac{I_B}{I_{OH}}\right)\frac{1+\cos\beta}{2}\right] I_D + \rho \frac{1-\cos\beta}{2}(I_B + I_D) \tag{4}$$

d. Klucher model (Klucher, 1979). It is known that the isotropic model (Eq. (3)) underestimates irradiance on tilted planes during clear days. The Klucher model aims to correct this effect.

$$I = \frac{\cos\theta}{\cos\theta_z} I_B + \frac{1+\cos\beta}{2}\left(1 + F\sin^3\frac{\beta}{2}\right) \times (1 + F\cos^2\theta\sin^3\theta_z) I_D - \rho\frac{1-\cos\beta}{2}(I_B + I_D) \tag{5}$$

where

$$F = 1 - \left(\frac{I_B}{I_B + I_D}\right)^2 \tag{6}$$

e. Reindl model (Reindl et al., 1990). It is a non-isotropic model that establishes Eq. (7).

$$I = \frac{\cos\theta}{\cos\theta_z} I_B + \left[\left(\frac{\cos\theta}{\cos\theta_z}\right)\frac{I_B}{I_{OH}} + \left(1 - \frac{I_B}{I_{OH}}\right)\frac{1+\cos\beta}{2}\left(1 + \sqrt{\frac{I_B}{I_B + I_D}}\sin^3\frac{\beta}{2}\right)\right] I_D + \rho\frac{1-\cos\beta}{2}(I_B + I_D) \tag{7}$$

f. Muneer model (Usher and Muneer, 1989). This model considers that non-isotropy of diffuse irradiance is modulated

by factor b_M thanks to Eqs. (8) and (9). In fact, Eq. (8) coincides with Eq. (3) when $b_M = 0$.

$$I = \frac{\cos\theta}{\cos\theta_z} I_B + \left[\left(\frac{\cos\theta}{\cos\theta_z}\right)\frac{I_B}{I_{OH}} + \left(1 - \frac{I_B}{I_{OH}}\right)\frac{I_{D\beta}}{I_D}\right] I_D + \rho\frac{1-\cos\beta}{2}(I_B + I_D) \quad (8)$$

being

$$\frac{I_{D\beta}}{I_D} = \frac{1+\cos\beta}{2} + \frac{2b_M}{\pi(3+2b_M)}\left(\sin\beta - \beta\cos\beta - \pi\sin^2\left(\frac{\beta}{2}\right)\right) \quad (9)$$

g. Perez model (Perez et al., 1990)

$$I = \frac{\cos\theta}{\cos\theta_z} I_B + \left[(1-F_1)\frac{1+\cos\beta}{2} + F_1\frac{a}{b} + F_2\sin\beta\right] I_D + \rho\frac{1-\cos\beta}{2}(I_B + I_D) \quad (10)$$

For the application of Eq. (10), the model uses F_1 and F_2, coefficients expressing the degree of circumsolar and horizon/zenith anisotropy respectively, as well as the parameters a_P and b_P defined by the authors as expressed in Eqs. (11) and (12) (Perez et al., 1990).

$$a_P = \max(\cos\theta; 0) \quad (11)$$

$$b_P = \max(\cos 85^\circ; \cos\theta_z) \quad (12)$$

For the right choice of solar tracking equations, it is necessary to know the function of usable irradiance I. It is considered in this study that I can be given by any of the Eqs. (2), (3), (4), (5), (7), (8) or (10). Given that, this paper follows a vectorial approach, the following parameters will be considered:

$$\cos\beta = \vec{k}\cdot\vec{n} \quad (13)$$

$$\cos\theta = \vec{s}\cdot\vec{n} \quad (14)$$

$$\cos\theta_z = \vec{s}\cdot\vec{k} \quad (15)$$

Eqs. (2), (3), (5), (7), (8), (9) and (10) can be expressed according to the unit vectors, being respectively Eqs. (16), (17), (18), (19), (20), (21) or (22). It must be highlighted the vectorial dependence of $\vec{s}\cdot\vec{n}$ and $\vec{k}\cdot\vec{n}$ for these equations with respect to the orientation of the collector plane.

$$I = \frac{\vec{s}\cdot\vec{n}}{\vec{s}\cdot\vec{k}} I_B \quad (16)$$

$$I = \frac{\vec{s}\cdot\vec{n}}{\vec{s}\cdot\vec{k}} I_B + \frac{1+\vec{k}\cdot\vec{n}}{2} I_D + \rho\frac{1-\vec{k}\cdot\vec{n}}{2}(I_B + I_D) \quad (17)$$

$$I = \frac{\vec{s}\cdot\vec{n}}{\vec{s}\cdot\vec{k}} I_B + \left[\frac{\vec{s}\cdot\vec{n}}{\vec{s}\cdot\vec{k}}\frac{I_B}{I_{OH}} + \left(1 - \frac{I_B}{I_{OH}}\right)\frac{1+\vec{k}\cdot\vec{n}}{2}\right] I_D + \rho\frac{1-\vec{k}\cdot\vec{n}}{2}(I_B + I_D) \quad (18)$$

$$I = \frac{\vec{s}\cdot\vec{n}}{\vec{s}\cdot\vec{k}} I_B + \frac{1+\vec{k}\cdot\vec{n}}{2}\left(1 + F\left(\frac{1-\vec{k}\cdot\vec{n}}{2}\right)^{3/2}\right) \times \left(1 + F(\vec{s}\cdot\vec{n})^2\left[1 - (\vec{s}\cdot\vec{k})^2\right]^{3/2}\right) I_D + \rho\frac{1-\vec{k}\cdot\vec{n}}{2}(I_B + I_D) \quad (19)$$

$$I = \frac{\vec{s}\cdot\vec{n}}{\vec{s}\cdot\vec{k}} I_B + \left[\frac{\vec{s}\cdot\vec{n}}{\vec{s}\cdot\vec{k}}\frac{I_B}{I_{OH}} + \left(1 - \frac{I_B}{I_{OH}}\right)\frac{1+\vec{k}\cdot\vec{n}}{2}\left(1 + \sqrt{\frac{I_B}{I_B+I_D}}\left(\frac{1-\vec{k}\cdot\vec{n}}{2}\right)^{3/2}\right)\right] I_D + \rho\frac{1-\vec{k}\cdot\vec{n}}{2}(I_B + I_D) \quad (20)$$

$$I = \frac{\vec{s}\cdot\vec{n}}{\vec{s}\cdot\vec{k}} I_B + \left[\frac{\vec{s}\cdot\vec{n}}{\vec{s}\cdot\vec{k}}\frac{I_B}{I_{OH}} + \left(1 - \frac{I_B}{I_{OH}}\right)\frac{I_{D\beta}}{I_D}\right] I_D + \rho\frac{1-\vec{k}\cdot\vec{n}}{2}(I_B + I_D) \quad (21)$$

$$\frac{I_{D\beta}}{I_D} = \left(\frac{1+\vec{k}\cdot\vec{n}}{2}\right) + \frac{2b_M}{\pi(3+2b_M)} \times \left(\sqrt{1-(\vec{k}\cdot\vec{n})^2} - (\vec{k}\cdot\vec{n})\arccos(\vec{k}\cdot\vec{n}) - \pi\left(\frac{1-\vec{k}\cdot\vec{n}}{2}\right)\right) \quad (22)$$

$$I = \frac{\vec{s}\cdot\vec{n}}{\vec{s}\cdot\vec{k}} I_B + \left[(1-F_1)\frac{1+\vec{k}\cdot\vec{n}}{2} + F_1\frac{\vec{s}\cdot\vec{n}}{b_P} + F_2\sqrt{1-(\vec{k}\cdot\vec{n})^2}\right] I_D + \rho\frac{1-\vec{k}\cdot\vec{n}}{2}(I_B + I_D) \quad (23)$$

2.3. Mathematical approach to single-axis trackers

This paper uses the unit vector $\vec{e}$ to describe the generic movement of any single-axis tracking system. This is a fixed unit vector included in the rotation axis of the collector plane. Given that the collector surface – and thus $\vec{n}$ – can only rotate about $\vec{e}$, Eq. (24) must always be satisfied:

$$\vec{e}\cdot\vec{n} = \cos\chi \quad (24)$$

Being χ the constant angle formed by $\vec{e}$ and $\vec{n}$.

Table 1 shows the characteristic values of χ for the main single-axis trackers described in the literature.

This paper proposes the use of a cylindrical chart for the solar position in order to show graphically the possibilities of movement of single-axis trackers. In this chart, the line to describe the celestial sphere, to the point in which $\vec{n}$ is oriented is overlapped. Fig. 2, then, shows the family of curves of the pointing points of the tracking systems from Table 1 in the cylindrical chart.

This paper considers movement equations that allow the maximization of irradiance on the collector plane. Mathematically, this

Table 1
Values of χ for the main single-axis trackers.

Type	$\vec{e}$	χ
Vertical axis	$0\,\vec{i} + 0\,\vec{j} + 1\,\vec{k}$	β
E-W horizontal axis	$1\,\vec{i} + 0\,\vec{j} + 0\,\vec{k}$	$\pi/2$
N-S horizontal axis	$0\,\vec{i} + 1\,\vec{j} + 0\,\vec{k}$	$\pi/2$
N-S inclined axis	$0\,\vec{i} - \sin\tau\,\vec{j} + \cos\tau\,\vec{k}$	$\pi/2$
Polar	$0\,\vec{i} - \sin\varphi\,\vec{j} + \cos\varphi\,\vec{k}$	$\pi/2$

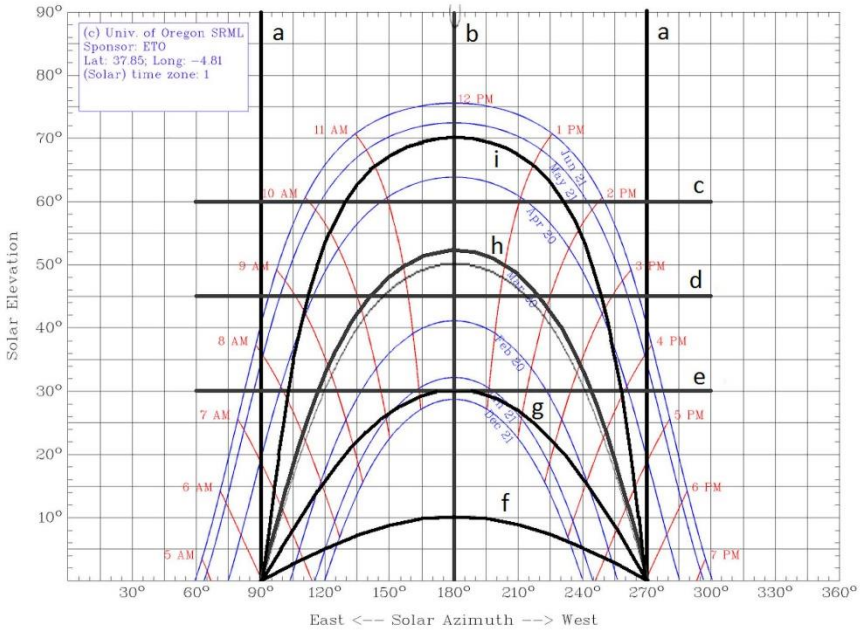

Fig. 2. Cylindrical chart for Córdoba, Spain ($\varphi = 37.85°$N) with the pointing paths of the main single-axis trackers. (a) N-S horizontal axis. (b) E-W horizontal axis. (c) $\beta = 30°$ Vertical axis. (d) $\beta = 45°$ Vertical axis. (e) $\beta = 60°$ Vertical axis. (f) N-S inclined axis $\tau = 10°$. (g) N-S inclined axis $\tau = 30$ °. (h) N-S polar axis. (i) N-S inclined axis $\tau = 70°$ (the figure was adapted from the software at the University of Oregon Solar Radiation Monitoring Laboratory, http://solardat.uoregon.edu/SunChartProgram.php).

equates to find the vector $\vec{n}$ to maximize function shown in Eq. (25) according to the conditions given by Eqs. (26), (24) and (27).

$$I = I(\vec{s}\cdot\vec{n}, \vec{k}\cdot\vec{n}) \tag{25}$$

$$\vec{n}\cdot\vec{n} = 1 \tag{26}$$

$$\vec{e}\cdot\vec{n} = \cos\chi \tag{24}$$

$$\vec{e}\cdot\vec{e} = 1 \tag{27}$$

For this purpose, the method of Lagrange multipliers is used, as it conducts to the maximum or minimum of a multivariable function when there are some constraints between the input values (Zill and Wright, 2011). As a consequence, it is proposed function Φ with independent variables $\vec{n}$, λ, μ and v, where the new variables or Lagrange multipliers λ, μ and v are methodically introduced.

$$\Phi(\vec{n},\lambda,\mu,v) = I(\vec{s}\cdot\vec{n}, \vec{k}\cdot\vec{n}) + \lambda(1-\vec{n}\cdot\vec{n}) + \mu(\cos\chi - \vec{e}\cdot\vec{n}) + v(1-\vec{e}\cdot\vec{e}) \tag{28}$$

The differentiation with respect to $\vec{n}$ arises:

$$d\Phi = \left[\frac{\partial I}{\partial(\vec{s}\cdot\vec{n})}\vec{s} + \frac{\partial I}{\partial(\vec{k}\cdot\vec{n})}\vec{k} - 2\lambda\vec{n} - \mu\vec{e}\right] d\vec{n} + [1-\vec{n}\cdot\vec{n}]d\lambda + [\cos\chi - \vec{e}\cdot\vec{n}]d\mu + [1-\vec{e}\cdot\vec{e}]dv \tag{29}$$

Following Lagrange methods implies equating to zero the brackets in Eq. (29), obtaining Eqs. (30), (26), (24) and (27). The resolution of these gives the values of $\vec{n}$.

$$\frac{\partial I}{\partial(\vec{s}\cdot\vec{n})}\vec{s} + \frac{\partial I}{\partial(\vec{k}\cdot\vec{n})}\vec{k} - 2\lambda\vec{n} - \mu\vec{e} = 0 \tag{30}$$

In the resolution of the equation systems is used the auxiliary vector $\vec{u}$, defined by

$$\vec{u} - \frac{\partial I}{\partial(\vec{s}\cdot\vec{n})}\vec{s} - \frac{\partial I}{\partial(\vec{k}\cdot\vec{n})}\vec{k} \tag{31}$$

Eq. (30) establishes that $\vec{u}, \vec{e}, \vec{n}$ are coplanar, so it represents that there is a linear combination of these, which is equal to zero. If a unit vector $\vec{p}$ is defined – also coplanar with $\vec{u}, \vec{e}$, and perpendicular to $\vec{e}$ – the Eq. (32) can be found for $\vec{p}$.

$$\vec{p} = \frac{\vec{u} - (\vec{u}\cdot\vec{e})\vec{e}}{|\vec{u} - (\vec{u}\cdot\vec{e})\vec{e}|} = \frac{\vec{u} - (\vec{u}\cdot\vec{e})\vec{e}}{\sqrt{u^2 - (\vec{u}\cdot\vec{e})^2}} \tag{32}$$

Fig. 3 shows a scheme of the coplanar vector $\vec{e}, \vec{u}, \vec{p}$ and $\vec{n}$.

This figure shows that $\vec{e}$ and $\vec{p}$ are unit and perpendicular vectors. Consequently, they create an orthogonal basis on which $\vec{n}$ can be expressed from the angle formed with one of them.

This way, the expression of $\vec{n}$ solving the system given by Eqs. (39), (26), (24) and (27) can be found in Eq. (33).

$$\vec{n} = \cos\chi\,\vec{e} + \sin\chi\,\vec{p} \tag{33}$$

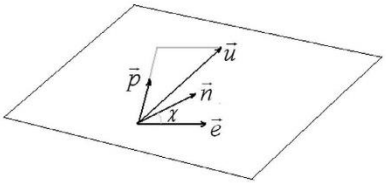

Fig. 3. Graphic representation of coplanar vectors $\vec{e}, \vec{u}, \vec{p}$ and $\vec{n}$.

This equation can be expressed in terms of $\vec{u}$.

$$\vec{n} = \cos\chi\,\vec{e} + \sin\chi\frac{\vec{u} - (\vec{u}\cdot\vec{e})\,\vec{e}}{\sqrt{u^2 - (\vec{u}\cdot\vec{e})^2}} = \left(\cos\chi - \frac{(\vec{u}\cdot\vec{e})\sin\chi}{\sqrt{u^2 - (\vec{u}\cdot\vec{e})^2}}\right)\vec{e} + \left(\frac{\sin\chi}{\sqrt{u^2 - (\vec{u}\cdot\vec{e})^2}}\right)\vec{u} \tag{34}$$

$$\vec{n} = \left(\cos\chi - \frac{\left(\frac{\partial I}{\partial(\vec{s}\cdot\vec{n})}\vec{s}\cdot\vec{e} + \frac{\partial I}{\partial(\vec{k}\cdot\vec{n})}\vec{k}\cdot\vec{e}\right)\sin\chi}{\sqrt{\left(\frac{\partial I}{\partial(\vec{s}\cdot\vec{n})}\right)^2 + \left(\frac{\partial I}{\partial(\vec{k}\cdot\vec{n})}\right)^2 + 2\left(\frac{\partial I}{\partial(\vec{s}\cdot\vec{n})}\right)\left(\frac{\partial I}{\partial(\vec{k}\cdot\vec{n})}\right)\vec{s}\cdot\vec{k} - \left(\frac{\partial I}{\partial(\vec{s}\cdot\vec{n})}\vec{s}\cdot\vec{e} + \frac{\partial I}{\partial(\vec{k}\cdot\vec{n})}\vec{k}\cdot\vec{e}\right)^2}}\right)\vec{e} + \left(\frac{\sin\chi\frac{\partial I}{\partial(\vec{s}\cdot\vec{n})}}{\sqrt{\left(\frac{\partial I}{\partial(\vec{s}\cdot\vec{n})}\right)^2 + \left(\frac{\partial I}{\partial(\vec{k}\cdot\vec{n})}\right)^2 + 2\left(\frac{\partial I}{\partial(\vec{s}\cdot\vec{n})}\right)\left(\frac{\partial I}{\partial(\vec{k}\cdot\vec{n})}\right)\vec{s}\cdot\vec{k} - \left(\frac{\partial I}{\partial(\vec{s}\cdot\vec{n})}\vec{s}\cdot\vec{e} + \frac{\partial I}{\partial(\vec{k}\cdot\vec{n})}\vec{k}\cdot\vec{e}\right)^2}}\right)\vec{s} + \left(\frac{\sin\chi\frac{\partial I}{\partial(\vec{k}\cdot\vec{n})}}{\sqrt{\left(\frac{\partial I}{\partial(\vec{s}\cdot\vec{n})}\right)^2 + \left(\frac{\partial I}{\partial(\vec{k}\cdot\vec{n})}\right)^2 + 2\left(\frac{\partial I}{\partial(\vec{s}\cdot\vec{n})}\right)\left(\frac{\partial I}{\partial(\vec{k}\cdot\vec{n})}\right)\vec{s}\cdot\vec{k} - \left(\frac{\partial I}{\partial(\vec{s}\cdot\vec{n})}\vec{s}\cdot\vec{e} + \frac{\partial I}{\partial(\vec{k}\cdot\vec{n})}\vec{k}\cdot\vec{e}\right)^2}}\right)\vec{k} \tag{35}$$

This paper suggests Eq. (35) as a unified expression for all the cases of single-axis trackers.

Example 1. N-S horizontal single-axis tracker with concentration. This is the case of multiple installations of parabolic-cylinder concentration tracking systems. Considering that the only usable component of the irradiance is the direct irradiance, Eq. (16) is considered for its determination, which implies Eqs. (36) and (37).

$$\frac{\partial I}{\partial(\vec{s}\cdot\vec{n})} = I_{DN} \tag{36}$$

$$\frac{\partial I}{\partial(\vec{k}\cdot\vec{n})} = 0 \tag{37}$$

Considering the values of $\vec{e}$ and χ in Table 1, applying Eq. (35) we obtain Eq. (38).

$$\vec{n} = \left(-\frac{I_{DN}s_y}{\sqrt{I_{DN}^2 - (I_{DN}s_y)^2}}\right)\vec{j} + \left(\frac{I_{DN}}{\sqrt{I_{DN}^2 - (I_{DN}s_y)^2}}\right)\vec{s} - \left(\frac{0}{\sqrt{I_{DN}^2 - (I_{DN}s_y)^2}}\right)\vec{k} \tag{38}$$

Simplifying, Eq. (39) is obtained

$$\vec{n} = \left(-\frac{s_y}{\sqrt{1 - s_y^2}}\right)\vec{j} + \left(\frac{1}{\sqrt{1 - s_y^2}}\right)\vec{s} = \left(\frac{s_x}{\sqrt{1 - s_y^2}}\right)\vec{i} + \left(\frac{s_x}{\sqrt{1 - s_y^2}}\right)\vec{k} \tag{39}$$

It is easy to see, when substituting in Eq. (39) the values given in Eq. (1), the coincidence with the equations previously published for this case.

Example 2. Obtaining the optimal position vector for the collector plane located on a polar tracker with $\chi = 90^\circ$, and considering the irradiance model given by Eq. (17) as the most appropriate. Considering that these collectors are proposed for photovoltaic collectors, which use the three components of irradiance, as well as the irradiance model proposed in Eq. (17) to be adequate, we obtain:

$$\frac{\partial I}{\partial(\vec{s}\cdot\vec{n})} = I_{DN} \tag{40}$$

$$\frac{\partial I}{\partial(\vec{k}\cdot\vec{n})} = \frac{I_D}{2} - \frac{\rho I_G}{2} \tag{41}$$

Given that Eq. (35) is applied where $\vec{k}\cdot\vec{e}$ and $\vec{s}\cdot\vec{e}$ intervene, we get the following values for Eqs. (42) and (43):

$$\vec{k}\cdot\vec{e} = \cos\varphi \tag{42}$$

$$\vec{s}\cdot\vec{e} = (\cos\Omega t\cos\delta\sin\varphi - \sin\delta\cos\varphi)(-\cos\varphi) + (\cos\Omega t\cos\delta\cos\varphi - \sin\delta\sin\varphi)(\sin\varphi) = \sin\delta \tag{43}$$

Applying Eq. (35), we obtain Eq. (44):

$$\vec{n} = \left(\frac{-I_{DN}\sin\delta + \left(\frac{I_D}{2} - \frac{\rho I_G}{2}\right)\cos\varphi}{\sqrt{I_{DN}^2\cos^2\delta + \left(\frac{I_D}{2} - \frac{\rho I_G}{2}\right)^2\sin^2\varphi + 2I_{DN}\left(\frac{I_D}{2} - \frac{\rho I_G}{2}\right)(s_z - \sin\delta\cos\varphi)}}\right)\vec{e} + \left(\frac{I_{DN}}{\sqrt{I_{DN}^2\cos^2\delta + \left(\frac{I_D}{2} - \frac{\rho I_G}{2}\right)^2\sin^2\varphi + 2I_{DN}\left(\frac{I_D}{2} - \frac{\rho I_G}{2}\right)(s_z - \sin\delta\cos\varphi)}}\right)\vec{s} + \left(\frac{\left(\frac{I_d}{2} - \frac{\rho I_G}{2}\right)}{\sqrt{I_{DN}^2\cos^2\delta + \left(\frac{I_D}{2} - \frac{\rho I_G}{2}\right)^2\sin^2\varphi + 2I_{DN}\left(\frac{I_D}{2} - \frac{\rho I_G}{2}\right)(s_z - \sin\delta\cos\varphi)}}\right)\vec{k} \tag{44}$$

Simplifying Eq. (44), we get Eqs. (45) and (46)

$$\vec{n} = \left(\frac{-I_{DN}\sin\delta + \left(\frac{l_D}{2} - \frac{\rho l_G}{2}\right)\cos\varphi}{\sqrt{I_{DN}^2\cos^2\delta + \left(\frac{l_D}{2} - \frac{\rho l_G}{2}\right)^2 \sin^2\varphi + 2I_{DN}\left(\frac{l_D}{2} - \frac{\rho l_G}{2}\right)(s_z - \sin\delta\cos\varphi)}} \right) \times (0\,\vec{i} - \sin\varphi\,\vec{j} + \cos\varphi\,\vec{k}) + \left(\frac{I_{DN}}{\sqrt{I_{DN}^2\cos^2\delta + \left(\frac{l_D}{2} - \frac{\rho l_G}{2}\right)^2 \sin^2\varphi - 2I_{DN}\left(\frac{l_D}{2} - \frac{\rho l_G}{2}\right)(s_z - \sin\delta\cos\varphi)}} \right) \times (s_x\,\vec{i} + s_y\,\vec{j} - s_z\,\vec{k}) + \left(\frac{\left(\frac{l_D}{2} - \frac{\rho l_G}{2}\right)}{\sqrt{I_{DN}^2\cos^2\delta + \left(\frac{l_D}{2} - \frac{\rho l_G}{2}\right)^2 \sin^2\varphi - 2I_{DN}\left(\frac{l_D}{2} - \frac{\rho l_G}{2}\right)(s_z - \sin\delta\cos\varphi)}} \right) \vec{k} \tag{45}$$

$$\vec{n} = \left(\frac{I_{DN}s_x}{\sqrt{I_{DN}^2\cos^2\delta + \left(\frac{l_D}{2} - \frac{\rho l_G}{2}\right)^2 \sin^2\varphi + 2I_{DN}\left(\frac{l_D}{2} - \frac{\rho l_G}{2}\right)(s_z - \sin\delta\cos\varphi)}} \right) \vec{i} + \left(\frac{I_{DN}(s_y + \sin\delta\sin\varphi) + \left(\frac{l_D}{2} - \frac{\rho l_G}{2}\right)\cos\varphi\sin\varphi}{\sqrt{I_{DN}^2\cos^2\delta + \left(\frac{l_D}{2} - \frac{\rho l_G}{2}\right)^2 \sin^2\varphi + 2I_{DN}\left(\frac{l_D}{2} - \frac{\rho l_G}{2}\right)(s_z - \sin\delta\cos\varphi)}} \right) \vec{j} + \left(\frac{I_{DN}(s_z - \sin\delta\cos\varphi) + \left(\frac{l_D}{2} - \frac{\rho l_G}{2}\right)\sin^2\varphi}{\sqrt{I_{DN}^2\cos^2\delta + \left(\frac{l_D}{2} - \frac{\rho l_G}{2}\right)^2 \sin^2\varphi + 2I_{DN}\left(\frac{l_D}{2} - \frac{\rho l_G}{2}\right)(s_z - \sin\delta\cos\varphi)}} \right) \vec{k} \tag{46}$$

2.4. Two-axis tracking

The function to maximize in two-axis tracking is the expressed in Eq. (25), with the single restriction imposed by Eq. (26). The Lagrange function is given by the Eq. (47).

$$\Phi(\vec{n}, \lambda) = I(\vec{s}\cdot\vec{n}, \vec{k}\cdot\vec{n}) + \lambda(1 - \vec{n}\cdot\vec{n}) \tag{47}$$

The differentiation respect to $\vec{n}$ and λ gives:

$$d\Phi = \left[\frac{\partial I}{\partial(\vec{s}\cdot\vec{n})}\vec{s} + \frac{\partial I}{\partial(\vec{k}\cdot\vec{n})}\vec{k} - 2\lambda\vec{n} \right] d\vec{n} + [1 - \vec{n}\cdot\vec{n}]d\lambda \tag{48}$$

Equating to zero the brackets in Eq. (48), Eqs. (49) and (26) are obtained, whose resolution gives the value of $\vec{n}$ expressed in Eq. (50).

$$\frac{\partial I}{\partial(\vec{s}\cdot\vec{n})}\vec{s} + \frac{\partial I}{\partial(\vec{k}\cdot\vec{n})}\vec{k} - 2\lambda\vec{n} = 0 \tag{49}$$

$$\vec{n} = \frac{\frac{\partial I}{\partial(\vec{s}\cdot\vec{n})}\vec{s} + \frac{\partial I}{\partial(\vec{k}\cdot\vec{n})}\vec{k}}{\sqrt{\left(\frac{\partial I}{\partial(\vec{s}\cdot\vec{n})}\right)^2 + \left(\frac{\partial I}{\partial(\vec{k}\cdot\vec{n})}\right)^2 + 2\left(\frac{\partial I}{\partial(\vec{s}\cdot\vec{n})}\right)\left(\frac{\partial I}{\partial(\vec{k}\cdot\vec{n})}\right)\vec{s}\cdot\vec{k}}} \tag{50}$$

Example 3. Two-axis tracker with concentration. This is the case of parabolic discs. Considering that the only usable component of the irradiance is the direct irradiance, Eq. (16) is considered, thus:

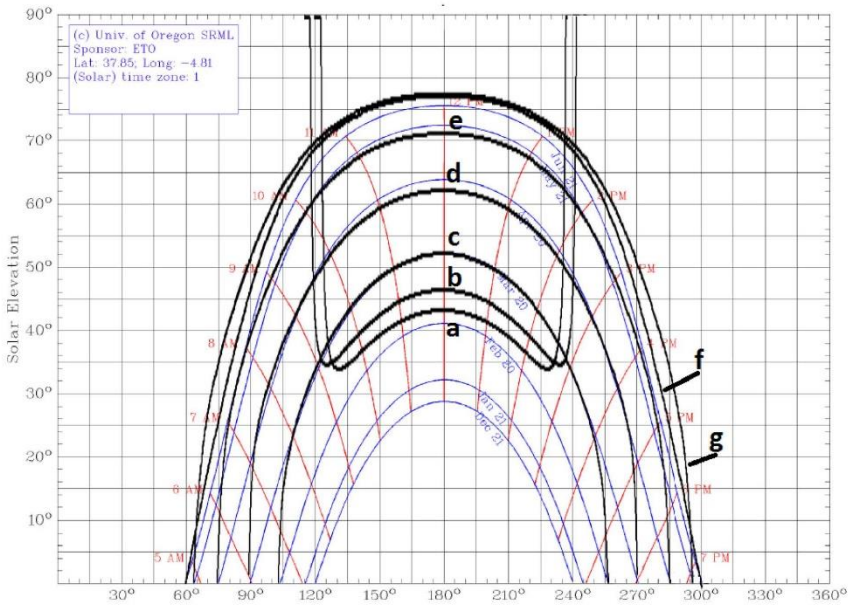

Fig. 4. Cylindrical chart for Córdoba, Spain (φ = 37.85°N) with the pointing paths of the two-axis tracker under the hypothesis of isotropic sky for the days in half of the months: (a) December; (b) January; (c) February; (d) March; (e) April; (f) May; (g) June.

$$\frac{\partial I}{\partial(\vec{s}\cdot\vec{n})} = I_{DN} \tag{36}$$

$$\frac{\partial I}{\partial(\vec{k}\cdot\vec{n})} = 0 \tag{37}$$

It is easy to observe here that Eq. (50) leads to Eq. (51).

$$\vec{n} = \vec{s} \tag{51}$$

Example 4. Two-axis tracker for PV modules that use the three components of irradiance. Considering the irradiance model suggested in Eq. (17) to be adequate, Eqs. (39) and (40) are obtained.

$$\frac{\partial I}{\partial(\vec{s}\cdot\vec{n})} = I_{DN} \tag{40}$$

$$\frac{\partial I}{\partial(\vec{k}\cdot\vec{n})} = \frac{I_D}{2} - \frac{\rho I_G}{2} \tag{41}$$

Applying Eq. (50), we get Eq. (52)

$$\vec{n} = \frac{I_{DN}\,\vec{s} + \left(\frac{I_D}{2} - \frac{\rho I_G}{2}\right)\vec{k}}{\sqrt{I_{DN}^2 + \left(\frac{I_D}{2} - \frac{\rho I_G}{2}\right)^2 + I_{DN}(I_D - \rho I_G)s_z}} \tag{52}$$

In Eq. (52), it can be observed that always that $\left(\frac{I_D}{2} - \frac{\rho I_G}{2}\right)$ is positive, the normal vector in this tracking mode would have a higher elevation than in the case of astronomical tracking.

A cylindrical chart is normally used to represent the solar position and path on the celestial vault. Nevertheless, it can also be used to represent other movements or trajectories (Ramírez-Faz and López-Luque, 2012). In this paper, the cylindrical chart is used to represent the movement of any planar collector over a solar tracker by representing on the chart the set of directions pointed by vector $\vec{n}$. The daily movement of the tracker hence corresponds to a trajectory over the chart.

Fig. 4 shows, on a cylindrical chart, the recommended tracking paths for the representative values of winter and spring according to the hypothesis of isotropic sky given by Eq. (52). When comparing these paths to the solar paths (typical from the astronomical tracking), it can be observed how Eq. (52) recommends a higher elevation of $\vec{n}$ with respect to $\vec{s}$ for all cases. The model proposed here shows a quite different behavior from the astronomical one during the sunrise and the sunset on those days with low radiation levels, as it recommends completely horizontal positions for a better collection of diffuse radiation.

3. Results

Eqs. (35) and (50) are themselves results of this paper. It is convenient, however, to calculate energy collection in the collector plane of a tracker when irradiance follows any of the functions given by Eqs. (16), (17), (18), (19), (20), (21) and (23), and the tracking vector is the optimal vector generated by Eqs. (35) or (50). Furthermore, it is also useful to compare this collection to the values calculated for an astronomical tracking system.

These comparisons have been developed for a wide set of European locations with latitude greater than 40° N. The models show similar behavior in all cases. Therefore, the case of Paris, France, (φ = 48.73°N) has been selected to be shown as representative.

Table 2
Global radiation values per month measured in Paris, France.

Month	H (MJ/m^2 day)
Jan	2.73
Feb	5.17
Mar	8.80
Apr	13.57
May	17.04
Jun	19.63
Jul	17.64
Aug	16.18
Sep	11.36
Oct	6.41
Nov	3.03
Dec	2.01

Table 2 shows the considered daily horizontal radiation for representative days in each month. Table 3 is obtained for a horizontal N-S single-axis tracking system comparing tracking criteria and irradiance models.

Table 3 shows a systematic improvement in the collection when the position of the collector is determined by Eq. (35). In the months with a higher proportion of diffuse irradiance, increases over 10% are observed; moreover, an increase of about 1% is obtained in those months of high radiation.

4. Conclusions

This paper shows the deduction of general equations that optimize the energy Radiation of collectors installed on single-axis Eq. (35) and two-axis Eq. (50) tracking systems. The equations proposed are generic for any continuous tracking system, and the symmetry in the positions of the tracker with respect to the meridian plane are not required. Astronomical tracking, proposed by numerous authors as the optimal tracking system, should be checked for each case (type of usability and validated model that satisfactorily explains irradiance). Consequently, it should not be considered a priori as the most adequate system in all cases. In fact, the cases studied here enable us to observe how the astronomical movement may provide energy collections inferior to the data determined when the values of $\vec{n}$ given by Eqs. (35) or (50) are used.

The equations proposed here include the astronomical tracking model if the value given by Eq. (16) is considered as usable irradiance. Other models that consider the diffuse component of the irradiance make that vector $\vec{n}$ includes a component in direction $\vec{k}$ with respect to the astronomical model. This means that these models predict that the collector plane should be more horizontal than the astronomical model.

In the simplest models of irradiance Eqs. (16)–(18), the partial derivatives with respect to $\vec{s}\cdot\vec{n}$ and $\vec{n}\cdot\vec{k}$ give constant values. In these cases, Eqs. (35) and (50) directly provide the value of $\vec{n}$ for the optimal collection situation. However, when the partial derivatives depend on $\vec{n}$, Eqs. (35) and (50) become solvable equations where the components of $\vec{n}$ can be solved. It is recommended for these cases the numerical method of iteration. The authors have been able to check experimentally that replacing the values of an approach $\vec{n}^{(i)}$ of $\vec{n}$ in the second member of Eqs. (35) and (50), the member of the right $\vec{n}^{(i+1)}$ is obtained, being $\vec{n}^{(i+1)}$ a better approach than $\vec{n}^{(i)}$. It is advisable to start the iterations from

Table 3
Results of the simulation of solar radiation with a horizontal N-S single-axis tracking system and different tracking criteria and irradiance model.

Month	Isotropic sky			Hay-Davies model			Klucher model			Reindl model			Muneer model			Perez model		
	(a) H (MJ/m² day)	(b) H (MJ/m² day)	(c) %	(d) H (MJ/m² day)	(e) H (MJ/m² day)	(f) %	(g) H (MJ/m² day)	(h) (MJ/m² day)	(i) %	(j) H (MJ/m² day)	(k) H (MJ/m² day)	(l) %	(m) H (MJ/m² day)	(n) H (MJ/m² day)	(o) %	(p) H (MJ/m² day)	(q) H (MJ/m² day)	(r) %
Jan	2.44	2.70	10.7	2.46	2.72	10.2	2.52	2.76	9.4	2.49	2.72	8.9	2.35	2.70	15.1	2.49	2.70	8.4
Feb	4.79	5.18	8.3	4.84	5.22	7.8	5.06	5.41	6.8	4.90	5.23	6.6	4.65	5.19	11.6	4.97	5.22	5.0
Mar	8.43	8.93	5.9	8.57	9.02	5.3	9.16	9.56	4.4	8.68	9.04	4.2	8.28	8.94	8.1	8.78	9.05	3.0
Apr	13.70	14.14	3.2	13.98	14.35	2.7	15.09	15.43	2.2	14.17	14.42	1.8	13.60	14.19	4.3	14.17	14.43	1.8
May	17.76	18.16	2.2	18.15	18.47	1.7	19.49	19.78	1.5	18.39	18.58	1.0	17.72	18.24	2.9	18.26	18.52	1.4
Jun	21.32	21.62	1.4	21.86	22.08	1.0	23.38	23.59	0.9	22.14	22.25	0.5	21.42	21.79	1.7	21.79	22.01	1.0
Jul	18.36	18.78	2.3	18.76	19.09	1.8	20.06	20.36	1.5	19.00	19.19	1.0	18.31	18.86	3.0	18.85	19.11	1.4
Aug	17.31	17.61	1.7	17.75	17.97	1.2	19.26	19.42	1.1	17.99	18.11	0.6	17.36	17.73	2.1	17.77	17.98	1.2
Sep	11.47	11.85	3.3	11.71	12.04	2.8	12.68	12.97	2.3	11.88	12.10	1.8	11.39	11.89	4.4	11.89	12.12	1.9
Oct	6.00	6.45	7.5	6.08	6.50	6.9	6.42	6.80	5.9	6.16	6.51	5.7	5.85	6.46	10.4	6.24	6.50	4.2
Nov	2.70	3.01	11.5	2.72	3.02	11.1	2.79	3.08	10.3	2.75	3.02	10.0	2.59	3.01	16.3	2.74	3.00	9.4
Dec	1.76	1.98	12.4	1.77	1.98	12.0	1.80	2.00	11.3	1.79	1.98	10.9	1.68	1.98	17.6	1.76	1.97	12.0
Year	10.53	10.89	3.5	10.75	11.07	2.9	11.50	11.79	2.5	10.89	11.12	2.1	10.46	10.94	4.6	10.84	11.08	2.2

(a) Radiation on a surface on a N-S single-axis tracking system with movement based on the solar position with irradiance described by Eq. (17).
(b) Radiation on a surface on a N-S single-axis tracking system with movement based on Eq. (35) with irradiance described by Eq. (17).
(c) Percentage increase of (b) with respect to (a).
(d) Radiation on a surface on a N-S single-axis tracking system with movement based on the solar position with irradiance described by Eq. (18).
(e) Radiation on a surface on a N-S single-axis tracking system with movement based on Eq. (35) with irradiance described by Eq. (18).
(f) Percentage increase of (e) with respect to (d).
(g) Radiation on a surface on a N-S single-axis tracking system with movement based on the solar position with irradiance described by Eq. (19).
(h) Radiation on a surface on a N-S single-axis tracking system with movement based on Eq. (35) with irradiance described by Eq. (19).
(i) Percentage increase of (h) with respect to (g).
(j) Radiation on a surface on a N-S single-axis tracking system with movement based on the solar position with irradiance described by Eq. (20).
(k) Radiation on a surface on a N-S single-axis tracking system with movement based on Eq. (35) with irradiance described by Eq. (20).
(l) Percentage increase of (k) with respect to (j).
(m) Radiation on a surface on a N-S single-axis tracking system with movement based on the solar position with irradiance described by Eq. (22).
(n) Radiation on a surface on a N-S single-axis tracking system with movement based on Eq. (35) with irradiance described by Eq. (22).
(o) Percentage increase of (n) with respect to (m).
(p) Radiation on a surface on a N-S single-axis tracking system with movement based on the solar position with irradiance described by Eq. (23).
(q) Radiation on a surface on a N-S single-axis tracking system with movement based on Eq. (35) with irradiance described by Eq. (23).
(r) Percentage increase of (q) with respect to (p).

$\vec{n}^{(i)} = \vec{s}$. In all the cases, the convergence allows to finish the process with less than twenty iterations.

A reflection about the movement of solar trackers based on sensors that continuously search for the position of the collector plane optimizing the collector irradiance would suggest that this movement may be more approximated to the calculated with Eqs. (35) and (50) (using the adequate irradiance model) than to the astronomical model. In this light, it could be considered that Eqs. (35) and (50) could be the equations for predicting the movement of solar trackers based on sensors optimizing the irradiance of the collector plane.

References

Ahmad, M.J., Tiwari, G.N., 2009. Optimization of tilt angle for solar collector to receive maximum radiation. Open Renew. Energy J. 2, 19–24. http://dx.doi.org/10.2174/1876387100902010019.

Bakirci, K., 2012. General models for optimum tilt angles of solar panels: Turkey case study. Renew. Sustain. Energy Rev. 16, 6149–6159. http://dx.doi.org/10.1016/j.rser.2012.07.009.

Baltas, P., Tortoreli, M., Russell, P.E., 1986. Evaluation of power output for fixed and step tracking photovoltaic arrays. Sol. Energy 37, 147–163. http://dx.doi.org/10.1016/0038-092X(86)90072-1.

Blanco-Muriel, M., Alarcón-Padilla, D.C., López-Moratalla, T., Lara-Coira, M., 2001. Computing the solar vector. Sol. Energy 70, 431–441. http://dx.doi.org/10.1016/S0038-092X(00)00156-0.

Braun, J.E., Mitchell, J.C., 1983. Solar geometry for fixed and tracking surfaces. Sol. Energy 31, 439–444. http://dx.doi.org/10.1016/0038-092X(83)90046-4.

Chang, T.P., 2009a. Output energy of a photovoltaic module mounted on a single-axis tracking system. Appl. Energy 86, 2071–2078. http://dx.doi.org/10.1016/j.apenergy.2009.02.006.

Chang, T.P., 2009b. Performance analysis of tracked panel according to predicted global radiation. Energy Convers. Manage. 50, 2029–2034. http://dx.doi.org/10.1016/j.enconman.2009.04.007.

Chong, K.K., Wong, C.W., 2009. General formula for on-axis sun-tracking system and its application in improving tracking accuracy of solar collector. Sol. Energy 83, 298–305. http://dx.doi.org/10.1016/j.solener.2008.08.003.

Cruz-Peragón, F., Casanova-Peláez, P.J., Díaz, F.A., López-García, R., Palomar, J.M., 2011. An approach to evaluate the energy advantage of two axes solar tracking systems in Spain. Appl. Energy 88, 5131–5142. http://dx.doi.org/10.1016/j.apenergy.2011.07.018.

Drago, P., 1978. A simulated comparison of the useful energy gain in a fixed and a fully tracking flat plate collector. Sol. Energy 20, 419–423. http://dx.doi.org/10.1016/0038-092X(78)90160-3.

Duffie, J.A., Beckman, W.A., 2013. Solar Engineering of Thermal Processes: Fourth Edition. doi: http://dx.doi.org/10.1002/9781118671603.

Evseev, E.G., Kudish, A.I., 2009. The assessment of different models to predict the global solar radiation on a surface tilted to the south. Sol. Energy 83, 377–388. http://dx.doi.org/10.1016/j.solener.2008.08.010.

García, M., Marroyo, L., Lorenzo, E., Pérez, M., 2008. Experimental energy yield in 1.5v and 2v PV concentrators with conventional modules. Prog. Photovoltaics Res. Appl. 16, 261–270. http://dx.doi.org/10.1002/pip.801.

Grena, R., 2008. An algorithm for the computation of the solar position. Sol. Energy 82, 462–470. http://dx.doi.org/10.1016/j.solener.2007.10.001.

Gueymard, C., 1987. An anisotropic solar irradiance model for tilted surfaces and its comparison with selected engineering algorithms. Sol. Energy 38, 367–386. http://dx.doi.org/10.1016/0038-092X(87)90009-0.

Hay, J.E., 1993. Calculating solar radiation for inclined surfaces: practical approaches. Renew. Energy 3, 373–380. http://dx.doi.org/10.1016/0960-1481(93)90104-O.

Huang, B.J., Sun, F.S., 2007. Feasibility study of one axis three positions tracking solar PV with low concentration ratio reflector. Energy Convers. Manage. 48, 1273–1280. http://dx.doi.org/10.1016/j.enconman.2006.09.020.

Huld, T., Cebecauer, T., Šúri, M., Dunlop, E.D., 2010. Analysis of one-axis tracking strategies for PV systems in Europe. Prog. Photovoltaics Res. Appl. 18, 183–194. http://dx.doi.org/10.1002/pip.948.

Huld, T., Suri, M., Dunlop, E.D., 2008. Comparison of potential solar electricity output from fixed-inclined and two-axis tracking photovoltaic modules in Europe. Prog. Photovoltaics Res. Appl. 16, 47–59. http://dx.doi.org/10.1002/pip.773.

Jolly, P.G., 1986. Derivation of solar angles using vector algebra. Sol. Energy 37, 429–430.

Khorasanizadeh, H., Mohammadi, K., Mostafaeipour, A., 2014. Establishing a diffuse solar radiation model for determining the optimum tilt angle of solar surfaces in Tabass, Iran. Energy Convers. Manage. 78, 805–814. http://dx.doi.org/10.1016/j.enconman.2013.11.048.

Klucher, T.M., 1979. Evaluation of models to predict insolation on tilted surfaces. Sol. Energy 23, 111–114. http://dx.doi.org/10.1016/0038-092X(79)90110-5.

Lee, C.-Y., Chou, P.-C., Chiang, C.-M., Lin, C.-F., 2009. Sun tracking systems: a review. Sensors 9, 3875–3890. http://dx.doi.org/10.3390/s90503875 (14248220).

Li, Z., Liu, X., Tang, R., 2011. Optical performance of vertical single-axis tracked solar panels. Renew. Energy 36, 64–68. http://dx.doi.org/10.1016/j.renene.2010.05.020.

Liu, B.Y.H., Jordan, R.C., 1963. A rational procedure for predicting the long-term average performance of flat-plate solar-energy collectors. Sol. Energy 7, 53–74. http://dx.doi.org/10.1016/0038-092X(63)90006-9.

Lorenzo, E., Pérez, M., Ezpeleta, A., Acedo, J., 2002. Design of tracking photovoltaic systems with a single vertical axis. Prog. Photovoltaics Res. Appl. 10, 533–543. http://dx.doi.org/10.1002/pip.442.

Loutzenhiser, P.G., Manz, H., Felsmann, C., Strachan, P.A., Frank, T., Maxwell, G.M., 2007. Empirical validation of models to compute solar irradiance on inclined surfaces for building energy simulation. Sol. Energy 81, 254–267. http://dx.doi.org/10.1016/j.solener.2006.03.009.

Martín, N., Ruiz, J.M., 2001. Calculation of the PV modules angular losses under field conditions by means of an analytical model. Sol. Energy Mater. Sol. Cells 70, 25–38. http://dx.doi.org/10.1016/S0927-0248(00)00408-6.

Meinel, A.B., Meinel, M.P., 1979. Applied solar energy. Appl. Energy.

Mousazadeh, H., Keyhani, A., Javadi, A., Mobli, H., Abrinia, K., Sharifi, A., 2009. A review of principle and sun-tracking methods for maximizing solar systems output. Renew. Sustain. Energy Rev. 13, 1800–1818. http://dx.doi.org/10.1016/j.rser.2009.01.022.

Narvarte, L., Lorenzo, E., 2008. Tracking and ground cover ratio. Prog. Photovoltaics Res. Appl. 16, 703–714. http://dx.doi.org/10.1002/pip.847.

Neville, R.C., 1978. Solar energy collector orientation and tracking mode. Sol. Energy 20, 7–11. http://dx.doi.org/10.1016/0038-092X(78)90134-2.

Parkin, R.E., 2010. Solar angles revisited using a general vector approach. Sol. Energy 84, 912–916. http://dx.doi.org/10.1016/j.solener.2010.02.005.

Perez, R., Ineichen, P., Seals, R., Michalsky, J., Stewart, R., 1990. Modeling daylight availability and irradiance components from direct and global irradiance. Sol. Energy 44, 271–289. http://dx.doi.org/10.1016/0038-092X(90)90055-H.

Perpiñan, O., Lorenzo, E., Castro, M.A., Eyras, R., 2009. Energy payback time of grid connected PV systems: comparison between tracking and fixed systems. Prog. Photovoltaics Res. Appl. 17, 137–147. http://dx.doi.org/10.1002/pip.871.

Ramírez-Faz, J., López-Luque, R., 2012. Development of a methodology for quantifying insolation variables in windows and building openings. Renew. Energy 37, 426–433. http://dx.doi.org/10.1016/j.renene.2011.05.040.

Rapp-Arrarás, Í., Domingo-Santos, J.M., 2009. Algorithm for the calculation of the horizontal coordinates of the Sun via spatial rotation matrices. Renew. Energy 34, 876–882. http://dx.doi.org/10.1016/j.renene.2008.06.005.

Reda, I., Andreas, A., 2004. Solar position algorithm for solar radiation applications. Sol. Energy 76, 577–589. http://dx.doi.org/10.1016/j.solener.2003.12.003.

Reindl, D.T., Beckman, W.A., Duffie, J.A., 1990. Evaluation of hourly tilted surface radiation models. Sol. Energy 45, 9–17. http://dx.doi.org/10.1016/0038-092X(90)90061-G.

Riley, D., Hansen, C., 2014. Sun-relative pointing for dual-axis solar trackers employing azimuth and elevation rotations. J. Sol. Energy Eng. 137, 31008. http://dx.doi.org/10.1115/1.4029379.

Salas, V., Olias, E., 2009. Overview of the photovoltaic technology status and perspective in Spain. Renew. Sustain. Energy Rev. 13, 1049–1057. http://dx.doi.org/10.1016/j.rser.2008.03.011.

Skartveit, A., Asle Olseth, J., 1986. Modelling slope irradiance at high latitudes. Sol. Energy 36, 333–344. http://dx.doi.org/10.1016/0038-092X(86)90151-9.

Sproul, A.B., 2007. Derivation of the solar geometric relationships using vector analysis. Renew. Energy 32, 1187–1205. http://dx.doi.org/10.1016/j.renene.2006.05.001.

Stanciu, C., Stanciu, D., 2014. Optimum tilt angle for flat plate collectors all over the World – a declination dependence formula and comparisons of three solar radiation models. Energy Convers. Manage. 81, 133–143. http://dx.doi.org/10.1016/j.enconman.2014.02.016.

Torres-Roldán, M., López-Luque, R., Varo-Martínez, M., 2015. Design of an innovative and simplified polar heliostat for integration in buildings and urban environments. Sol. Energy 119, 159–168. http://dx.doi.org/10.1016/j.solener.2015.06.041.

Tsalides, P., Thanailakis, A., 1985. Direct computation of the array optimum tilt angle in constant-tilt photovoltaic systems. Sol. Cells 14, 83–94.

Usher, J.R., Muneer, T., 1989. Case studies in solar radiation modelling. Math. Comput. Model. 12, 1155–1165. http://dx.doi.org/10.1016/0895-7177(89)90236-7.

Yadav, A.K., Chandel, S.S., 2013. Tilt angle optimization to maximize incident solar radiation: a review. Renew. Sustain. Energy Rev. 23, 503–513. http://dx.doi.org/10.1016/j.rser.2013.02.027.

Yoon, K., Yun, G., Jeon, J., Kim, K.S., 2014. Evaluation of hourly solar radiation on inclined surfaces at Seoul by Photographical method. Sol. Energy 100, 203–216. http://dx.doi.org/10.1016/j.solener.2013.11.011.

Zill, D., Wright, W., 2011. Multivariable Calculus. Springer.

Anexo II

Segundo artículo del compendio: “Un novedoso enfoque para instalaciones con seguidores solares fotovoltaicos de dos ejes”.

Publicado en la revista Renewable Energy, editorial Elsevier.

Enviado el 15 de diciembre de 2018, aceptado el 12 de junio de 2019.

Factor de impacto en 2018: 5,439.

Renewable Energy 145 (2020) 1214–1221

Contents lists available at ScienceDirect

Renewable Energy

journal homepage: www.elsevier.com/locate/renene

A novel backtracking approach for two-axis solar PV tracking plants

L.M. Fernández-Ahumada [a], J. Ramírez-Faz [b], R. López-Luque [c], M. Varo-Martínez [c, *], I.M. Moreno-García [d], F. Casares de la Torre [b]

[a] Computing and Numeric Analysis, University of Cordoba, Campus of Rabanales, 14071 Cordoba, Spain
[b] Electrical Engineering, University of Cordoba, Campus of Rabanales, 14071 Cordoba, Spain
[c] Applied Physics, University of Cordoba, Campus of Rabanales, 14071 Cordoba, Spain
[d] Electronic and Computers Engineering, University of Cordoba, Campus of Rabanales, 14071 Cordoba, Spain

ARTICLE INFO

Article history:
Received 15 December 2018
Received in revised form
29 April 2019
Accepted 12 June 2019
Available online 15 June 2019

Keywords:
PV solar plants
Two-axis solar tracker
Power losses by shading in PV plants
Backtracking

ABSTRACT

Solar tracking is a technique required to increase energy production in multiple photovoltaic (PV) facilities. In these plants, during low-elevation solar angle hours, shadows appear between the collectors causing a dramatic decrease in production. This paper presents a novel optimal tracking strategy to prevent the creation of these shadows. The presented method determines whether or not there is shading between collectors. Thus, when the collectors are not shaded, a tracking trajectory for maximum irradiance on the collectors is suggested. However, when the collectors are shaded, backtracking is proposed. Therefore, energy production in plants with this novel tracking method can be 1.31% higher than that in PV installations with astronomical tracking. Moreover, this method allows the study of PV facilities for which there have been no published approaches, such as plants with non-rectangular collectors or those located on topographically heterogeneous surfaces.

1. Introduction

Technologies based on the use of solar energy have recently received more attention, and their development aims to respond to the growing need for renewable energy. In this context, scientific advances in the field of photovoltaics (PV) are allowing this technology to become an alternative sustainable energy source [1,2]. However, these advances are not always properly applied to PV plant design and/or operation, and, consequently, the optimal development that these advances require for PV plants has not yet been achieved.

This is evident in the case of using solar tracking to increase the ability of PV plants to harness solar resources. Solar trackers can be classified as one- or two-axis trackers. In one-axis trackers, the collector's surface rotates around a fixed axis, while the surface moves around two fixed axes in two-axis trackers, which allows the collector plane to orientate towards any direction of the celestial sphere [3]. In this research area, authors [4–6] have analysed the effects of the type of tracking on energy production at different latitudes, and their results show that, in any case, the higher the latitude, the more effective the tracking, with differences reaching 57% [7].

In solar tracking PV plants, the collector's orientation is commonly governed by equations based on the astronomical movement of the Sun, which can predict the position of the Sun in the celestial sphere with an accuracy of an order of mrad [8–10]. In this field, mathematical equations based on applying spherical trigonometry to solar movement have been developed to calculate the elevation and azimuth position for one- and two-axis trackers for each moment [7,10–14]. Recently, in contrast to this method, it is possible to deduce all of the astronomical factors governing the movement of the Sun and the orientation of solar tracking systems from the definition of 'solar vector' (unit vector along the direction towards the centre of the solar disk) and applying vector algebra [15–19].

Applying the astronomical model to solar tracking means that the angle formed between the direct solar rays and the normal angle to the collector's surface θ must be as low as possible. With astronomical tracking, the value of the direct irradiance component is maximized, which is appropriate for applications focused on this component (such as concentration technologies). However, in PV, all irradiance components (direct, diffuse, and reflected irradiance)

* Corresponding author. Applied Physics Department, University of Cordoba. Albert Einstein Building, Campus of Rabanales, Carretera Nacional IV, km 396, Cordoba, Spain.
E-mail address: fa2vamam@uco.es (M. Varo-Martínez).

https://doi.org/10.1016/j.renene.2019.06.062
0960-1481/

are useable. Therefore, this type of tracking is not the most suitable. As Duffie and Beckman [11] and Mousazadeh et al. [2] noted, on cloudy days, when the solar disk is not visible and direct radiation does not reach the collectors, collectors located on a fixed horizontal position would collect more energy than those with astronomical tracking. Despite this, no work has been conducted to determine the appropriate equations for optimising solar tracking on cloudy days. Thus, it is necessary to study the influence of diffuse and reflected components on solar tracking in greater depth to determine the equations that can allow maximum radiative capture.

Additionally, one of the most important aspects to consider in plants with astronomical solar tracking is shading between the modules, which mainly occurs during the first and last hours of the day and causes production losses, as well as the appearance of hot spots in the modules [7].

To characterise and optimise the design of tracking plants, Diaz-Dorado et al. [20,21] developed a model that considers the arrangement of the cells within the photovoltaic modules, as well as the exact position of each module within the tracking surface, to determine the shading effects for all cells in the tracker. In this model, shading is characterised following a conventional tracking strategy to achieve perpendicularity between the direct solar rays and the collector's surface [20,21].

To estimate power losses caused by shading, Martinez-Moreno et al. [22] have proposed a predictive model that does not require any specific information regarding the connections between the cells and modules. This model has been validated by different authors [23,24] who have developed more extensive models based on Martinez-Moreno's model to determine the productivity of PV plants. Similarly, Perpiñan [25] developed a method for estimating and optimising energy costs based on plant design parameters, specifically the ground cover ratio (GCR, which is the ratio between the PV module area and the terrain occupied by the PV plant). For this, the method uses Gordon and Wenger's hypothesis [26] when determining energy losses due to shading, which considers the losses proportional to the percentage of the shaded area. Navarte and Lorenzo [27] studied the productivity of a PV plant considering different types of solar tracking and three simple hypotheses for estimating losses by shading.

Panico et al. [28] proposed backtracking as an approach to minimise the effects of shading. This technique involves deviating the direction of the solar trackers from the solar position to avoid shading between the collectors when necessary. Different authors [7,28,29] have demonstrated the advantages of backtracking, as follows:

A. Advantages of land use: By avoiding the effects of shading, the distances between trackers can be reduced, resulting in greater GCR.
B. Operating advantages: The work conducted by Lorenzo and Navarte [7] indicates that, in all cases, energy balance is more favourable in plants with backtracking than in those allowing shading between collectors.
C. Design advantages: The absence of shading and, therefore, of hot spots, suggests lower maintenance costs.

Therefore, the reliability of plants with backtracking is greater than that in plants that allow shading [7,29]. Consequently, many technological solutions to implement backtracking are being developed [30–32].

To determine the orientation of the collectors during backtracking, different methods based on the geometric determination of shadows between polygons have been proposed [4,7,33]. However, these methods are often limited to simple geometric situations such as:

i. Exclusively rectangular collectors.
ii. Regular ground layouts where only the shading between contiguous collectors is considered.
iii. Flat topographic surfaces.
iv. Horizontal topographic surfaces.
v. Movement around the azimuthal and elevational axes without considering other combinations of axes that entail the rotation of the collector around the normal axis to the collector's surface.

Considering the aforementioned limitations, this study presents a simple and more generic backtracking method to avoid shadows and optimise solar energy collection. The method is based on the vector treatment of the geometry of the Sun-Earth position, as well as the implicit geometry of solar tracking plants. Furthermore, this method does not *a priori* assume the astronomical tracking hypothesis commonly assumed in the literature, which aims to maintain the position of the collector's surface perpendicular to the direct solar rays [15]. Thus, the proposed method allows the following, which are novelties in comparison to conventional methodologies:

1. The study of plants with non-rectangular surface collectors.
2. The analysis of facilities where collectors are not necessarily located at the regular nodes of a geometric grid.
3. The determination and comparison of the effects of different tracking modes.
4. The consideration of plants located on real topographical surfaces, and not only flat or horizontal surfaces.
5. The consideration of global irradiance on collectors, instead of being limited to direct irradiance (typical for astronomical tracking).

Therefore, the method presented here will be useful for optimising the design of new photovoltaic two-axis tracker plants, as well as for controlling the movement of current plants by improving and optimising their electrical production.

2. Materials and methods

2.1. Astronomical and vector fundamentals

To optimise the trajectory of solar trackers in PV plants, this work is based on the definition of the solar vector $\vec{s}$ in an Earth reference system, where the Ox axis is oriented to the West, the Oy axis is oriented to the South, and the Oz axis is oriented to the zenithal direction, with $\vec{i}$, $\vec{j}$, *and* $\vec{k}$ the respective unit vectors (Fig. 1). The solar vector is given by equation (1), where δ is the solar declination [16], ϕ is the latitude and Ωt is the hourly angle, which is defined as the product of the Earth's rotation speed ($\Omega = 2\pi/24 rad/h$) and the time elapsed since the solar noon.

$$\vec{s} = s_x\vec{i} + s_y\vec{j} + s_z\vec{k} = \sin\Omega t\ \cos\delta\,\vec{i} + (\cos\Omega t\cos\delta\sin\varphi - \sin\delta\cos\varphi)\,\vec{j} + +(\cos\Omega t\cos\delta\cos\varphi + \sin\delta\sin\varphi)\,\vec{k} \quad (1)$$

Fig. 1 also shows the polygon Π, which represents the perimeter of the collector's surface, and the vector normal to that surface, $\vec{n}$. The components of the vector $\vec{n}$ in the Earth reference system, depending on the azimuth (γ) and elevation (α) angles of the collectors, are given by equation (2).

$$\vec{n} = cos\alpha\cdot sin\gamma\,\vec{i} + cos\alpha\cdot cos\gamma\,\vec{j} + sin\alpha\,\vec{k} \quad (2)$$

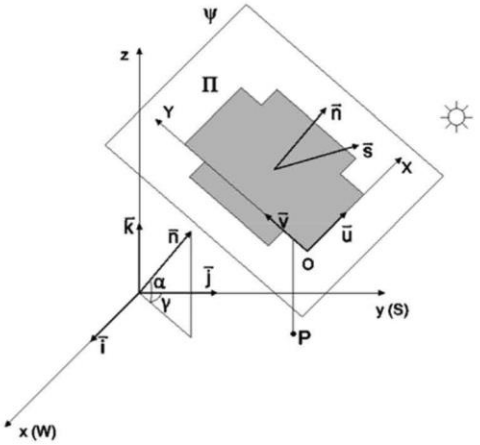

Fig. 1. Representation of the collector's surface in the Earth reference system.

Additionally, the projection plane is considered as the plane that contains the collector's surface. A flat coordinate system associated with this plane is defined (OXY) with unit vectors $\vec{u}$ and $\vec{v}$. During tracking, the system will move while rigidly attached to the collector polygon. As a result, the mathematical expressions for $\vec{u}$ and $\vec{v}$ will depend on the collector's orientation at every moment, given by α and γ, and be conditioned by the type of tracking. Equations (3)–(16) present the expressions for the most frequent tracking typologies (shown in Fig. 2).

- Azimuth-elevation tracking (A-E)

$$\vec{u} = -cos\gamma\,\vec{i} + sin\gamma\,\vec{j} \tag{3}$$

$$\vec{v} = sin\alpha\cdot cos\gamma\,\vec{i} - sin\alpha\cdot cos\gamma\,\vec{j} + cos\alpha\,\vec{k} \tag{4}$$

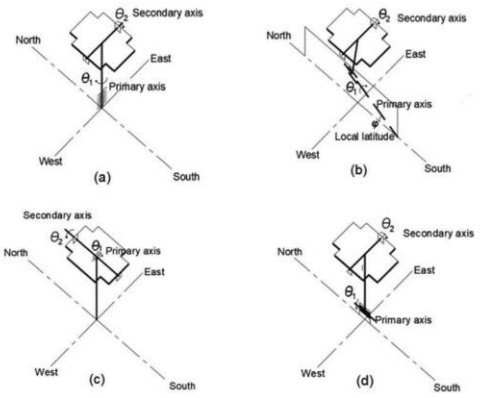

Fig. 2. Common tracking strategies: a) Azimuth-elevation tracking (A–E), b) Equatorial tracking (EQ), c) Elevation-Rolling tracking (E–R), and d) Rolling-Elevation tracking (R–E).

- Equatorial tracking (EQ)

$$\vec{u} = -cos\theta_1\,\vec{i} + sin\theta_1\cdot cos\varphi\,\vec{j} + sin\theta_1\cdot sin\varphi\,\vec{k} \tag{5}$$

$$\vec{v} = -sin\theta_2\cdot sin\theta_1\,\vec{i} - (cos\theta_1\cdot sin\theta_2\cdot cos\varphi + cos\theta_2\cdot sin\varphi)\,\vec{j} - (cos\theta_1\cdot sin\theta_2\cdot sin\varphi - cos\theta_2\cdot sin\theta_1)\,\vec{k} \tag{6}$$

where

$$\theta_1 = tan^{-1}\left(\frac{cos\alpha\cdot sin\gamma}{cos\alpha\cdot cos\gamma\cdot cos\varphi - sin\alpha\cdot sin\varphi}\right) \tag{7}$$

$$\theta_2 = sin^{-1}(cos\alpha\cdot cos\gamma\cdot sin\varphi + sin\alpha\cdot cos\varphi) \tag{8}$$

- Elevation-Rolling tracking (E-R)

$$\vec{u} = -cos\theta_2\,\vec{i} + sin\theta_1\cdot sin\theta_2\,\vec{j} + cos\theta_1\cdot sin\theta_2\,\vec{k} \tag{9}$$

$$\vec{v} = -cos\theta_1\,\vec{j} + sin\theta_1\,\vec{k} \tag{10}$$

where

$$\theta_1 = tan^{-1}(cos\gamma\cdot cotan\alpha) \tag{11}$$

$$\theta_2 = sin^{-1}(cos\alpha\cdot sin\gamma) \tag{12}$$

- Rolling-Elevation tracking (R-E)

$$\vec{u} = -cos\theta_1\,\vec{i} + sin\theta_1\,\vec{k} \tag{13}$$

$$\vec{v} = sin\theta_1\cdot cos\theta_2\,\vec{i} + sin\theta_2\,\vec{j} + cos\theta_1\cdot cos\theta_2\,\vec{k} \tag{14}$$

where

$$\theta_1 = tan^{-1}(sin\gamma\cdot cos\alpha) \tag{15}$$

$$\theta_2 = cos^{-1}(cos\gamma\cdot cos\alpha) \tag{16}$$

2.2. Geometrical methodology

Based on the geometric fundamentals defined in the previous section, this work studies shadows to dichotomously determine whether there is an intersection between the PV collectors at a specific time, rather than to quantify the shape and size of the shaded polygons. Therefore, by calculating the irradiance received by the collector's surfaces for a given hour at different positions when there is no shading, the maximum irradiance position can be elucidated. Moreover, by conducting this study over a certain period, it is possible to define the trajectory of the collectors that optimises energy capture by a PV plant for each day of the year.

In this study, it is considered that all collectors have the same

geometric shape and move in the same manner. Considering this, it can be stated that the planes that contain the collector surfaces are always parallel. Therefore, regardless of the solar position with respect to the collectors, the solar projection Π'_i of any collector Π_i on plane Ψ containing the reference tracker Π_0 will produce a polygon with the same shape and dimensions as the collector polygon i (Fig. 3). From this projection, it can be concluded that Π_i shades Π_0 if polygons Π_0 and Π'_i intersect.

As all collectors are considered equal and the perimeters of the projected collectors in the solar direction maintain their geometry, polygon Π'_i could be considered as a translation of the reference collector Π_0 contained on plane Ψ, with $\vec{d}_i$ as the translation vector. Similarly, as the collectors remain parallel, the distance between any two equivalent points (A_i and A_0) of collectors Π_i and Π_0 is constant. That is, $\overrightarrow{A_0A_i} = \overrightarrow{P_oP_i}$. Consequently, to determine $\vec{d}_i$, the parallelogram rule is applied to the vectors involved in the described geometric problem (Fig. 3), which produces equation (17).

$$\overrightarrow{P_oP_i} = \overrightarrow{A_0A_i} = \vec{d}_i + \tau \cdot \vec{s} \tag{17}$$

Furthermore, to determine τ, the scalar product between equation (17) and the vector normal to plane Ψ, $\vec{n}$, is calculated, which produces equation (18), where $\vec{n} \cdot \vec{d}_i$ is zero as both vectors are perpendicular.

$$\vec{n} \cdot \overrightarrow{P_oP_i} = \vec{n} \cdot \vec{di} + \vec{n} \cdot \tau \cdot \vec{s} \tag{18}$$

Consequently, scalar τ is given by equation (19).

$$\tau = \frac{\overrightarrow{P_oP_i} \cdot \vec{n}}{\vec{s} \cdot \vec{n}} \tag{19}$$

Substituting (19) into (17), the translation vector of projection Π'_i with respect to reference collector Π_0 on plane Ψ, $\vec{d}_i$, can be obtained (Equation (20)).

$$\vec{d}_i = \overrightarrow{P_oP_i} - \frac{\overrightarrow{P_oP_i} \cdot \vec{n}}{\vec{s} \cdot \vec{n}} \vec{s} \tag{20}$$

Thus, expression (20) allows the components of $\vec{d}_i$ in Earth reference system Oxyz to be calculated. However, as $\vec{d}_i$ belongs to the OXY plane, the Cartesian components in the collector plane can be determined by equations (21) and (22).

$$d_X = \vec{d} \cdot \vec{u} \tag{21}$$

$$d_Y = \vec{d} \cdot \vec{v} \tag{22}$$

Once the projections have been obtained, a test based on Minkowski algebra [17–19] is conducted to determine whether the polygons intersect and, therefore, whether there would be shading. For this, all the feasible polygons on Ψ resulting from moving Π_0 are drawn so that any point on its perimeter matches the origin of the 0XY reference system associated with plane Ψ (Fig. 4). Polygon Σ is defined as the envelope of this family of polygons. Therefore, it is possible to affirm that Π_0 and Π'_i intersect if the representation of the corresponding $\vec{d}_i$, vector moved to the origin of the 0XY reference system, is fully included in Σ (Fig. 4).

To ensure that reference collector Π_0 is not shaded at a given time, it is necessary to check that it is not shaded by any other collector in the PV plant. Given that envelope Σ is the same for any pair of collectors as they all exhibit the same geometry and remain parallel, it would be sufficient to determine whether the $\vec{d}_i$ vectors (for $i = 1$, N-1, with N being the number of PV panels in the plant) linked to each pair of collector surfaces, Π_0-Π_i, are included in envelope Σ for cases that meet the following conditions:

I. Collector Π_i is visible from the reference collector Π_0: $\overrightarrow{P_oP_i} \cdot \vec{n} > 0$.
II. The sun does not irradiate the rear side of the collectors: $\vec{s} \cdot \vec{n} > 0$.
III. It is a specific moment of the solar day: $\vec{s} \cdot \vec{k} > 0$.

Under these conditions, a single $\vec{d}_i$ included in the Σ envelope will indicate that the studied collector is shaded.

2.3. Optimisation of the collector position under the no shading hypothesis

According to the described method, for each moment in time, whether the reference collector is shaded or not for different collector orientations (given by its azimuth, γ, and elevation, α) can be analysed. Based on this analysis, for any specific moment in time, it is also possible to represent the delimitation of the two regions in a cylindrical chart (γ, α): one corresponding to shaded collectors and another corresponding to non-shaded collectors. In addition, as will be demonstrated in the application, the irradiance received by the

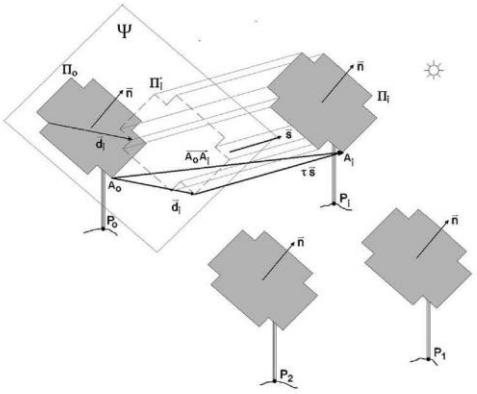

Fig. 3. Geometry of the set of trackers.

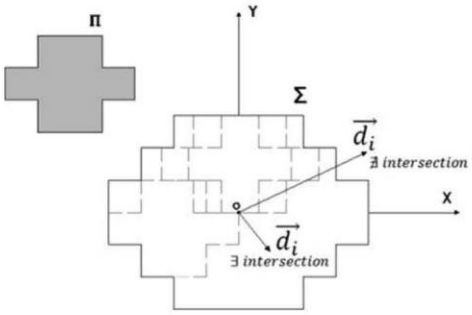

Fig. 4. Obtaining enveloping polygon Σ from Π

collectors at each orientation can be also represented on the same chart using irradiance isovalue curves. From these two delimited areas and using the irradiance isovalue curves, the point with maximum irradiance for each moment in time, and, consequently, the optimum orientation of the solar trackers, can be selected. Repeating this process for different moments in time the same day can allow the optimal tracking trajectory (with maximum irradiance and without shading) to be defined.

3. Results and discussion

Once the proposed methodology has been described, the optimal trajectories for tracking and backtracking at the "El Molino" PV solar plant located in Cordoba, Spain, are obtained (latitude = 37.75492°N; longitude = 5.04548°W). This plant is an Azimuth Elevation tracker plant arranged in a rectangular grid with an east-west distance (d_{EW}) of 20 m and north-south distance (d_{NS}) of 14 m (Fig. 5).

Based on the geometry of the collectors (Fig. 6a and b), Fig. 7 shows the envelope Σ for the collectors' surface. In practice, the polygons constituting the collectors (Fig. 6a) only have right angles. Therefore, the surrounding polygon Σ has only right angles (Fig. 7), simplifying the test to determine whether the $\vec{d_i}$ vectors are included in Σ. Therefore, in this example, each $\vec{d_i}$ is included in the Σ envelope if condition (23) or (24) is verified.

$$|d_{iX}| < 8\ m \text{ and } |d_{iY}| < 4\ m \tag{23}$$

$$|d_{iX}| < 6.4\ m \text{ and } |d_{iY}| < 5\ m \tag{24}$$

The analysis method proposed here was applied every 5 min for one astronomical year. As this methodology involves a dichotomous test to establish whether or not there is shading at a specific collector orientation defined by its azimuth (γ) and elevation (α), a binary search for the elevation limit between the shaded and non-shaded areas has been programmed for fixed azimuth values. It has been verified that eight iterations are sufficient for estimating this limit with an error below 0.3 deg.

For Julian Day 349 at 8:20 (true solar time; TST), Fig. 8 shows a cylindrical chart representing the boundary between the shaded (grey region, corresponding to the cases for which at least one $\vec{d_i}$ is included in Σ) and not-shaded (blue region, corresponding to the cases for which all vectors $\vec{d_i}$ are not included in Σ) areas. Moreover, the irradiance isolines were included in the non-shaded area. As the proposed methodology only considers the collector positions at which there would be no shading, a single irradiance model is assumed. Therefore, Liu-Jordan's equation [34] (Equation (25)) was considered as it was used by Fernandez-Ahumada et al. [15], where I_B and I_D are direct and diffuse irradiances, respectively, and ρ is the albedo. In this study, $\rho = 0.2$ is considered following [34]. Therefore, it is possible to determine the solar irradiance captured by the collectors for each orientation without shading using equation (25).

Fig. 5. Application example: Spatial distribution of the collectors of the El Molino PV plant (Cordoba, Spain).

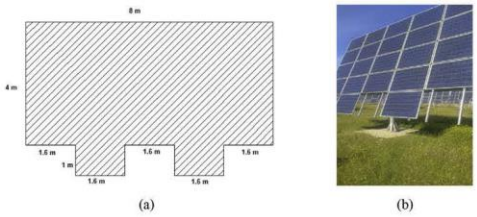

Fig. 6. Application example: Shape and dimensions of the photovoltaic collectors in the El Molino PV plant (Cordoba, Spain).

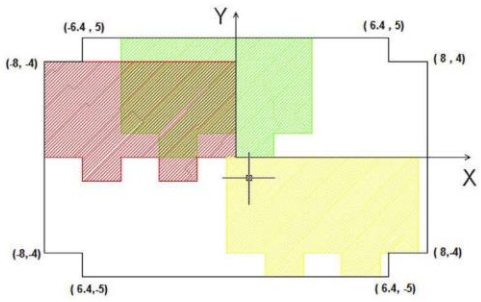

Fig. 7. Application example: Shape and dimensions of polygon Σ enveloping the set of polygons generated by sliding Π_0 onto the origin of the coordinates (values in metres).

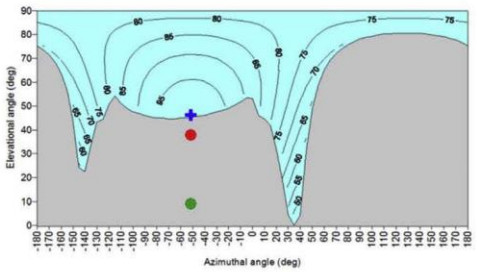

Fig. 8. Application example: Splitting of the spatial directions and selection of the angles (γ, α) that optimise irradiance (W/m^2) for the reference collector in the El Molino PV plant (Cordoba, Spain) on Julian day 349 at 8:20 TST.

$$I = \frac{\vec{s}\cdot\vec{n}}{\vec{s}\cdot\vec{k}} I_B + \frac{1+\vec{k}\cdot\vec{n}}{2} I_D + \rho \frac{1-\vec{k}\cdot\vec{n}}{2} (I_B + I_D) \quad (25)$$

Similarly, Fig. 8 presents the collector orientation for three different tracking strategies:

a. Astronomical tracking with no shading (ATNS, represented by a green circle): tracking governed by an astronomic equation for an ideal PV plant where the distances between the collectors are sufficiently large to avoid shading.
b. Maximum irradiance tracking with no shading (MITNS, represented by a red circle): the optimal tracking strategy proposed by Fernandez-Ahumada et al. [15], which seeks maximum irradiance levels on an ideal isolated collector that is not affected by shadows from adjoining collectors.
c. Maximum irradiance backtracking (MIBT, represented by a blue cross): tracking strategy proposed in this study, which seeks maximum irradiance levels while avoiding shading between the collectors by backtracking when necessary.

Therefore, for this day and time, this novel backtracking approach proposes that the tracker should point towards the maximum irradiance direction within the non-shaded region (blue cross in Fig. 8). Fig. 8 also shows that the orientations corresponding to ATNS and MITNS are within the region where there are shadows between the collectors and, consequently, the irradiance captured by the PV modules is reduced. However, it should be noted that, in this case, the minimum and maximum limits of the azimuth or elevation are not considered. Consequently, if these constructive limits exist, they should also be represented as additional restrictions in the cylindrical charts.

Moreover, based on the method outlined above, the path to be tracked by the collector for the day of study can be proposed. Therefore, Fig. 9 shows the trajectories corresponding to the three different analysed tracking strategies: ATNS (green line), MITNS (red line), and MIBT (blue line). As shown, the proposed MIBT trajectory (blue curve) exhibits sections where it does not coincide with the MITNS trajectory (red curve) corresponding to the maximum solar irradiance collection under an ideal situation with no shading. For these periods, backtracking is proposed as the movement that optimises energy collection by the plant, as it considers the real shadows between the collectors, which reduce the levels of irradiance from their optimal values considered by MITNS.

Finally, the daily radiation was determined for each approach to compare energy production under the three potential strategies (ATNS, MITNS, and MIBT). The values for the three cases were obtained by integrating equation (25) on representative days. Therefore, although the three tracking strategies imply no shading between collectors, in contrast to MIBT, ATNS and MITNS are only valid for isolated trackers and not for plants with many PV modules. Accordingly, the simulated energy production of these two ideal tracking strategies can be considered as maximum potential values and should be used as a reference to evaluate the improvements made by the proposed tracking method.

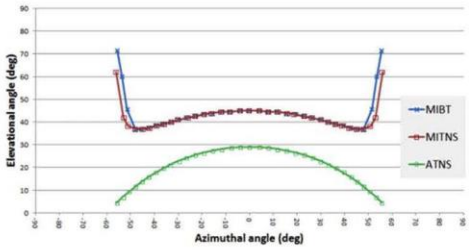

Fig. 9. Application example: Potential collector pointing trajectories of the PV plant "El Molino" (Cordoba, Spain) on the Julian day = 349.

Table 1 shows the simulated energy production (kWh) values for each month against the peak power (kWp) of the collectors. In line with Fernandez-Ahumada's results [15], energy production under MITNS is higher than that under ATNS. Similarly, it has been verified that, for several months, energy production by solar plants under MIBT reaches values between the optimal values of MITNS and ATNS. Production by MIBT solar plants is 0.89% lower than that by MINTS plants, but 1.31% higher than that by ATNS plants.

The proposed method improves the results obtained by Navarte and Lorenzo [27] in their characterisation of the energy losses due to shading in plants with different astronomical tracking typologies (one and two-axis). They demonstrated that, in all cases, energy production losses increase with GCR. Therefore, in comparison to the ideal astronomical tracking, they estimated that the uncertainty of energy production is within 2% for GCR = 0.09. These results are similar to those published by Panico [28], even though this study is restricted to one-axis trackers. Specifically, Panico found that the losses due to shading in installations with GCR = 0.09 compared to astronomical tracking are 2.5% [28]. These values are also within the intervals proposed by Gordon and Wenger [26], who demonstrated that energy losses by shading in plants with GCR = 0.09 depend on the collectors' geometry and spatial layout.

Consequently, all published studies indicate that shading causes energy losses in comparison to energy generation under ideal astronomical tracking. Therefore, this study shows that solar energy collection by plants with the proposed tracking strategy, MIBT, is better than that by plants with astronomical tracking and only 0.98% lower than that by plants with the ideal MITNS tracking. However, owing to the scarcity of publications in this area, the authors of this paper consider that it is necessary to continue studying the influence of design parameters on energy collection by plants with MIBT, as well as to implement this novel tracking strategy in actual PV installations to evaluate its development.

4. Conclusions

In this study, a new methodology for defining the optimal tracking strategy without shading of sets of two-axis motion PV tracker collectors is proposed. In contrast to astronomical tracking, the proposed method indicates that collectors do not have to be constantly perpendicular to the direct solar rays, as it considers the diffuse and reflected irradiance, as well as the direct irradiance, reaching PV collectors. Therefore, when collectors are not shaded, a tracking trajectory seeking maximum irradiance on the collectors is suggested. However, when the collectors are shaded, backtracking is proposed. Therefore, based on the concepts of solar vectors and vector algebra, this method analyses shading between the collectors. However, the proposed technique is not based on the calculation of the area of polygon intersections; rather, it is based on whether or not such intersections are present. Consequently, in contrast with other tracking strategies found in previous studies, this novel method is based on algorithms that are significantly more simple and fast. Thus, owing to its novelties and advantages, this method is easier to be used to simulate energy production with different radiative models and is applicable to situations for which no published generic methods can be found, such as PV plants:

Table 1
Comparative analysis of the energy production levels of PV solar plants with different tracking strategies.

Month	MIBT (kWh/kWp)	MITNS (kWh/kWp)	ATNS (kWh/kWp)	Decrease in MIBT vs. MITNS (%)	Increase in MIBT vs. ATNS (%)
January	82.4	84.2	83.7	2.16	−1.51
February	114.7	116.0	114.0	1.09	0.59
March	144.3	146.3	144.4	1.36	−0.11
April	160.8	163.0	161.4	1.35	−0.39
May	177.1	179.6	178.4	1.41	−0.76
June	250.5	251.1	244.5	0.24	2.44
July	291.0	291.3	280.7	0.08	3.68
August	269.3	269.6	259.0	0.09	4.01
September	197.7	198.4	192.1	0.34	2.93
October	125.4	127.3	125.9	1.49	−0.35
November	86.6	88.5	88.0	2.11	−1.52
December	65.0	67.4	67.4	3.54	−3.49
Year	1965.0	1982.7	1939.5	0.89	1.31

i. With non-rectangular surface collectors
ii. With collectors that are not located on the regular nodes of a geometric mesh
iii. With different tracking modes
iv. With trackers located on real topographical surfaces

The energy production by PV plants with this new tracking strategy, called MIBT, has been analysed and compared to two ideal tracking strategies:

1) ATNS: Astronomical tracking in an ideal PV plant where the distances between the collectors are large enough to avoid shading.
2) MITNS: optimal tracking that seeks the maximum irradiance levels on an ideal isolated collector not affected by potential shadows from adjoining collectors [15].

The results show that MIBT improves the energy collection by 1.31% in comparison to ATNS, and the energy collection is only 0.89% lower than that by MITNS plants. Therefore, considering these results and the advantages of this method, the authors consider that this method will not only be useful for designing new facilities, but could also help to improve the productivity and management of many PV plants by redefining tracking strategies.

Acknowledgements

This research is partially supported by the CLARA Project, which has received funding from the European Union's Horizon 2020 research and innovation programme under Grant Agreement No 730482. The authors thank Magtel Operaciones SL for their collaboration in this research.

References

[1] V. Salas, E. Olias, Overview of the photovoltaic technology status and perspective in Spain, Renew. Sustain. Energy Rev. 13 (2009) 1049–1057, https://doi.org/10.1016/j.rser.2008.03.011.
[2] H. Mousazadeh, A. Keyhani, A. Javadi, H. Mobli, K. Abrinia, A. Sharifi, A review of principle and sun-tracking methods for maximizing solar systems output, Renew. Sustain. Energy Rev. 13 (2009) 1800–1818, https://doi.org/10.1016/j.rser.2009.01.022.
[3] C.-Y. Lee, P.-C. Chou, C.-M. Chiang, C.-F. Lin, Sun tracking systems: a review, Sensors 9 (2009) 3875–3890, https://doi.org/10.3390/s90503875 (14248220).
[4] E. Lorenzo, M. Pérez, A. Ezpeleta, J. Acedo, Design of tracking photovoltaic systems with a single vertical axis, Prog. Photovoltaics Res. Appl. 10 (2002) 533–543, https://doi.org/10.1002/pip.442.
[5] O. Perpiñan, E. Lorenzo, M.A. Castro, R. Eyras, Energy payback time of grid connected PV systems: comparison between tracking and fixed systems, Prog. Photovoltaics Res. Appl. 17 (2009) 137–147, https://doi.org/10.1002/pip.871.
[6] T. Huld, M. Suri, E.D. Dunlop, Comparison of potential solar electricity output from fixed-inclined and two-axis tracking photovoltaic modules in Europe, Prog. Photovoltaics Res. Appl. 16 (2008) 47–59, https://doi.org/10.1002/pip.773.
[7] E. Lorenzo, L. Narvarte, J. Muñoz, Tracking and Back-Tracking, 2011.
[8] M. Blanco-Muriel, D.C. Alarcón-Padilla, T. López-Moratalla, M. Lara-Coira, Computing the solar vector, Sol. Energy 70 (2001) 431–441, https://doi.org/10.1016/S0038-092X(00)00156-0.
[9] I. Reda, A. Andreas, Solar position algorithm for solar radiation applications, Sol. Energy 76 (2004) 577–589, https://doi.org/10.1016/j.solener.2003.12.003.
[10] J.E. Braun, J.C. Mitchell, Solar geometry for fixed and tracking surfaces, Sol. Energy 31 (1983) 439–444, https://doi.org/10.1016/0038-092X(83)90046-4.
[11] J.A. Duffie, W.A. Beckman, Solar Engineering of Thermal Processes, fourth ed., 2013, https://doi.org/10.1002/9781118671603.
[12] D. Riley, C. Hansen, Sun-relative pointing for dual-Axis solar trackers employing azimuth and elevation rotations, J. Sol. Energy Eng. 137 (2014), 031008, https://doi.org/10.1115/1.4029379.
[13] P.G. Jolly, Derivation of solar angles using vector algebra, Sol. Energy 37 (1986) 429–430.
[14] Í. Rapp-Arrarás, J.M. Domingo-Santos, Algorithm for the calculation of the horizontal coordinates of the Sun via spatial rotation matrices, Renew. Energy 34 (2009) 876–882, https://doi.org/10.1016/j.renene.2008.06.005.
[15] L.M. Fernández-Ahumada, F.J. Casares, J. Ramírez-Faz, R. López-Luque, Mathematical study of the movement of solar tracking systems based on rational models, Sol. Energy 150 (2017) 20–29, https://doi.org/10.1016/j.solener.2017.04.006.
[16] E.G. Evseev, A.I. Kudish, The assessment of different models to predict the global solar radiation on a surface tilted to the south, Sol. Energy 83 (2009) 377–388, https://doi.org/10.1016/j.solener.2008.08.010.
[17] B. Chazelle, The polygon containment problem, Adv. Comput. Res. 1 (1983) 1–33.
[18] T. Lozano-Perez, Spatial Planning: A Configuration Space Approach, 1980.
[19] F. Avnaim, J.-D. Boissonnat, Polygon placement under translation and rotation, RAIRO Theor. Inform. Appl. 23 (1989) 5–28, https://doi.org/10.1051/ita/1989230100051.
[20] E. Díaz-Dorado, J. Cidrás, C. Carrillo, A method to estimate the energy production of photovoltaic trackers under shading conditions, Energy Convers. Manag. 150 (2017) 433–450, https://doi.org/10.1016/J.ENCONMAN.2017.08.022.
[21] E. Díaz-Dorado, J. Cidrás, C. Carrillo, Discrete I–V model for partially shaded PV-arrays, Sol. Energy 103 (2014) 96–107, https://doi.org/10.1016/J.SOLENER.2014.01.037.
[22] F. Martínez-Moreno, J. Muñoz, E. Lorenzo, Experimental model to estimate shading losses on PV arrays, Sol. Energy Mater. Sol. Cells 94 (2010) 2298–2303, https://doi.org/10.1016/J.SOLMAT.2010.07.029.
[23] T.O. Fartaria, M.C. Pereira, Simulation and computation of shadow losses of direct normal, diffuse solar radiation and albedo in a photovoltaic field with multiple 2-axis trackers using ray tracing methods, Sol. Energy 91 (2013) 93–101, https://doi.org/10.1016/J.SOLENER.2013.02.008.
[24] Y. Hu, Y. Yao, A methodology for calculating photovoltaic field output and effect of solar tracking strategy, Energy Convers. Manag. 126 (2016) 278–289, https://doi.org/10.1016/J.ENCONMAN.2016.08.007.
[25] O. Perpiñán, Cost of energy and mutual shadows in a two-axis tracking PV system, Renew. Energy 43 (2012) 331–342, https://doi.org/10.1016/J.RENENE.2011.12.001.
[26] J.M. Gordon, H.J. Wenger, Central-station solar photovoltaic systems: field layout, tracker, and array geometry sensitivity studies, Sol. Energy 46 (1991) 211–217, https://doi.org/10.1016/0038-092X(91)90065-5.
[27] L. Narvarte, E. Lorenzo, Tracking and ground cover ratio, Prog. Photovoltaics Res. Appl. 16 (2008) 703–714, https://doi.org/10.1002/pip.847.
[28] D. Panico, P. Garvison, H. Wenger, D. Shugar, Backtracking: a novel strategy for tracking PV systems, in: Conf. Rec. Twenty-Second IEEE Photovolt. Spec. Conf, IEEE, 1991, pp. 668–673, https://doi.org/10.1109/PVSC.1991.169294, n.d.
[29] M.C.-R.M. Pedro, Modelling of Shading Effects in Photovoltaic Optimization, 2016.

[30] Control Seguimiento Solar, Sun Tracker Control, Solar Nachführung - Suntrack, (n.d.).
[31] Solar Production Machines - Machinery and Plant Construction - Siemens Global Website, (n.d.).
[32] Lauritzen Solutions, (n.d.).
[33] D. Schneider, Control algorithms for large-scale single-axis photovoltaic trackers, Acta Polytech 52 (2012), https://doi.org/10.14311/1648.
[34] B.Y.H. Liu, R.C. Jordan, A rational procedure for predicting the long-term average performance of flat-plate solar-energy collectors, Sol. Energy 7 (1963) 53–74, https://doi.org/10.1016/0038-092X(63)90006-9.

Anexo III

Tercer artículo del compendio: “Una metodología para el acceso solar de edificios en ciudades sostenibles”.

Publicado en la revista Sustainability, editorial MDPI.

Enviado el 18 de septiembre de 2019, aceptado el 15 de noviembre de 2019.

Factor de impacto en 2018: 2,592.

sustainability

MDPI

Article

A Methodology for Buildings Access to Solar Radiation in Sustainable Cities

L. M. Fernández-Ahumada [1], J. Ramírez-Faz [2], R. López-Luque [3], A. Márquez-García [4] and M. Varo-Martínez [3,*]

1 Department of Computing and Numeric Analysis, University of Cordoba, Campus of Rabanales, 14071 Cordoba, Spain; lmfernandez@uco.es
2 Department of Electrical Engineering, University of Cordoba, Campus of Rabanales, 14071 Cordoba, Spain; jramirez@uco.es
3 Department of Applied Physics, University of Cordoba, Campus of Rabanales, 14071 Cordoba, Spain; fa1lolur@uco.es
4 Research Group of Physics for Renewable Energies, University of Cordoba, Campus of Rabanales, 14071 Cordoba, Spain; alvaromarquezugr@gmail.com
* Correspondence: fa2vamam@uco.es; Tel.: +34-957-218-602

Received: 18 September 2019; Accepted: 15 November 2019; Published: 22 November 2019

Abstract: The growing need to improve the environmental and energy sustainability of buildings involves the use of solar radiation incident on their surfaces. However, in cities, this task is complicated due to the constructive geometry that leads to shading between buildings. In this context, this work presents a study of solar access to the façades of buildings in cities. The methodology is based on the determination of the incident annual solar radiation in 121 significant points of each façade considering the twelve representative days of the year. To characterize the influence of the different city typologies on solar access, the urban solar coefficient is proposed. A study of two neighborhoods in Cordoba (Spain) with different urban settings have been analyzed. Specifically, two typologies of neighborhoods have been compared: one with "L-shaped" and "U-shaped blocks" and another with "Grouped blocks". For both of them, the Urban Solar Coefficient has been calculated, obtaining a higher mean value for the neighborhood with "L-shaped" and "U-shaped blocks" (0.317) than for the one with "Grouped blocks" (0.260). Accordingly, the results show that urban morphology can influence the Urban Solar Coefficient and solar access. Finally, a regression model for each neighborhood has been obtained in order to determine the dependence of the Urban Solar Coefficient on neighborhood geometry factors.

Keywords: sustainable cities; solar access; solar radiation on buildings

1. Introduction

Cities in developed countries are undergoing fast growth due to different factors such as the increase in the global population [1] or migration from rural environments and underdeveloped countries, among others [2,3]. In fact, more than half of the world's population now lives in cities and this number is expected to reach 66% by 2050 [4,5]. As a result of this urban population increase, major problems related to the sustainability of cities are emerging, such as the worsening of air quality as a consequence of the use of fossil fuels for transportation or heating of buildings [3,5–7]. Specifically, in terms of energy supply, it is estimated that 75% of total energy is consumed in cities [3] and that this consumption will double over the next three decades [8,9]. These circumstances, together with the environmental problems associated with fossil fuels [10], have encouraged research and development of renewable energies in order to improve energy efficiency and sustainability in cities [5,9]. Among

these renewable energy sources, solar energy stands out as a source of clean energy, abundant and available, to a greater or lesser extent, throughout the Earth [11].

In addition, urban planning has always searched, as the main goal, an ideal integration of living spaces (buildings and squares), communication systems (roads and streets) and land area (topography) [12]. However, the lack of available space in cities has caused the appearance of new neighborhood configurations, which only give importance to the rise of population density [13]. Therefore, nowadays, parameters such as population density, street width, and accessibility, determine the typology of new neighborhoods [14]. Nevertheless, despite the harnessing of solar energy in cities becoming an obligation in new dwellings to make them sustainable, solar radiation levels are not frequently taken into account when making decisions about urban planning.

In fact, to develop energy efficiency measures in new buildings it is necessary to know the levels of solar radiation reaching every piece of the building which could be used to install solar panels or thermal collectors [15,16]. In addition, this information about solar radiation can also be used for the estimation of natural lighting on its windows and, consequently, to guarantee solar rights [17], especially in cities with a great presence of skyscrapers. Daylight also has a positive influence on the health and human behavior of the residents [18,19] and it contributes to improving the indoor climate, increasing thermal comfort, and, consequently, reducing the energy demand of a dwelling [19–24]. For all these reasons, an in-depth knowledge of the level of available solar radiation on the façades of buildings in cities is necessary [25].

Furthermore, complete knowledge of the solar radiation on façades in complex cities also allows developing new passive solar building designs [26], making it easier to choose the ideal materials for windows (transparent or translucent polymer) and their layout in each case [27]. These techniques turn out to be especially interesting in areas where the heating loads in buildings represent an important part of the electricity bill. With this in mind, Building Performance Simulation (BPS) tools compare different design alternatives related to the efficiency and energy consumption in buildings, providing useful and quick information to the technicians [28]. Owing to the importance of the level of solar irradiance on façades and roofs [29,30], architects should consider it during the early phases of their projects. In this line of work, Tang Minfang [31] studied the effect of the azimuth angle and the height of the main façades of a building on the available solar radiation and Salazar Trujillo [32] described the influence of solar radiation on the temperatures inside the rooms in order to improve energy efficiency.

However, in cities, this analysis can prove complex [23], due to several interactions existing, including those with neighboring buildings or the effect of the trees [33] and the fact that each neighborhood must be studied independently [34].

Geographic Information System (GIS) techniques allow representing complex cities and can be used for the estimation of the most appropriate parts of a building for the installation of PV panels [35] or identifying the zones of optimal solar energy potential [36]. Besides, using these techniques, the results may be scalable and automated, in comparison with points-based methods [37]. A good example of a methodology based in GIS is the Solar Energy Planning (SEP) developed by Gadsden et al. [38], which not only can predict the energy consumed by dwellings but also the achievable power saving when using PV systems, solar-assisted hot water or passive solar design.

Several software applications have been developed to study the distribution of solar radiation in complex cities. One of the most important is the Heliodon. This tool, designed by Benoit Beckers and Luc Masset, graphically represents the solar irradiance reaching building façades. However, to minimize the computation time, it only considers the direct component of solar radiation [39]. Additionally, Solene software, designed by the Centre de Recherche Méthodologique d'Architecture (CERMA) analyzes sunlight in cities [40]. It allows determining shadows between buildings as well as daylight both inside and outside a building. Accordingly, it is quite useful as a tool for architects who can easily simulate daylight when deciding window distribution on façades and roofs.

In this paper, a new characterization of the solar radiation reaching the building façades of neighborhoods of different typologies is presented. As an innovation, it takes into account not only direct solar radiation but also the diffuse and reflected components. In that way, a new framework for characterizing solar radiation reaching building façades in urban environments is provided. This framework is applied in two neighborhoods with different typologies in Cordoba (Spain) in order to determine the influence of the neighborhood morphology on solar access. Finally, a new correlation to estimate the solar radiation on the façades of the buildings of each neighborhood has been determined.

2. Data: Neighborhoods Selected

In this paper, two different neighborhoods of Cordoba (Spain) have been analyzed. Cordoba is made up of different typologies of neighborhoods. Specifically, the oldest ones, located near the center, present an irregular net. However, since the middle of the 20th century, the growth of the city has been planned in advance in order to design a street layout capable of distributing the traffic flow through the neighborhoods and to improve accessibility to buildings. In addition, due to the high temperatures registered in summer in Cordoba, recent buildings have recreational spaces such as swimming pools, areas of play, etc.

2.1. Case A. U-Shaped Blocks and L-Shaped Blocks Neighborhood

In this first case, a neighborhood made up of "U-shaped" and "L-shaped" blocks (Figure 1) is studied. This building structure is nowadays the most common solution for the growth of the city selected, Cordoba. This urban development planning is conceived for a horizontal growth of the city and the roads and the blocks of the neighborhood maintain an "orthogonal urban net". These neighborhoods are characterized by low population density, high accessibility and extensive recreational spaces among buildings [41,42].

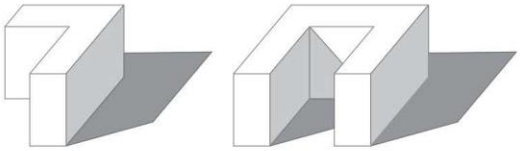

Figure 1. L-Shaped and U-Shaped blocks.

For this first study, the neighborhood selected, which will be denoted by the letter A, is located in the north of Cordoba (37°53′50.0″ N 4°47′50.6″ W) and was built in 2007 (Figure 2). Since it is a real neighborhood, it is made up of different kinds of buildings. However, most of them are U-shaped and L-shaped blocks or have a similar structure with two-by-two parallel façades. Accordingly, it will be considered as a U-shaped and L-shaped block neighborhood. Figure 3 shows the perimeter and the height of all the buildings of neighborhood A. Specifically, the buildings of neighborhood A have an average height of 17 m [41].

Figure 2. 3D view of a U-shaped and L-shaped neighborhood (Case A) of Cordoba (Spain).

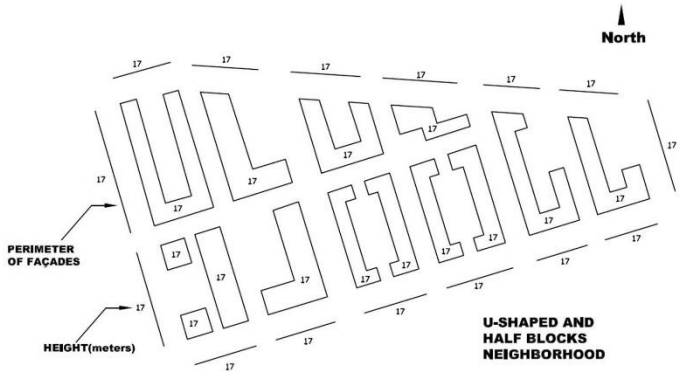

Figure 3. Perimeter and heights of the buildings of a U-shaped and L-shaped block neighborhood (Case A) of Cordoba (Spain).

2.2. *Case B. Grouped Blocks Neighborhood*

Secondly, a neighborhood made up of "grouped blocks" (Figure 4) is considered. This typology of urban planning is often used when the available space is reduced. This usually happens when an old block located in the center of a city is pulled down and a new one is rebuilt in its place. In this context, the roads and the street layout cannot be modified so that the number of dwellings planned will determine the height of the building and its population density.

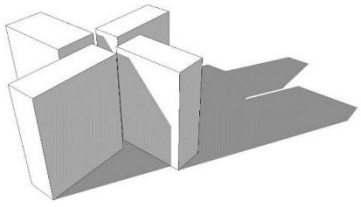

Figure 4. Grouped blocks.

In this case, the neighborhood selected, B (Figure 5), is situated in a consolidated area of the city of Cordoba (37°52′57.7″ N 4°47′48.3″ W) and it was built in the sixties. The buildings have the maximum height allowed in Cordoba, that is, 7 floors and, consequently, their average height is 25 m [41].

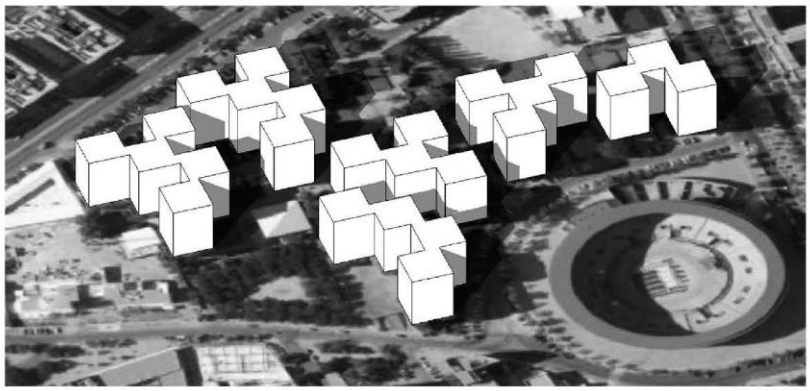

Figure 5. 3D view of a grouped block neighborhood (Case B) of Cordoba (Spain).

The building configuration used in this neighborhood is the "grouped blocks" with a distribution of attached buildings in which most of the façades are external. The available space between the blocks is used for recreational uses, gardens, etc. This is a common cause of the vertical growth of the city. Figure 6 shows the perimeter and the height of all the buildings of the neighborhood B studied.

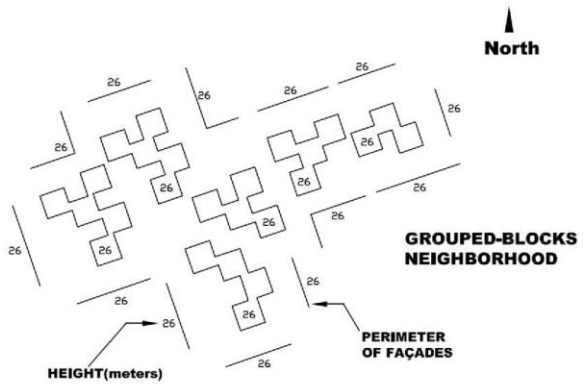

Figure 6. Perimeter and heights of the buildings of a grouped block neighborhood (Case B) of Cordoba (Spain).

3. Methodology

To describe the solar radiation reaching the building façades of a neighborhood and its dependence on the neighborhood typologies, firstly, the level of solar radiation received on different points of the façades of the buildings of each selected neighborhood is determined. For this purpose, a dimensionless factor called Urban Solar Coefficient (USC) is proposed (Equation (1)). This factor is defined as the proportion between the annual average horizontal solar radiation in the neighborhood,

$\overline{H_{g,a}}$ (in kWh/m^2), and the annual average solar radiation reaching a particular point of a façade of the neighborhood, $\overline{H_{g,a,p}}$ (in kWh/m^2). Thus, the parameter USC represents a measure of the capacity of an urban environment to access the solar resource.

$$\mathrm{USC} = \frac{\overline{H_{g,a}}}{\overline{H_{g,a,p}}} \quad (1)$$

This dimensionless parameter is exclusive for each point of a façade and it represents its solar capacity. Due to the effect of the shadows of neighboring buildings, the level of solar radiation reaching a specific point of a building façade depends on the geometry of the neighborhood (height of the point studied, distance to other façades and so on). Once the USC of each point of each façade has been computed, a statistical analysis of the USC values obtained is developed. From the USC data for the façades of all the buildings of each neighborhood, different regression models have been estimated to determine the dependence of USC on the neighborhood geometry factors. According to this, a simple and accurate empirical mathematical expression for the dependence of USC on the geometry for each neighborhood has been proposed (Equation (2)):

$$\mathrm{USC}(\mathrm{H}, \mathrm{D}, \theta) = c_1 \cdot I_b + c_2 \cdot \mathrm{H} + c_3 \cdot \mathrm{D} + c_4 \cdot \sin\theta + c_5 \cdot \cos\theta \quad (2)$$

where:

H: Height of the studied point (in meters)
D: Distance between the façade studied and the closest one (in meters)
θ: Azimuth angle of the selected façade (in degrees)
c_1, c_2, c_3, c_4, c_5: Correlation coefficients. They may be estimated for each neighborhood typology.

3.1. Solar Radiation Model

In order to obtain the existing correlation, for each typology of neighborhood, between the different variables and the Urban Solar Coefficient (USC) on every point of the façades, the proposed tool uses a specific solar radiation model that considers the three components of the global solar irradiance received on a façade, that is, direct, diffuse and reflected irradiance. Among these three components, global solar irradiance depends mainly on direct irradiance which comes straight from the sun without being scattered. Diffuse irradiance is the solar irradiance reaching the façade after having been scattered from the direct solar beam. Finally, in cities, reflected irradiance, that is, the irradiance reflected by any other surface or façade must also be considered. Its intensity depends on the reflection coefficient or albedo of other surfaces. Thus, the global solar irradiance received on a façade is given by Equation (3).

$$I = \frac{\vec{n} \cdot \vec{s}}{\vec{k} \cdot \vec{s}} \cdot I_b + \frac{1 + \vec{n} \cdot \vec{k}}{2} \cdot I_d + \frac{1 - \vec{n} \cdot \vec{k}}{2} \cdot \rho \cdot (I_b + I_d) \quad (3)$$

where:

$\vec{n}$: Normal vector to the external surface of the façade of the building
$\vec{s}$: Solar vector
$\vec{k}$: Normal vector of the tangent plane of the location considered
ρ: Albedo
I_b: Direct irradiance on horizontal surface
I_d: Diffuse irradiance on horizontal surface

In this solar radiation model, the direct (I_b) and diffuse (I_d) irradiances on the horizontal surface have been estimated from synthetic series of data of horizontal global radiation. These series are based on 10-year daily measurements. Thus, global solar radiation for a specific period of time can be determined by integrating, over time, the global irradiance (I) on a point given by Equation (3).

However, Equation (3) shows poor results when estimating solar radiation on façades since it does not consider the influence of the height on the diffuse and reflected irradiance. In order to improve this method, a new expression has been developed considering that diffuse and reflected irradiance depends on the portion of sky seen from the studied point. That is, a point with a great height will see a bigger portion of the sky vault and it will receive more diffuse irradiance. On the other hand, a point located close to the floor will see a greater portion of the neighboring buildings so that irradiance reflected from them will be greater. To quantify this behavior, a dimensionless term, called Sky View Factor (SVF) has been defined. It estimates the portion of the celestial vault seen from a specific point [43].

Accordingly, SVF will determine whether the most important component of the global solar irradiance reaching a specific point of a façade will be the diffuse or reflected irradiance (Equation (4)) [44].

$$I = \frac{\vec{n} \cdot \vec{s}}{\vec{k} \cdot \vec{s}} \cdot I_b + SFV \cdot I_d + (1 - SFV) \cdot \rho \cdot (I_b + I_d) \quad (4)$$

3.2. *Software Application for the Analysis*

In this paper, the average annual solar radiation on the building façades of two different neighborhoods has been studied. For this purpose, using Equation (4), it is necessary to estimate the solar irradiance received on different points of each façade for all the buildings and both neighborhoods. Specifically, in each façade, 121 points are considered. In addition, each neighborhood is made up of more than 100 façades. Due to the great number of points to analyze, different functions and subroutines in Visual Basic environment have been developed to automatize the calculation. Table 1 lists these subroutines.

Table 1. Summary of subroutines developed.

Name of Subroutine	Features
Shadow	It takes the value 0 if the point is Shaded and 1 if it is lighted
Sky View Factor	Portion of the sky seen from the point [0–0.5]
Daily Radiation	Energy in kWh/ m^2 with a 6 min integration interval
Irradiance	Measure of the irradiance in W/m^2 on the point

3.2.1. Shadow Subroutine

This function determines whether a specific point on the façade of a building is shaded or not. The result will be 0 if the point is shaded and 1 if not.

In order to locate this point, each façade is represented in a local reference system of two orthogonal axis ρ and μ whose values range from 0 to 1 in steps of 0.1 (Figure 7). Thus, in each façade, 121 different points can be studied.

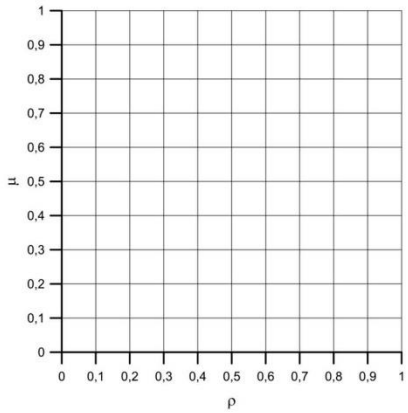

Figure 7. Grid façade representation.

Accordingly, the shadow function uses as input parameters the selected façade and two parameters which indicate the specific point of the façade to be studied. Additionally, other input parameters are the Julian day, the solar time and the latitude of the location of the neighborhood.

To determine whether the point is shaded or lighted, first, its Cartesian coordinates are defined in the global reference system of the city. Then, for the Julian day, latitude and solar time selected, the subroutine will estimate the position of the sun and the straight line from the sun to the façade point of the study. After that, the intersections between this line and the planes representing the neighboring façades will be calculated (Figure 8) by solving the equation system given by Equation (5). Thus, the selected façade point will be shaded if the following conditions are satisfied: $a > 1$, $0 < b < 1$ and $0 < c < 1$.

$$\begin{pmatrix} X_0 \\ Y_0 \\ Z_0 \end{pmatrix} + a \begin{pmatrix} S_x \\ S_y \\ S_z \end{pmatrix} = \begin{pmatrix} X_1 \\ Y_1 \\ Z_1 \end{pmatrix} + b \begin{pmatrix} V_{12x} \\ V_{12y} \\ V_{12z} \end{pmatrix} + c \begin{pmatrix} V_{23x} \\ V_{23y} \\ V_{23z} \end{pmatrix} \quad (5)$$

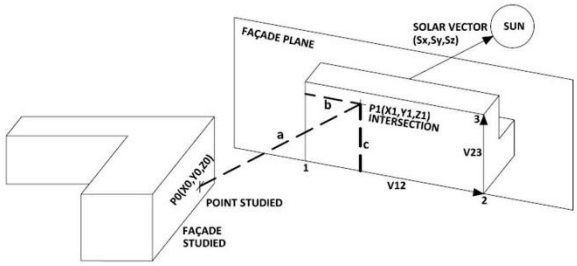

Figure 8. Representation of the geometric problem.

Figure 9 shows the different situations that must be discussed when studying whether the selected point is shaded or not. The output given by the shadow subroutine will be 0 (shadowed point) when there is one intersection point on the façade of an adjacent building (condition 1), when the angle between the normal vector of the external surface of the façade and the solar vector is greater than $\pi/2$ rad (condition 2) or when the moment of time considered is before sunrise or after sunset (condition 3).

In any other case, the studied point will be lighted and, consequently, the output of the Shadow Function will be 1.

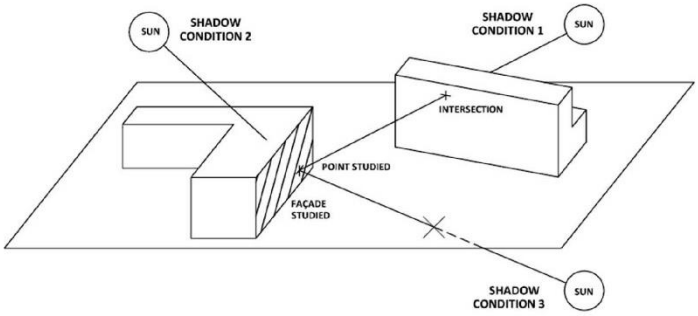

Figure 9. Representation of the shading conditions.

3.2.2. Sky View Factor Subroutine

A shadowed point of a façade will not receive direct solar irradiance, but diffuse or reflected irradiance could reach it. Specifically, the higher the point considered, the greater the portion of the celestial vault seen from it. Thus, the higher points of the façade receive more diffuse irradiance than the lower ones, which will receive more reflected radiation from nearby façades. Since the diffuse component of the solar radiation is greater than the reflected one, the higher points of the façade will receive higher radiation levels.

A new subroutine, called Sky View Factor (SVF), has been developed to simulate this phenomenon. Specifically, for each one of the 121 points considered on a façade, 1012 rays in different directions are generated (Figure 10). For each of them, it determines whether the ray points to the celestial vault or, on the contrary, it reaches the ground or a surrounding building (applying conditions defined in Figure 9). From that analysis, the Sky View Factor (SVF) is defined as the ratio between the number of rays pointing to the celestial vault and the total amount of rays generated. Accordingly, this parameter does not depend on the time but only on the point under consideration and the geometry of the neighborhood selected. In that way, the SVF and its complementary value make it possible to calculate more realistically the diffuse and reflected solar radiation that reaches a point on the façade of a building in a neighborhood considering the obstacles posed by the buildings that surround it.

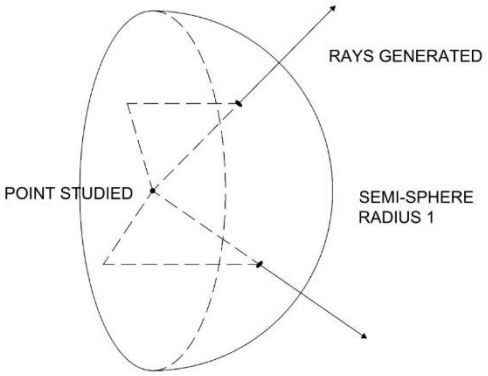

Figure 10. Generation of the rays on the selected point. Adapted from [45].

3.2.3. Instantaneous Irradiance Subroutine

This subroutine estimates the irradiance (W/m^2) reaching a specific point of a façade at a solar time using Equation (4) and considering as input data: the façade selected and the coordinates of the point understudy in the local reference system, the latitude, the Julian day, the solar time, the albedo and the solar radiation on a horizontal plane at this latitude and moment of time. Specifically, to simplify the calculation, for the albedo, a mean value of 0.2 has been considered [46].

3.2.4. Daily Solar Radiation Subroutine

From the result of the Instantaneous Irradiance subroutine, this function calculates the daily solar radiation (kWh/m^2) for each point of the façade understudy and a Julian day. Specifically, it calculates the irradiance every 6 min throughout each complete day, multiplies the result by 0.1 h and adds all the values of the day obtaining the daily radiation. Accordingly, the result of this function provides valuable information for evaluating the feasibility of a photovoltaic or thermal installation on the façade of a building.

Figure 11 shows the flowchart of the Visual Basic application designed for the calculations.

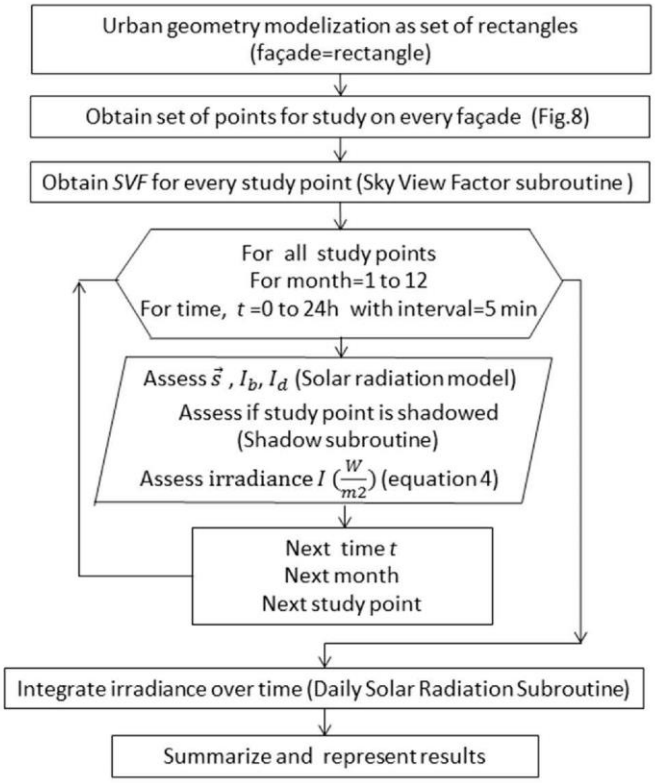

Figure 11. Flowchart of the Visual Basic application developed.

4. Discussion and Regressions

As explained before, the USC value has been calculated for the 121 points considered (Figure 7) on each façade of neighborhoods A and B. Specifically, 14,036 USC values for neighborhood A and 13,673 USC values for neighborhood B have been obtained. To simplify the graphical representation and visualization of the data, an auxiliary variable, USC_{100}, is defined according to Equation (6).

$$USC_{100} = 100 \cdot USC \tag{6}$$

Figure 12 shows the USC_{100} absolute frequency histogram for neighborhood A. For this representation, consecutive classes of index i have been defined so that i meets Equation (7).

$$i - 1 < USC_{100} \leq i \tag{7}$$

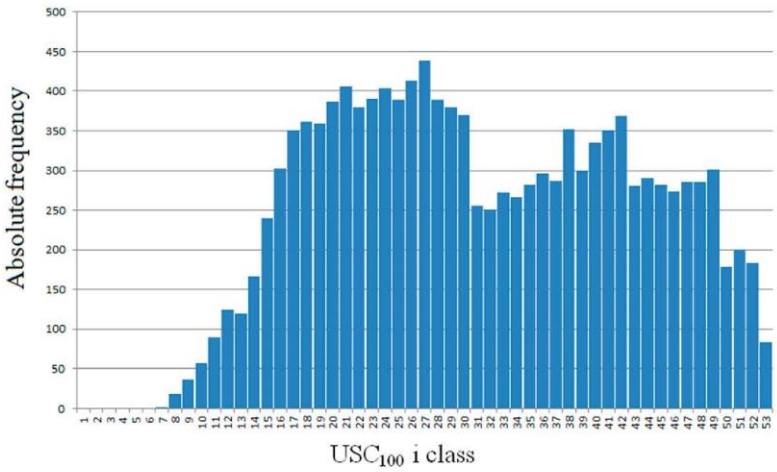

Figure 12. USC_{100} (Urban Solar Coefficient) histogram for neighborhood A.

This condition is equivalent to define i according to Equation (8).

$$i = \text{integer}(USC_{100}) + 1 \tag{8}$$

Thus, as an example, if USC = 0.341, it will belong to class 35.

Similarly, Figure 13 shows the USC_{100} absolute frequency histogram for neighborhood B.

Figure 12 shows a displacement of USC values in neighborhood A with respect to values in neighborhood B (Figure 13), which implies better access to solar resources in neighborhood A in general. This effect is linked to the lower height of the buildings in neighborhood A, as well as to the distribution in a simpler geometry. The intertwined geometry of neighborhood B favors the existence of north-facing walls that are also obstructed in all directions. Normally the lowest points of this type of façades are associated with the lowest values of the USC index. In both neighborhoods, as expected, the maximum USC values are reached at the highest points of the façades that are best oriented to the south and have a low level of obstruction. The value of the maximums of USC is slightly higher in neighborhood B, which could be explained by the greater height of the buildings and their better South orientation.

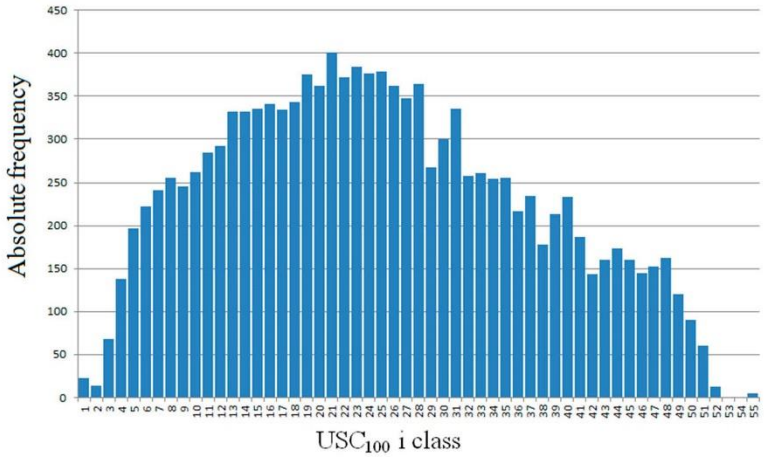

Figure 13. USC_{100} histogram for neighborhood B.

Table 2 shows the values of the descriptive statistics of USC for both distributions, from which significant differences in the mean and the median have been observed. Both parameters indicate that access to the solar resource is about 20% higher in neighborhood A than in neighborhood B.

Table 2. Descriptive statistic values for USC in both neighborhoods.

Descriptive Statistic Values	Neighborhood A	Neighborhood B
N sample	14,036	13,673
Minimum	0.063	0.012
Maximum	0.528	0.540
Average	0.317	0.260
Median	0.304	0.249
Variance	0.013	0.017
Standard Deviation	0.116	0.132

The exposed methodology also allows mapping the USC_{100} variable in façades. This enables us to deepen the details of the differences in access to the solar resource at each point of the same façade. Figures 14 and 15 show the variability of USC_{100} in representative façades of neighborhoods A and B respectively. They also allow quantifying, in specific façades, the dependence of the USC_{100} gradient on the height. It is worth highlighting that in the façades analyzed, the increase of this gradient is greater on the highest points than on the lowest ones. This behavior is more evident as the height of the building increases.

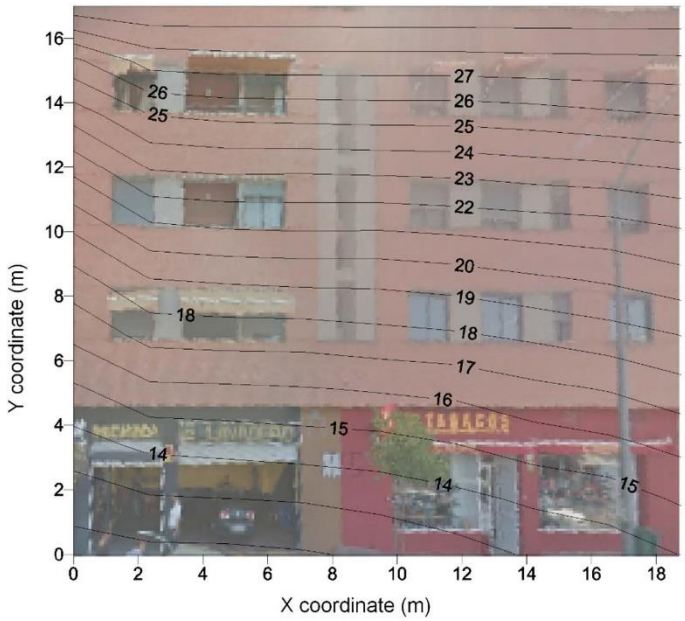

Figure 14. USC_{100} map for a representative façade of neighborhood A.

Finally, with the USC data of all the façades and buildings, a regression analysis has been performed for each neighborhood in order to analyze the variables with the most significant influence on the USC value.

Studying the influence of façade facing, street width and height of the studied point on the outcome of the USC factor at each point studied, linear regression is proposed (Equation (9)).

$$USC(H, D, \theta) = c_1 + c_2 \cdot H + c_3 \cdot D + c_4 \cdot \cos\theta \quad (9)$$

where:

H: Height of the studied point over the ground (in meters)
D: Street width (in meters)
θ: Façade facing (in grades)
c_1, c_2, c_3, c_4: Constants

Equation (10) shows the result of the regression for neighborhood A. It is observed that the height of the studied point over the floor and the street width keep a direct relationship with the USC factor while in the case of the cosine of the orientation of the façade is reversed. Its correlation coefficient has a value of 0.919.

$$USC(H, D, \theta) = 0.197 + 0.012 \cdot H + 0.001 \cdot D - 0.115 \cdot \cos\ \theta \quad (10)$$

On the other hand, the regression for neighborhood B (Equation (11)) has a correlation value of 0.86 which is lower than the value obtained for neighborhood A. In this case, as in the previous one, the influence of the height of the point considered and the street width is direct and the orientation of the façade reverse.

$$USC(II, D, \theta) = 0.074 + 0.010 \cdot II + 0.002 \cdot D - 0.091 \cdot \cos\ \theta \quad (11)$$

These regressions allow knowing the value of the USC factor, and therefore the annual radiation received at any point on the façade was chosen, knowing only the typology of the neighborhood and the annual radiation on a horizontal surface.

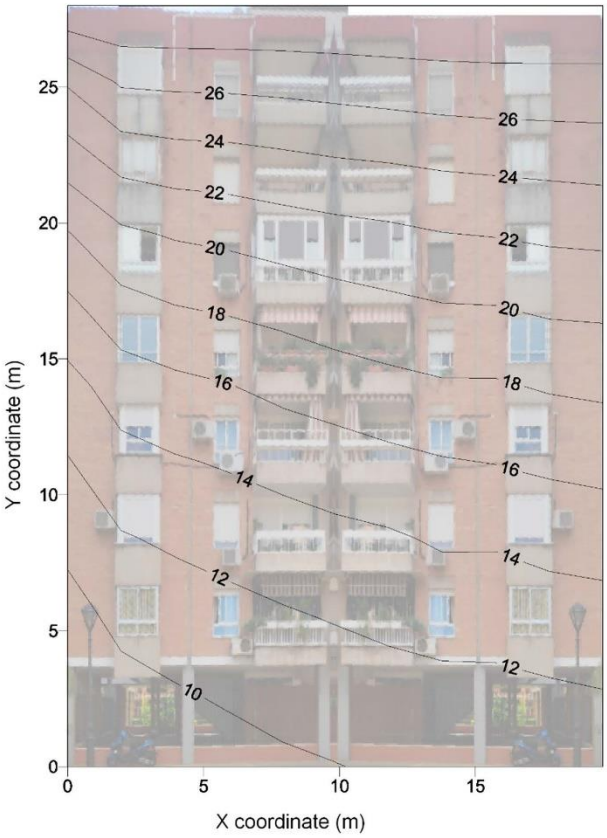

Figure 15. USC_{100} map for a representative façade of neighborhood B.

5. Conclusions

In this paper, a novel model for calculating the solar radiation that reaches the façade of a building in a complex neighborhood is presented. The equation proposed allows obtaining accurate results for the irradiance, considering how the position of the adjacent buildings affects to the diffuse and reflected irradiance received on the façade. For this purpose, the Sky View Factor (SVF) is calculated. Considering the obstacles posed by surrounding buildings, it represents the portion of celestial vault viewed from each point of the façade. Accordingly, the SVF depends on the position of the point on the façade of the building but remains constant as long as the geometry of the neighborhood is not altered.

Four subroutines, programmed in Visual Basic Excel environment, have been developed to solve the problem of shading, the quantification of the obstacles seen, and the radiation received on a complete façade. Therefore, these subroutines allow the calculation of the solar radiation reaching any point of a selected façade of a neighborhood. From it, it is possible to display the results of the radiation on the façade in an intuitive way, through a solar radiation contour map.

The model and the program created have been used to characterize two typologically different neighborhoods through their capacity for solar energy harnessing. To this aim, the Urban Solar Coefficient (USC) has been defined, relating the annual radiation on horizontal surface of the study area and the annual radiation received at a chosen point on a façade. Calculating this factor on 121 points on each façade and for all the façades compounding the neighborhood, the distribution of the USC values for each neighborhood and the two different histograms that characterize the radiation according to the urban typology have been obtained. A comparative statistical analysis of the USC data for each neighborhood shows that the maximum values of USC are registered in neighborhood B (0.540) since its buildings are higher than the ones in neighborhood A, with a relative maximum USC value of 0.528. On the contrary, the relative minimum value in neighborhood A (0.063) is higher than in neighborhood B (0.012) due to the fact that the geometry of the neighborhood A is simpler, and its buildings are lower and more separated which reduces the effect of obstacles. On the whole, the mean value is higher in neighborhood A (0.317) than in neighborhood B (0.260) which implies the best access to solar resources in the first area than in the second one.

Finally, with the results obtained, one regression for each neighborhood has been proposed to determine the dependence of USC on the geometry of the buildings. These regressions allow calculating easily the amount of radiation received on the points of the façades, in neighborhoods that meet the characteristics described in this paper. In this way, the methodology and the tool proposed provide the calculation of the solar irradiance incident on any point of the façade of a given neighborhood. However, the tool presents some limitations and it is planned to be improved in upcoming works with the inclusion of a new subroutine that represents, in 3D contour maps, the values of irradiance in all the facades of the buildings of a certain neighborhood. Likewise, a network of sensors is being designed to automatically monitor the experimental irradiance received on a given façade in order to validate the methodology and tool proposed in this work.

Despite these limitations, the methodology and tool proposed could be very useful, among other applications, to plan urban designs of new neighborhoods that guarantee the solar rights and favor an optimum harnessing of the solar resource, whether for natural lighting or for the generation of energy from renewable sources, which will have a positive impact on the sustainability of cities.

Author Contributions: Conceptualization, L.M.F.-A. and R.L.-L.; methodology, J.R.-F. and M.V.-M.; software, A.M.-G.; validation, L.M.F.-A. and M.V.-M.; formal analysis, L.M.F.-A., J.R.-F. and R.L.-L.; bibliographic search, L.M.F.-A. and M.V.-M.; data curation, J.R.-F. and R.L.-L.; writing—original draft preparation, L.M.F.-A., A.M.-G. and M.V.-M.; writing—review & editing, L.M.F.-A., J.R.-F., R.L.-L. and M.V.-M.; supervision, J.R.-F. and R.L.-L.

Funding: This research received no external funding.

Conflicts of Interest: The authors declare no conflict of interest.

References

1. United Nations. World Population Prospects 2019 (Report). Available online: https://population.un.org/wpp/Publications/Files/WPP2019_Highlights.pdf (accessed on 18 September 2019).
2. Eremia, M.; Toma, L.; Sanduleac, M. The smart city concept in the 21st century. *Procedia Eng.* **2017**, *181*, 12–19. [CrossRef]
3. Milošević, M.R.; Milošević, D.M.; Stević, D.M.; Stanojević, A.D. Smart city: Modeling key indicators in Serbia using IT2FS. *Sustainability* **2019**, *11*, 3536. [CrossRef]
4. United Nations. World Urbanization Prospects 2018 (Report). Available online: https://population.un.org/wup/Publications/Files/WUP2018-Report.pdf (accessed on 18 September 2019).

5. Sandman, H.; Levänen, J.; Savela, N. Using empathic design as a tool for urban sustainability in low-resource settings. *Sustainability* **2018**, *10*, 2493. [CrossRef]
6. Martos, A.; Pacheco-Torres, R.; Ordóñez, J.; Jadraque-Gago, E. Towards successful environmental performance of sustainable cities: Intervening sectors. A review. *Renew. Sustain. Energy Rev.* **2016**, *57*, 479–495. [CrossRef]
7. Lindfors, A.; Feiz, R.; Eklund, M.; Ammenberg, J. Assessing the potential, performance and feasibility of urban solutions: methodological considerations and learnings from biogas solutions. *Sustainability* **2019**, *11*, 3756. [CrossRef]
8. Alamdari, P.; Nematollahi, O.; Alemrajabi, A.A. Solar energy potentials in Iran: A review. *Renew. Sustain. Energy Rev.* **2013**, *21*, 778–788. [CrossRef]
9. Mardonova, M.; Choi, Y. Assessment of photovoltaic potential of mining sites in Uzbekistan. *Sustainability* **2019**, *11*, 2988. [CrossRef]
10. Østergaard, P.A.; Duic, N.; Noorollahi, Y.; Mikulcic, H.; Kalogirou, S. Sustainable development using renewable energy technology. *Renew. Energy* **2020**, *146*, 2430–2437. [CrossRef]
11. Panwar, N.L.; Kaushik, S.C.; Kothari, S. Role of renewable energy sources in environmental protection: A review. *Renew. Sustain. Energy Rev.* **2011**, *15*, 1513–1524. [CrossRef]
12. Belakehal, A.; Tabet Aoul, K.; Bennadji, A. Sunlighting and daylighting strategies in the traditional urban spaces and buildings of the hot arid regions. *Renew. Energy* **2004**, *29*, 687–702. [CrossRef]
13. Glaeser, E.L.; Kahn, M.E. Sprawl and urban growth. *Handb. Reg. Urban Econ.* **2004**, *4*, 2481–2527.
14. Van Esch, M.M.E.; Looman, R.H.J.; De Bruin-Hordijk, G.J. The effects of urban and building design parameters on solar access to the urban canyon and the potential for direct passive solar heating strategies. *Energy Build.* **2012**, *47*, 189–200. [CrossRef]
15. Drif, M.; Pérez, P.J.; Aguilera, J.; Aguilar, J.D. A new estimation method of irradiance on a partially shaded PV generator in grid-connected photovoltaic systems. *Renew. Energy* **2008**, *33*, 2048–2056. [CrossRef]
16. Zhang, X.; Wei, Z. A hybrid model based on principal component analysis, wavelet transform, and extreme learning machine optimized by Bat algorithm for daily solar radiation forecasting. *Sustainability* **2019**, *11*, 4138. [CrossRef]
17. Alzoubi, H.H.; Alshboul, A.A. Low energy architecture and solar rights: Restructuring urban regulations, view from Jordan. *Renew. Energy* **2010**, *35*, 333–342. [CrossRef]
18. Edwards, L.; Torcellini, P. A Literature Review of the Effects of Natural Light on Building Occupants. Available online: https://www.nrel.gov/docs/fy02osti/30769.pdf (accessed on 18 September 2019).
19. Calama-González, C.; León-Rodríguez, Á.; Suárez, R. Daylighting and energy performance evaluation of an egg-crate device for hospital building retrofitting in a Mediterranean climate. *Sustainability* **2018**, *10*, 2714. [CrossRef]
20. Ihm, P.; Nemri, A.; Krarti, M. Estimation of lighting energy savings from daylighting. *Build. Environ.* **2009**, *44*, 509–514. [CrossRef]
21. Gago, E.J.; Muneer, T.; Knez, M.; Köster, H. Natural light controls and guides in buildings. Energy saving for electrical lighting, reduction of cooling load. *Renew. Sustain. Energy Rev.* **2015**, *41*, 1–13. [CrossRef]
22. Torres-Roldán, M.; López-Luque, R.; Varo-Martínez, M. Design of an innovative and simplified polar heliostat for integration in buildings and urban environments. *Sol. Energy* **2015**, *119*, 159–168. [CrossRef]
23. Torres-Roldán, M.; López-Luque, R.; Varo-Martínez, M. Assessment of the pointing error of heliostats with a single not polar rotation axis for urban applications. *Sol. Energy* **2016**, *137*, 281–289. [CrossRef]
24. Spacek, A.D.; Neto, J.M.; Biléssimo, L.D.; Junior, O.H.A.; Neto, G.P.D.F.; Giansella, R.D.S.; De Santana, M.V.F.; Malfatti, C.D.F. Proposal for an experimental methodology for evaluation of natural lighting systems applied in buildings. *Energies* **2017**, *10*, 1014. [CrossRef]
25. Polo, M.-E.; Pozo, M.; Quirós, E. Directional statistics in solar potential of rooftops at three different neighborhoods of a medium size city. *Proceedings* **2018**, *2*, 1275. [CrossRef]
26. Gómez-Munoz, V.M.; Porta-Gándara, M.A. General model to build awnings and external walls with optimum shading interaction. *Renew. Energy* **2004**, *29*, 605–613. [CrossRef]
27. Smith, G.B. Materials and systems for efficient lighting and delivery of daylight. *Sol. Energy Mater. Sol. Cells* **2004**, *84*, 395–409. [CrossRef]
28. Kanters, J.; Horvat, M.; Dubois, M.C. Tools and methods used by architects for solar design. *Energy Build.* **2014**, *68*, 721–731. [CrossRef]

29. Brito, M.C.; Freitas, S.; Guimarães, S.; Catita, C.; Redweik, P. The importance of facades for the solar PV potential of a Mediterranean city using LiDAR data. *Renew. Energy* **2017**, *111*, 85–94. [CrossRef]
30. Bayón-Cueli, C.; Barbón, A.; Bayón, L.; Barbón, N. A cost-energy based methodology for small-scale linear Fresnel reflectors on flat roofs of urban buildings. *Renew. Energy* **2020**, *146*, 944–959. [CrossRef]
31. Mingfang, T. Solar control for buildings. *Build. Environ.* **2002**, *37*, 659–664. [CrossRef]
32. Salazar Trujillo, J.H. Solar performance and shadow behaviour in buildings. Case study with computer modelling of a building in Loranca, Spain. *Build. Environ.* **1998**, *33*, 117–130. [CrossRef]
33. Gómez-Muñoz, V.M.; Porta-Gándara, M.A.; Fernández, J.L. Effect of tree shades in urban planning in hot-arid climatic regions. *Landsc. Urban Plan.* **2010**, *94*, 149–157. [CrossRef]
34. Shao, J. Calculation of sunshine duration and saving of land use in urban building design. *Energy Build.* **1990**, *15*, 407–415. [CrossRef]
35. La Gennusa, M.; Lascari, G.; Rizzo, G.; Scaccianoce, G.; Sorrentino, G. A model for predicting the potential diffusion of solar energy systems in complex urban environments. *Energy Policy* **2011**, *39*, 5335–5343. [CrossRef]
36. Abd Alla, S.; Bianco, V.; Tagliafico, L.A.; Scarpa, F. An innovative approach to local solar energy planning in Riva Trigoso, Italy. *J. Build. Eng.* **2020**, *27*, 100968. [CrossRef]
37. Mardaljevic, J.; Rylatt, M. Irradiation mapping of complex urban environments: An image-based approach. *Energy Build.* **2003**, *35*, 27–35. [CrossRef]
38. Gadsden, S.; Rylatt, M.; Lomas, K.; Robinson, D. Predicting the urban solar fraction: A methodology for energy advisers and planners based on GIS. *Energy Build.* **2003**, *35*, 37–48. [CrossRef]
39. Antaluca, E.; Merino, L.; Beckers, B. Correlation between Measured and Calculated Solar Radiation Data in Compiègne, France. Available online: http://www.worldses.org/journals/environment/environment-2010.htm (accessed on 18 September 2019).
40. Miguet, F. A Further Step in Environment and Bioclimatic Analysis: The Software Tool Solene. Available online: http://www.ibpsa.org/proceedings/BS2007/p126_final.pdf (accessed on 18 September 2019).
41. Ayuntamiento de Córdoba (Spain) Plan General de Ordenación Urbanística (PGOU). Available online: http://www.gmucordoba.es/urbanismo/plan-general-de-ordenacion-urbanistica-pgou (accessed on 7 November 2019).
42. Instituto de Estadística y Cartografía de Andalucía. Distribución Espacial de la Población en Andalucía. Available online: http://www.juntadeandalucia.es/institutodeestadisticaycartografia/distribucionpob/index.htm (accessed on 7 November 2019).
43. Ramírez-Faz, J.; López-Luque, R.; Casares, F.J. Development of synthetic hemispheric projections suitable for assessing the sky view factor on vertical planes. *Renew. Energy* **2015**, *74*, 279–286. [CrossRef]
44. Fernández-Ahumada, L.M.; Casares, F.J.; Ramírez-Faz, J.; López-Luque, R. Mathematical study of the movement of solar tracking systems based on rational models. *Sol. Energy* **2017**, *150*, 20–29. [CrossRef]
45. Márquez-García, A.; Varo-Martínez, M.; López-Luque, R. *Solar Energy in Urban Environments: A New Solar Radiation Model for the Analysis of Energy on Façades*; LAP Lambert Academic Publishing: Alemania, Germany, 2013.
46. Duffie, J.A.; Beckman, W.A. *Solar Engineering of Thermal Processes: Fourth Edition*; John Wiley and Sons: Hoboken, NJ, USA, 2013.